Sensitivity Analysis of a Carbon Simulation Model and its Application in a Montane Forest Environment

SHIYONG XU

B. Sc., Nanjing Forestry University, 1985

A Thesis

Submitted to the School of Graduate Studies

of the University of Lethbridge

in Partial Fulfillment of the

Requirements for the Degree

MASTER OF SCIENCE

Department of Geography

University of Lethbridge

LETHBRIDGE, ALBERTA, CANADA

ABSTRACT

Accurate estimation of Net Primary Productivity (NPP), which is a key component of the terrestrial carbon cycle, is very important in studies of global climate. Ecosystem models have been used for NPP estimates. Determining how much each source of uncertainty contributes to modeled NPP is very important before ecosystem models can be used with confidence over larger areas and time periods. This research has systematically evaluated the boreal ecosystem productivity simulator (BEPS) carbon model in mountainous terrain, Kananaskis, Alberta. After parameterization of the model, sensitivity analysis was conducted as a controlled series of experiments involving sensitivity simulations with BEPS by changing a model input value in separate model runs. The results showed that NPP was sensitive to most model inputs measured in the study area, but that the most important input variables for BEPS were LAI and forest species. In addition, the NPP uncertainty resulting from topographic influence was approximately 3.5 %, which is equivalent to 140 kg C ha^{-1} yr^{-1}. This suggested that topographic correction for the model inputs was also important for accurate NPP estimation.

Using the topographically corrected data, the carbon dynamics were simulated, and average annual NPP production by forests in Kananaskis was estimated at 4.01 T ha^{-1} in 2003.

ACKNOWLEDGEMENTS

There are many people to whom I am indebted for the completion of this research. First and foremost, I would like to thank my thesis supervisor, Dr. Derek Peddle. He not only has offered funding, support and encouragement for my academic work, but also given me considerate care since I lived in Lethbridge. I would also like to thank my thesis committee members, Dr. Stefan Kienzle and Dr. Craig Coburn for their guidance and suggestions for this research, and Dr. Howard Cheng for his time in reviewing this thesis.

This research, including field and remote sensing data collection, was supported by NSERC research grants and other grants held by Dr. Derek R. Peddle, Department of Geography, University of Lethbridge. Additional financial support was made available through teaching assistantships provided by the School of Graduate Studies.

A special thank you to my field companions, Scott Soenen and Sam Lieff during summer 2003, Eric Van Gaalen for his reviewing an earlier draft of this thesis, as well as other graduate students and colleagues from Dr. Peddle's lab who collected field data used in this study. I would like to thank Grace Lebel and Judy Buchannan-Mappin of The University of Calgary Kananaskis Field Station for logistical support in the field, the use of GPS equipment, and for providing the climate data of the base station. The Miistakis Institute for the Rockies is thanked for DEM data and preprocessing. I would like to thank Neal Pilger for the use of partially preprocessed IKONOS imagery, and Scott Soenen for his help with satellite data topographic correction.

Also, I would like to thank the external thesis examiner, Dr. Xulin Guo of the

University of Saskatchewan and Dr. Andrew Hurly of the University of Lethbridge, chair of the thesis defense committee for comments and helpful suggestions.

In particular, I would like to thank Dr Jing Chen and Dr Jane Liu of the University of Toronto for generously providing me with the original BEPS model software. I also have benefited from numerous discussions with Dr Liu.

Finally, I am grateful to the Department of Geography at the University of Lethbridge which provided me with office space and research facilities.

TABLE OF CONTENTS

Approval Page.....ii

Abstract.....iii

Acknowledgements.....iv

Table of Contents.....vi

List of Figures.....xii

List of Tables.....xiv

List of Equations.....xvi

List of Abbreviations.....xviii

Chapter 1 INTRODUCTION

1.1 Introduction.....1

1.2 Research Objectives.....4

1.3 Organization of Thesis.....5

Chapter 2 LITERATURE REVIEW

2.1 Introduction.....6

2.2 Climate Change and Forests.....6

2.2.1 Global Warming.....6

2.2.2 Carbon Cycling in Forests.....7

2.2.3 Remote Sensing of Forests.....9

2.2.3.1 Principles used for remote sensing in forests.....9

2.2.3.2 Abstraction of forest biophysical parameters.....12

2.3 Process-Based Ecosystem Models.....19

2.3.1 Modeling review.....19

2.3.2 BEPS.....22

2.4 Inputs for BEPS.....23
2.4.1 Land Cover.....23
2.4.2 Leaf Area Index (LAI).....24
2.4.3 Forest Biomass.....25
2.4.4 Available Soil Water Capacity (AWC).....25
2.4.5 Climate Inputs for BEPS.....26
2.5 Chapter Summary.....27

Chapter 3 METHODS

3.1 Introduction.....28
3.2 Study Area.....29
3.3 Data Sets.....29
3.3.1 Field Data Collection.....29
3.3.1.1 Forest Stand Properties.....29
3.3.1.2 Endmember Spectra Collection.....31
3.3.1.3 Ground-based LAI measurements.....32
3.3.2 Remote Sensing Imagery.....33
3.3.2.1 IKONOS Data.....33
3.3.2.2 Image Preprocessing.....33
3.3.2.3 Topographic Correction.....34
3.3.3 Digital Elevation Data.....36
3.3.4 Climate Data.....36
3.4 BEPS Model Parameterization.....37
3.4.1 Tree Species Classification.....37
3.4.2 LAI and Biomass Estimation using SMA.....40
3.4.3 Available Soil Water Capacity.....43
3.4.4 Climate Variables.....44
3.4.4.1 Solar Radiation.....45
3.4.4.2 Temperature.....46

3.4.4.3 Precipitation.....47
3.4.4.4 Humidity.....49
3.5 General Sensitivity Test of BEPS in Kananaskis Forests.....50
3.5.1 Sensitivity of NPP to the Input Variables.....51
3.5.1.1 Tree Species.....51
3.5.1.2 LAI.....52
3.5.1.3 Biomass.....52
3.5.1.4 AWC.....52
3.5.1.5 Climate Variables.....53
3.5.2 NPP Independent Variation Sensitivity Analysis.....53
3.5.3 Factorial Sensitivity Test.....54
3.6 Sensitivity analysis of BEPS to topographic influences.....56
3.6.1. Tree species.....57
3.6.2 LAI.....57
3.6.3 Biomass.....57
3.6.4 Climate Variables.....58
3.7 Application of BEPS to the Study Areas.....59
3.8 Chapter Summary.....59

Chapter 4 RESULTS AND DISCUSSION

4.1 Introduction.....61
4.2 Field Results and BEPS Inputs.....61
4.2.1 Field Measurement Results.....61
4.2.2 BEPS Inputs.....63
4.3 Results of General Sensitivity for BEPS.....69
4.3.1 Modeled NPP for Each of the Model Inputs.....69
4.3.1.1 Tree Species.....69

4.3.1.2 LAI 70

4.3.1.3 Solar Radiation.....71

4.3.1.4 Minimum Temperature.....72

4.3.1.5 Maximum Temperature.....74

4.3.1.6 Humidity.....75

4.3.1.7 Biomass.....76

4.3.1.8 Precipitation and AWC.....77

4.3.2 NPP Independent Variation Sensitivity Analysis.....79

4.3.3 Factorial Sensitivity Test.....80

4.4 Results of Topographic Influence on the NPP Estimation.....81

4.4.1 Tree Species.....82

4.4.2 LAI.....83

4.4.3 Solar Radiation.....83

4.4.4 Minimum Temperature.....84

4.4.5 Maximum Temperature.....84

4.4.6 Precipitation.....85

4.4.7 Biomass.....85

4.4.8 Humidity.....86

4.4.9 All Inputs.....87

4.5 Results of Forest Carbon Growth from June to August.....88

4.6 Discussion and Future Perspective.....91

4.6.1 Estimation of the Model Inputs.....91

4.6.2 General Sensitivity Analysis.....92

4.6.3 Topographic Influence on NPP Modeling.....93

4.6.4 NPP Estimation.....94

4.7 Chapter summary.....95

Chapter 5 CONCLUSION

5.1 Summary of Results.....97

5.2 Conclusion.....97

5.3 Contribution to research.....99

5.4 Future work.....99

REFERENCES CITED.....101

Appendix 1 Climate data from June to August – Kananaskis in 2003.....109

Appendix 2 C codes for climate data extrapolation.....112

LIST OF FIGURES

Figure 2.1 An example of typical spectral reflectance curve 10

Figure 3.1 Study Area - Field plot locations.....30

Figure 3.2 Spectral signatures of white aspen.....32

Figure 3.3 ML classification using original image data.....39

Figure 3.4 ML classification using topographically corrected image data.....40

Figure 3.5 Ratio of precipitation of study site: base station for June.....48

Figure 4.1 AWC (cm) distribution in the study area 63

Figure 4.2 Estimated biomass (T ha^{-1}) using original image data..... .65

Figure 4.3 Estimated biomass (T ha^{-1}) using SCS+C topographically corrected data.....66

Figure 4.4 Estimated LAI using original image data.....67

Figure 4.5 Estimated LAI using SCS+C topographically corrected data.....68

Figure 4.6 NPP changes with forest types.....69

Figure 4.7 Average NPP values of different tree species.....70

Figure 4.8 NPP changes with LAI and time 71

Figure 4.9 Changes of average NPP values with LAI.....71

Figure 4.10 Changes of NPP with solar radiation and time 72

Figure 4.11 Average NPP changes with daily solar radiation 72

Figure 4.12 Changes of NPP with minimum temperature and time.....73

Figure 4.13 Average NPP changes with daily minimum temperature.....73

Figure 4.14 Changes of NPP with maximum temperature and time.....74

Figure 4.15 Average NPP changes with daily maximum temperature.....74

Figure 4.16 Changes of NPP with humidity and time.....75

Figure 4.17 Average NPP changes with daily humidity.....75

Figure 4.18 Changes of NPP with biomass and time.....76

Figure 4.19 Average NPP changes with biomass.....77

Figure 4.20 Average NPP changes with precipitation.....78

Figure 4.21 Average NPP changes with AWC.....78

Figure 4.22 Average NPP changes with precipitation and AWC.....79

Figure 4.23 Topographic influences on all of BEPS inputs 88

Figure 4.24 NPP (kg C m^{-2} for 92 days) distribution in the study area.....90

Figure 4.25 Modeled NPP and biomass for lodgepole pine using topographically corrected data.....93

LIST OF TABLES

Table 3.1 IKONOS spectral band characteristics.....33

Table 3.2 Overall accuracy of maximum likelihood supervised classification 38

Table 3.3 Reference endmember values based on ASD for the dominant species....42

Table 3.4 Empirical equations for estimating biomass by tree species.....42

Table 3.5 Measured average precipitation by climate stations.....49

Table 3.6 All of inputs for BEPS and their measured values in the study areas.....50

Table 3.7 Design matrix for 8-factor, one-eighth fraction factorial experiment.....55

Table 4.1 Statistics of plots by species.....62

Table 4.2 Equations derived from SMA to estimate LAI and biomass.....64

Table 4.3 Change in simulated mean NPP caused by increasing the parameter from the mean minus 1 Stdv to the mean plus 1 Stdv.....80

Table 4.4 Main effects of parameter variation in conifers.....81

Table 4.5 Two- and three-factor interaction effects of parameter variation.....81

Table 4.6 Results of topographic influence on NPP estimation by tree species..... 82

Table 4.7 Topographic influence on NPP estimation by LAI.....83

Table 4.8 Topographic influence on NPP estimation by solar radiation 83

Table 4.9 Topographic influence on NPP estimation by minimum temperature.....84

Table 4.10 Topographic influence on NPP estimation by maximum temperature....85

Table 4.11 Topographic influence on NPP estimation by precipitation.....85

Table 4.12 Topographic influence on NPP estimation by biomass.....86

Table 4.13 Topographic influence on NPP estimation by humidity.....86

Table 4.14 Topographic influence on NPP estimation by all input variables.....87

Table 4.15 Results of NPP estimation for the period from June to August.....89

LIST OF EQUATIONS

Equation 2-1 Gross Primary Productivity.....8

Equation 2-2 Net Primary Productivity.....8

Equation 2-3 Net Ecosystem Productivity.....8

Equation 2-4 Factors affecting reflectance.....10

Equation 2-5 for photochemical reflectance index.....16

Equation 2-6 SMA equation relating component spectra and fractions.....19

Equation 2-7 SMA fraction unity equation.....19

Equation 3-1 Converting DN to top of the atmosphere radiance.....34

Equation 3-2 Converting radiance to surface reflectance.....34

Equation 3-3 Topographic correction using SCS+C.....35

Equation 3-4 Topographic correction: derivation of the C term.....35

Equation 3-5 Wetness index.....44

Equation 3-6 Radiation on a slope.....45

Equation 3-7 Calculation of lapse rate.....46

Equation 3-8 Calculation of temperature.....46

Equation 3-9 Temperature adjustment.....47

Equation 3-10 Calculation of precipitation.....48

Equation 3-11 Calculation of saturated vapor pressure.....49

Equation 3-12 Calculation of daily temperature.....50

Equation 3-13 Calculation of ambient vapor pressure.....50

Equation 3-14 Calculation of relative humidity.....50

Equation 3-15 NPP relative difference.....56

LIST OF ABBREVIATIONS

AWC Available soil water-holding capacity

BEPS Boreal Ecosystem Productivity Simulator

Bio Bimass

BRDF Bi-Directional Reflectance Distribution Function

BRF Bi-directional Reflectance Factor

CASI Compact Airborne Spectrographic Imager

DBH Diameter at Breast Height

DEM Digital Elevation Model

DN Digital Number

EMR Electromagnetic Radiation

f_{PAR} Fraction of Absorbed Photosynthetically Active Radiation

GPP Gross Primary Productivity

GPS Global Positioning System

Hum Humidity

LAI Leaf Area Index

Max Maximum Temperature

MFM Multiple Forward Mode

Min Minimum Temperature

MI Model Inversion

ML Maximum Likelihood

NDVI Normalized Difference Vegetation Index

NEP Net Ecosystem Productivity

NIR Near Infrared

NPP Net Primary Productivity

PPT Precipitation

PRI Photochemical Reflectance Index

Rad Solar Radiation

ROI Region of Interest

RS Simple Ratio

SCS Sun-Canopy-Sensor

SMA Spectral Mixture Analysis

SVI Spectral Vegetation Indices

CHAPTER 1

1.0 Introduction

1.1 Introduction

Carbon is stored in the atmosphere, forests, soils, fossil fuels, and oceans. Atmospheric CO_2 exchanges rapidly with oceans and terrestrial ecosystems (Falkowski et al., 2000). Emissions and re-absorption of carbon (C) from natural ecosystem have been in equilibrium for millions of years. However, this balance has been disturbed by human activities. The increase in atmospheric CO_2 over the last 100 to 200 years is primarily the result of fossil fuel burning and land use changes (Houghton, 1995). These transformations alter the cycling of carbon accumulation and distribution on the land surface. Consequently, the atmospheric concentrations of greenhouse gases, which are mostly the derivatives of carbon, have been increasing rapidly. It is widely believed that higher concentrations of these gases are responsible for global warming (Cao and Woodward, 1998).

Fortunately, research has shown that the carbon needed to balance the CO_2 budget is probably absorbed by land plants and ultimately incorporated in soils or sediments (Houghton, 1995). The processes driving ecosystem carbon fluxes include photosynthesis, plant respiration and soil respiration. Net primary productivity (NPP) is defined as the difference between plant photosynthesis and respiration, and the difference between NPP and soil respiration is defined as net ecosystem productivity (NEP) (Cao and Woodward, 1998). Due to the spatial extent of forest biomes, their

relationships to climate and importance as a carbon store, it is important to understand the function of ecosystem processes. But it is difficult to extrapolate carbon dynamics from regional to global scales. For example, Canadian forests may either be a net source of carbon (Kurz and Apps, 1999) or sink (Chen et al, 2000). According to Houghton (2002), the difference between the net terrestrial sink and the emissions from land-use change, shown as a residual terrestrial sink, is also not well understood globally. Therefore, much effort should be made to study the terrestrial ecosystem carbon cycle.

The influence of environmental variability on forest C balances can be studied directly with field measurements of carbon fluxes. However, because of terrestrial heterogeneity and spatial distribution, temporal gaps in measurement records are inevitable, and spatial data gaps will also exist. Moreover, it is difficult to execute plot level experimental studies for larger environmental changes (Amthor et al., 2001).

It is therefore necessary to use computer models to fill temporal and spatial measurement gaps. Models can also be used to help understand global carbon cycling (Liu et al., 2002), and to conduct retrospective analyses of ecosystem responses to past climatic variability (Cao and Woodward, 1998). Various models have been applied to make spatially comprehensive estimates of NPP for large regions in the world.

Forest ecosystem models describe the processes of photosynthesis and evapotranspiration and may be used to estimate the rates of cycling of carbon (Running et al., 1989). At the same time, many ecological models have been built at spatial and temporal scales, locations, and with different driving inputs and

assumptions. For most models, the central work is the calculation of photosynthetic production. The major driving factor in this calculation is the radiation intercepted by plants.

Generally, there are three types of models according to differences in their radiation conversion, such as maximum productivity (Parton et al., 1993), light-use-efficiency (Moore et al., 1997; Goetz et al., 1996), and big-leaf (Running et al., 1989; Liu et al., 1997, 2002) models. For example, maximum productivity models assume that there is a maximum productivity for a given species as a function ofenvironmental factors. The model ensures this maximum is not exceeded. Light-use-efficiency models are formulated so that productivity is proportional to absorbed radiation, which is modified by a radiation use efficiency coefficient. Big-leaf models are conceptualized to scale photosynthesis rates from leaves to canopies and are useful in relating ground data to spatial image scales, and these have also been extended to regional ecosystems.

Model accuracy must be evaluated before ecosystem models can be applied to a specific location or biome with certain confidence for larger area extrapolation. This can be conducted by comparing model predictions to independent field measurements. For example, a boreal ecosystem productivity simulator (BEPS), which is based on big-leaf models, has been successfully used for mapping NPP in Canada (Liu et al, 1997, 2002). For the application of BEPS in Kananaskis, Alberta, Canada, absolute carbon flux or NPP measurements in the study areas are not available for the model evaluation. Furthermore, mountainous terrain provides an additional challenge for

using this model. Alternatively, to determine the model applicability in this montane environment, we can run the model by varying model input parameters, and the relationship between model accuracy and the extent of parameter changes can be shown. Through those experiments of model sensitivity analysis, we can assess how the model is sensitive to the variability of each of the model inputs and topography.

1.2 Research Objectives

Research is needed to improve our understanding of the interaction of environmental carbon dynamics. A better understanding of the relationship between carbon distribution and the hydrological characteristics of a catchment would improve ecological assessments and management of forests. Also, better forecasting tools are needed to enable ecosystem management, such as managing land cover to support biodiversity, watershed protection, and carbon sequestration studies (Mackay and Band, 1997; Urban, 2000). The sensitivity analysis in this research aims to show the model performance for the input parameter ranges measured in the study area. There are four main objectives for this research:

1. Determine the sensitivity of BEPS to its main input variables, such as LAI, species, and temperature, solar radiation, and precipitation;
2. Determine the most critical inputs of BEPS model;
3. Sensitivity analysis of BEPS to the topographic influence of the study areas;
4. Map LAI, biomass, and NPP in the study area.

1.3 Organization of Thesis

This thesis is organized into five chapters. This introductory chapter has presented the context for the study and outlined the basis and objectives of the research conducted, as well as the structure of the thesis.

Chapter Two consists of a literature review organized into three parts: global warming and forests, processed-based ecosystem models, and BEPS model inputs. In this chapter the issues of global warming are first addressed, and then followed by the important role forests have played in the terrestrial carbon cycling. Following that, as very important tools, remote sensing and ecosystem models are described with a focus on BEPS, including its input variables.

In Chapter Three, the research methods and experimental design are presented. The study area, data sets, measurements for forest spectral signature and structure parameters, and remotely sensed data are described. This is followed by the parameterization for BEPS inputs. The important parts for this chapter are BEPS general testing and its sensitivity to topographic variability.

Chapter Four presents the results of each of the BEPS inputs, the sensitivity analysis of BEPS to its main input variables and topography. This is followed by a discussion and summary of the results.

In Chapter Five, major conclusions from this thesis are presented. First, the results of the analysis are summarized, and conclusions are drawn. Then the contributions to research from this thesis are described. Finally, suggestions for future research are provided.

CHAPTER 2

2.0 Literature Review

2.1 Introduction

This chapter presents a literature review of forest physical parameter retrieval and carbon modelling. Beginning with global warming, this chapter also discusses forest and carbon cycling, the principles used for remote sensing in the forest ecosystem, retrieval of forest biophysical parameters, and carbon cycling simulation using process-based models, with particular detail provided about the process-based model, BEPS.

2.2 Global Warming, Forests, and Remote sensing

2.2.1 Global Warming

Global warming associated with the increase in greenhouse gases has become not only a scientific issue, but a major political issue as well (e.g. Kyoto Protocol). It will probably affect national policies, and including the future energy supply system. The level of atmospheric CO_2 has increased since the industrial revolution as a result of fossil fuel combustion and land use change. However, there is considerable uncertainty regarding the effects that these changes will have on global climate. According to Roberts (1989), an increase of only one degree or two in the average global temperature could mean an increase of between 4^{o} and 6^{o} in the temperate zone. Therefore, global warming may have a larger impact on Canadian forests since

most of them are situated in the temperate zone.

Although the oceans are currently the greatest carbon sinks, terrestrial carbon sinks are also very important, both in terms of their storage capacity and also with regard to resources management. Forests are a significant terrestrial carbon sink, especially in young, growing forests (Houghton, 2002). Meanwhile, forests are estimated to account for more than 75% of the carbon stored in terrestrial ecosystems and approximately 40% of the carbon exchange between the atmosphere and the terrestrial biosphere each year (Hamilton et al., 2002). Global warming has also heightened interest in the possible use of forests as credit towards reducing atmospheric carbon dioxide (e.g. Kyoto Protocol carbon credits) and in understanding how this potential may change as atmospheric CO_2 continues to increase in the future (Kasting, 1998).

2.2.2 Carbon Cycling in Forests

With about 10% of the world's forests, Canada's forestlands certainly play a major role in the balance of global carbon cycling. Plants provide all sources of food for the biosphere on earth through a primary photochemical process called photosynthesis. In the visible portion of the spectrum (400-700nm), plant chlorophyll pigments mainly absorb at blue and red wavelengths with regard to photosynthesis. Plants depend on the chemical energy as organic compounds for their maintenance and growth. The conversion processes from light energy to carbon include photosynthesis, where chloroplasts absorb light energy, and use this to convert

carbon dioxide and water into carbohydrates.

$$6CO_2 + H_2O \xrightarrow{sunlight} 6CH_2O + O_2$$

The conversion of the first products of photosynthesis, sugars, is controlled by many environmental and biological factors, such as biological and environmental influences. The productivity of forests can be described using the following equations (Sabbe et al., 2002):

Gross Primary Productivity (GPP) = f (S, f_{PAR}, F, C) (Equation 2-1)

Net Primary Productivity (NPP) = GPP-R_p (Equation 2-2)

Net Ecosystem Productivity (NEP) = NPP – R_s (Equation 2-3)

Net primary productivity (NPP) is an important component of the terrestrial carbon cycle. It is defined as the new carbon stored in living plants per unit time per unit surface area (Chen et al., 1999), and is the rate at which carbon is taken up by plants minus autotrophic respiratory losses (Equation 2-2). NPP can be broken down into the process of gross primary production (GPP), which is the gross rate of uptake, and plant respiration (R_p). GPP is the gross rate of uptake of carbon by photosynthesis. Using the approach of Kumar and Monteith (1981), GPP is estimated with a function f in Equation 2-1. The daily incoming global solar radiation is S; f_{PAR} is the fraction of incoming photosynthetically active radiation (PAR), which is absorbed by the vegetation. The dependency of GPP on the mean air temperature is represented as F in equation 2-1. The factor C takes into account dry matter conversion efficiency, the

proportion of PAR to global radiation and a CO_2 fertilization factor. Finally, NEP includes soil respiration losses R_s, by heterotrophic decomposition of soil organic matter (Equation 2-3).

2.2.3 Remote Sensing of Forests

Remote sensing from airborne and spaceborne platforms provides a means of mapping forest resources at a range of spatial scales. Local-scale mapping using aerial photography is a well-established technique for determining stocking density, forest cover and forest health over relatively small areas. Satellite remote sensing can be used to map forest resources over large areas, including regional to possibly continental or global scales. The information extracted from remotely sensed data can drive ecosystem-process simulation models which may be used to monitor the carbon production of forests and the rates of exchange of energy and matter with the atmosphere and hydrosphere (Wessman et al., 1998).

2.2.3.1 Principles Used for Remote Sensing in Forests

In remote sensing, the retrieval of forest biophysical parameters depends on the interaction of electromagnetic radiation with the surface and interpretation of the reflected or emitted signal values recorded by the sensor (Lillesand and Kiefer, 1994; Jenson, 1996). A lot of factors influence remotely sensed data. Therefore, , remote sensing signals are a function (f) of the atmosphere (a), location (x), time (t), wavelength (λ) and viewing geometry (θ) of the ground element (Equation 2-4).

$$R = f(a, x, t, \lambda, \theta) \qquad \text{(Equation 2-4)}$$

From this it follows that considerable changes in at least one of the variables of a, x, t, λ, or θ have to occur and cause a detectable change in R before remote sensing can be utilized to provide information about the environment. Most natural objects have characteristic features in the spectral signature that distinguishes them from others and many of these characteristic features occur in relatively narrow wavelength regions. For example, the optical properties of leaves in the PAR region depend on a number of factors, such as conditions of radiation, species, leaf thickness, leaf surface structure, chlorophyll and carotenoid content of leaves, dry matter content per leaf unit area and leaf internal structure. The spectral reflectance of vegetation is normally subdivided into three domains: visible, near infrared and mid infrared regions (Figure 2.1).

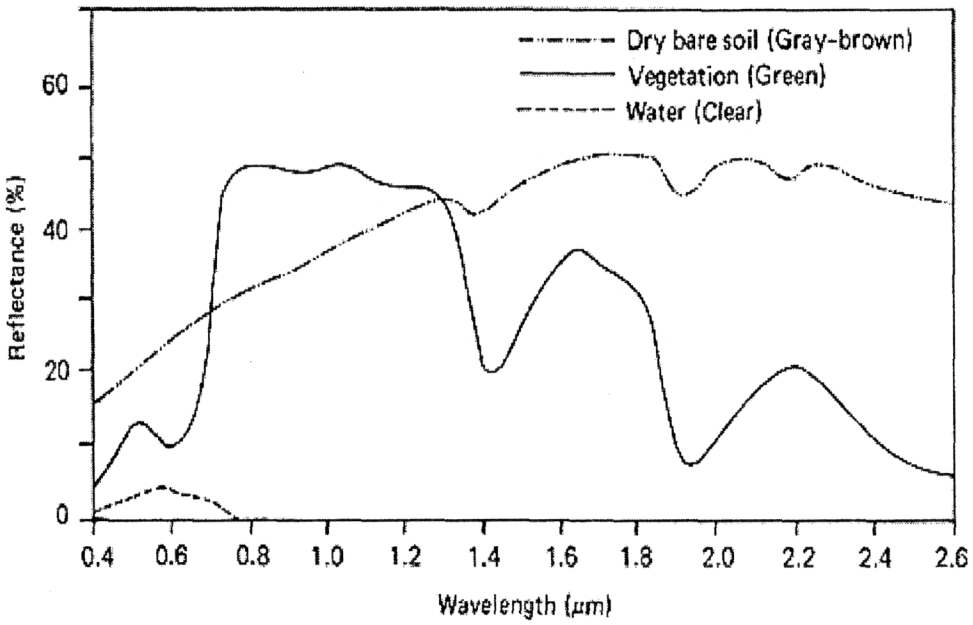

Figure 2.1 An example of typical spectral reflectance curve for vegetation, soil, and water (Lillesand and Kiefer, 1994)

The visible region of the vegetation reflectance spectrum is characterized by

low reflectance and transmittance due to strong absorptions by foliar pigments. In this region, chlorophyll pigments absorb violet-blue and red light for photosynthesis. Relative to absorption of red and blue light, a smaller proportion of green light is absorbed for photosynthesis; hence most plants appear green. The reflectance spectrum of green vegetation shows higher absorption around 420, 490 and 660nm and a visible reflectance peak near 550 nm. Most of these are caused by strong absorptions of chlorophyll. Plants generally have a high reflectance and transmittance in the near-infrared (NIR) region (Figure 2.1). The effects of leaf structure dominate the NIR. Strong water absorptions and minor absorption features of other foliar biochemical contents characterize mid-infrared domain (Figure 2.1). The reflectance in this region is much lower than in the NIR.

In addition to variations in the reflectance of forests as a function of leaf optical properties, the observed reflectance of forests is also affected by the sun-target-sensor geometry. Directional dependence of the surface reflectance on viewing angle is often characterized by comparing the radiance of the actual surface to the radiance of an ideal Lambertian surface illuminated and viewed in the same manner as the surface of interest. The ratio is called a reflectance factor, the surface radiative properties and the direction from which the surface is being viewed.

Vegetation canopies are anisotropic scatters since the distribution of leaves, the amount of leaf material and viewed fraction of leaf material in the direction of the sun and view affect the reflectance. That means they do not reflect radiance equally in all directions. The spectral variability of bi-directional reflectance

distribution function (BRDF) data is related to spectral and structural characteristics of vegetation canopies and allows the derivation of their overall structure from remote sensing data (Sandmeier and Deering, 1999).

Several scientists have ventured into approximating BRDF over canopies, using modelling (Li et al., 1985, 1986, 1992; Chen, 1997; Peddle, 1999). The BRDF is defined as the relation of that part of the total spectral radiance reflected into the direction which originates from the direction of incidence to the total spectral irradiance impinging on a surface from the direction. Therefore, the BRDF is difficult to measure because it is impossible to measure radiances of infinitesimally small solid angles. In practice the BRDF is approximated by the bi-directional reflectance factor (BRF) and normalized to the anisotropy factor (ANIF) for comparison between surfaces (Sandmeier and Deering, 1999).

2.2.3.2 Abstraction of Forest Biophysical Parameters

A number of studies have explored both empirically and theoretically, the relationship between pixel-level reflected, absorbed and transmitted radiation, and associated canopy biophysical characteristics (Hall et al., 1995). In fact, the spectral properties of all vegetation canopies is a function of forest biophysical or structural properties, and information on canopy biophysical properties should therefore be accessible from remotely sensed measurements (Peddle et al., 2002;Asner et al., 1997).

Variables such as LAI and biochemistry affect forest function in terms of light interception and absorption, nutrient cycling and productivity (North, 2002). They vary both spatially and temporally across forest areas and are difficult and expensive to measure. They are, however, the key spatial variables to drive forest ecosystem simulation models at a range of spatial scales. Measuring the growth and distribution of forests using remote sensing data is a central issue in global change research. Some biophysical variables, such as leaf area index (LAI), fraction of absorbed photosynthetically active radiation (f_{PAR}), and biomass are main drivers for ecosystem simulation models (Running and Coughlan, 1988; Liu et al., 1997). Forest managers may require other biophysical variables, such as stand age, average tree height, timber volume for forest management. Ground measurement of those variables is tedious, time consuming, and may be destructive. Therefore, it is difficult to achieve adequate spatial and temporal sampling using ground-based techniques for a reliable and near-continuous monitoring of forested areas. Remotely sensed imagery provides not only information on the amount of foliage and its biochemical properties, but also additional information related to the structure of the canopy. Forest biophysical variables thereby may be estimated over extensive areas.

To retrieve biophysical properties from remotely sensed data, the relationship between the remotely sensed signal and the variables of interest should be established and it often depends on developing techniques to infer this information from remote sensing imagery. Several methods to estimate biophysical variables from reflectance data have been developed. These include spectral vegetation indices (SVI),

model inversion (MI) (Weiss and Baret, 1999), and linear spectral mixture analysis (SMA) (Hall et al, 1995), which has been widely used to compute the abundance or percentages of cover types that make up a ground satellite pixel.

Empirical SVI

Forests absorb more visible solar radiation for photosynthesis and less near-infrared radiation. Reflectance values in the red (R) and near-infrared (NIR) spectral bands, denoted by ρ_r and ρ_n have been used to formulate various vegetation indices (VI) for retrieving vegetation information. The simple ratio (RS), ρ_n/ρ_r, and the normalized difference vegetation index (NDVI), $(\rho_n-\rho_r)/(\rho_{n+}\rho_r)$, are most frequently used to estimate LAI (Chen and Cihlar, 1996).

Empirical relationships can be established between vegetation indices and forest canopy parameters such as LAI, f_{PAR}, leaf nitrogen concentration, and forest biomass. At present, simpler empirical methods, for example the most popular used induces, SR and NDVI, remain widely used because of their simplicity and computational efficiency. But this method is often dependent upon location, time, and vegetation. Moreover, they require extensive field calibration to achieve a reasonable level of accuracy, which limits their quantitative capability for large-scale structure measurements. Additionally, because of the factors such as background effects and multiple scattering in the near infrared, SR or NDVI presents uncertainty. As a result, SVI does not explicitly account for non-vegetation components (e.g. background vegetation, soil, and shadow). NDVI also shows problems of saturation for higher

LAI. Furthermore, vegetation indices typically use only two bands, and therefore do not use the full amount of available information from multispectral and hyperspectral sensors. Also, not all vegetation indices account for non-vegetation components-some, such as SAVI, attempt to compensate for soil background, but other components (e.g. shadow) are not (Qi et al., 1994; Chen and Cihlar, 1996)

In order to improve the accuracy of LAI estimation, there are several other techniques used for estimating forest LAI. First, considering the effects of seasonal greenness change in forest stand floor, NDVI or SR is modified with seasonal background SR or NDVI when spectral indices and LAI empirical equations are derived (Chen, 1996). Additionally, except for removing the noise of raw image data, such as atmospheric and topographic correction (Jenson, 1996), image texture analysis and spectral mixture analysis (SMA) can also be applied for improved estimation of forest stand LAI. Wulder and Franklin (1996) added the texture variables to retrieve LAI and a higher correlation coefficient was found with independent variables of NDVI and texture compared to the use of the NDVI measure alone. Peddle et al.(2001) used the SMA approach in abstracting LAI and the result was better than any vegetation indices.

The estimation of forest LAI by the application of new vegetation indices has been based on either broad wavebands or high spectral resolution data. For instance, Chen et al. (2002) used three bands (R, NIR, and shortwave-infrared) of SPOT VEGETATION imagery to define a new vegetation index (named reduced simple

ratio) and estimate Canadian wide LAI. The results show that the new VI worked better than SR for scenes with mostly mixed pixels.

Hyperspectral resolution data, where measurements of surface radiance are made of many narrow wavebands have also been used to estimate forest LAI. For example, Gong et al. (1992) calculated the first or second derivatives of forest canopy reflectance through Compact Airborne Spectrographic Imager (CASI) data. This calculation may suppress the effects of variation in understory reflectance and allow more accurate estimation of LAI.

At the same time, some new vegetation indices are suggested. One of them is called photochemical reflectance index (PRI), and is used for tracking the physiological adjustments of plants (Stylinski et al., 2002). It is a narrow-waveband index based on reflectance at 531 and 570 nm (Equation 2-5):

$$PRI = \frac{R_{531} - R_{570}}{R_{531} + R_{570}} \qquad \text{(Equation 2-5)}$$

where R refers to reflectance, and the subscript refers to the wavebands in nanometers. PRI was found to track seasonal variations of carotenoid pigments and photosynthetic activity of mature evergreen chaparral shrubs. The results indicated that PRI and carotenoid pigment levels were well correlated with seasonal fluctuations; and by contrast, NDVI did not correlate with net CO_2 uptake. However, PRI as it is currently defined requires narrow band data which are not available with broadband multispectral satellite sensors.

Physically Based Model Inversion

The algorithms for LAI estimation have made much progress through a series of large multidisciplinary experiments such as Oregon Transect Ecosystem (OTTER) and the Boreal Ecosystem and Atmosphere Study (BOREAS) (Peterson et al., 1994; Peddle et al., 2001; Chen et al., 2002). Because empirical methods (using spectral vegetation indices) for biophysical estimation have limitations, many researchers started to resolve this problem by developing physically-based models and describing the interaction of electromagnetic radiation with leaves, branches and canopies of forests (Goel and Strebel, 1983; Li and Strahler, 1985; Chen and Leblanc, 1997). As a result, the algorithms of estimating forest LAI based on empirical methods has extended to the methods of physically-based model inversion. Model inversion is a process in which the model is run in a reverse mode, that is, the inputs to the inversion procedure are the reflectances and the output is a set of the biophysical parameters.

The inversion of these models provides an objective method for estimating biophysical characteristics from remotely sensed data. The process of inversion involves adjusting model parameters until the modeled reflectance best matches the reflectance provided by satellite (Goel and Strebel, 1983; Goel, 1988; Woodcock et al., 1997; Gemmell, 1998; Gemmell et al., 2002). These models can be used to simulate the reflectance of forest canopies by running them in the forward mode where data on the forest canopy variable are the inputs and the spectral signature is output. They have also been used to estimate forest parameters by applying them in

the inverse mode where the spectral signature is the input and estimates of forest biophysical variables are the outputs. Peddle et al. (2004) developed the Multiple-Forward-Mode (MFM) method to retrieve LAI and obtained a satisfactory result, with R^2=0.6 from NDVI compared to R^2=0.82 from MFM.

The MFM model approach works with all inputs and outputs stored in a look-up-table (LUT). According to existing knowledge, users input the specific ranges of forest parameters to the model, run the model with a specific increment step in forward mode, and all of the modeled reflectance for a pixel will be stored in the LUT. Comparing these simulated reflectance data with the pixel reflectance provided by satellite. If a match exists, the forest parameters as inputs corresponding to the pixel reflectance will be the outputs of interest.

SMA

Spectral Mixture Analysis (SMA) is a sub-pixel analysis technique that is designed to derive the fraction of each component contributing to a given pixel reflectance value. To analyze reflectance data from multicomponent surfaces, which is usually the case (e.g. canopy, background, and shadow), particular attention is paid to the effects of shadowing as an interaction between landscape components (Peddle et al., 1999a). An endmember, or component, is the spectral response of pixels having the closest approximation to pure cover types that are found in the image.

SMA relies on the selection of end members that closely represent and maximize the difference between pure surface cover types. Hence, the accurate spectral measurements of endmembers are very important. In most cases, an

endmember spectrum is obtained from field measurements with a spectroradiometer, or is taken from a spectral library. Alternatively, pure pixels can be located on imagery with sufficiently high spatial resolution that has been field-validated (Johnson, 2000).

The general equations that describe SMA are outlined in Equation 2-6 and Equation 2-7:

$$R_b = K_i r_{ib} + \delta_b \qquad \text{(Equation 2-6)}$$

$$K_i = 1.0 \qquad \text{(Equation 2-7)}$$

where R_b is the reflectance of a pixel in band *b*; K_i is the fractional abundance of endmember *i* in a single pixel (from a total of n endmembers); r_{ib} is the reflectance of band *b* of end member *i*; and δ_b is the residual error in band *b* of the model fit.
If the matrix of endmember spectra is provided, then a simple least squares inversion can be used to find the fractional abundance vector for each pixel.

2.3 Process-Based Ecosystem Models

2.3.1 Modelling Review

A model is an intentional simplification of reality, where the phenomena of interest can be examined, analyzed, and understood without additional complexity. While models are useful in science, it is also true that any model involves specific assumptions about how the world works. Computer simulation modelling of the terrestrial carbon cycle is a major focus in global change research efforts. These

models estimate plant productivity either through regression equations of system variables or process-based algorithms. Many models have attempted to simulate carbon, water, and nutrient dynamics at different scales (from stand, river basins to global) for different biomes (e.g. crops, forests, etc.). For this study, only biogeochemical models are described and used for a watershed scale.

There are many types of models generally used to estimate ecological functions, such as statistical models, parameter models, and process models (Liu et al., 1997). The first type derive NPP through regression analysis using the relationship between NPP and meteorological parameters or evapotranspiration or both; the second type uses a number of important parameters to NPP and uses the efficiency concept to model NPP from incident radiation and its absorption coefficient by plant canopies; and the third type simulates biological processes of ecosystems. Process-based models should be more reliable than the other two kinds of models (Liu et al., 1997). These kinds of models are based on our understanding of ecosystems and try to reveal the mechanisms of biomass production and plant-environmental interaction. Process models have the advantages of: 1) being theoretically grounded, 2) the ability to handle interactions and feedbacks of different processes, 3) the flexibility to describe details of biological processes under a variety of conditions, and (4) the verifiability of explicit hypotheses regarding plant physiological processes (Liu et al., 2002). However, the application of models of this type can be hindered by data availability and computing resources. Another challenge is the need for temporal and spatial scaling of a process model, because most process models originated at leaf

or stand levels (Chen et al., 1999). The type of landscape a model is appropriate for is also important.

Process-based models are able to estimate vegetation growth by simulating the processes of carbon assimilation, autotrophic and heterotrophic respiration and decomposition based on inputs such as radiation, temperature, precipitation, and nutrient availability. Numerous process-based plant productivity or carbon models have been developed to study ecosystem responses under different conditions and at different scales, including Century, TEM, BIOME-BGC and BEPS. Amthor et al. (2001) summarized the properties of nine ecosystem process modes including BIOME-BGC and BEPS, used in boreal forests. Among the modelling results of nine process models, the major parameters such as NPP and ET derived from BGC and BEPS were very close. Both of the two models use Farquhar's model (Farquhar et al., 1980) to calculate gross primary productivity (GPP).

The Biome BioGeochemical Cycles model (BIOME-BGC) (Kimball et al., 1997) is a multi-biome generalization of FOREST-BGC (Running and Coughlan, 1988; Running, 1994), originally developed to simulate forest stand development through key processes involved in the carbon, nitrogen, and water cycles. FOREST-BGC represents all essential ecosystem processes with minimal complexity. The main variables include standard meteorological information, soil water content, and leaf area index. It uses several simplifying strategies regarding land cover and meteorological conditions to facilitate application at multiple spatial scales (i.e., from stand to global levels). The model requires daily climate data and the definition of

several key climate, vegetation, and site conditions to estimate fluxes of carbon, nitrogen, and water through ecosystems.

Allometric relationships are used to initialize plant and soil carbon (C) and nitrogen (N) pools based on the leaf pools of these elements. Components of BIOME-BGC have previously undergone testing and validation, including the carbon dynamics. BIOME-BGC predicts photosynthesis, plant growth, maintenance respiration, litter production, decomposition, transpiration and precipitation interception losses, soil water evaporation, snow cover (water equivalent depth), and soil water status. BIOME-BGC as well as its predecessor, FOREST-BGC, has undergone extensive validation of the simulated water and carbon budgets in different North American ecosystems.

2.3.2 BEPS

The Boreal Ecosystem Productivity Simulator (BEPS) (Liu et al., 1997; Chen et al., 1999) is a daily time step process model derived from the FOREST-BGC family of models (Running and Coughlan, 1988) for application at the forest stand to regional scales. The biological principles in FOREST-BGC were adopted for modelling the processes governing carbon and water flows in the soil-plant-atmosphere system and is well documented and tested with measured NPP over various climatic zones (Running, 1994).

BEPS includes an advanced treatment of radiation transport through the canopy, including separation of sunlit and shaded leaf area. Leaf level photosynthesis

is related to remotely sensed leaf area index (LAI) estimates. The treatment of highly clumped canopies is a special feature for boreal coniferous forests. Important inputs for BEPS are LAI, available water-holding capacity of the soil, and daily meteorological variables (short wave radiation, minimum and maximum temperature, humidity, and precipitation). It estimates photosynthesis, plant growth, and maintenance respiration, litter production, decomposition, transpiration and precipitation interception losses, soil water evaporation, and soil water status.

BEPS is based on BIOME-BGC, however, it accounts for the effects of canopy architecture on radiation interception. Chen et al. (1999) found some daily step models like BIOME-BGC to be incapable of simulating the day-to-day variations, when applying these daily models to reliable data sets obtained from the Boreal Ecosystem–Atmosphere Study (BOREAS). The daily outputs were not reliable even though the annual totals can be brought to agreement with experimental data through parameter adjustments. To improve the daily modelling methodology without incurring much additional computation, they developed a new daily model through analytical spatial and temporal integration of canopy photosynthesis processes under some assumptions, as described in the following section.

2.4 Inputs for BEPS

2.4.2 Land Cover

Ecosystem type and ecosystem characteristics are among the basic variables determining the magnitude of the various terrestrial carbon. If the information on the

distribution of land cover types is known, the effect of various ecosystem characteristics can be parameterized in biogeochemical models such as BEPS (Liu et al., 1997, 2002). Over large areas, satellite remote sensing is the only feasible method for obtaining such up-to-date information.

In BEPS, some variables such as canopy conductance, plant respiration, foliage-clumping index etc., are vegetation-type dependent. So it is important to provide land cover maps with high quality. Based on various image-processing methods, land cover maps of study areas can be obtained from: 1) statistical attributes of the images of interest using traditional supervised multi-spectral image classification; 2) the application of an artificial neural network (ANN) to remotely sensed land cover, which has been an important recent development (Foody et al., 1997); 3) using geometric-optical spectral unmixing methods (Peddle, 1999a, b); and 4) using image texture information and knowledge-based methods (Peddle and Franklin, 1991; Peddle, 1995)

2.4.3 Leaf Area Index (LAI)

Leaf area index (LAI) quantifies the amount of foliage area per unit ground surface area. It is, therefore, an important parameter controlling many biological and physical process associated with vegetation, such as photosynthesis, respiration, transpiration, carbon and nutrient cycling, and precipitation (Running et al., 1988; Chen and Cihlar, 1996). Different methods such as spectral mixture analysis (SMA),

vegetation indices (e.g. NDVI, SR), and canopy reflectance model approaches have been used to estimate LAI.

2.4.4 Forest Biomass

Biomass is a critical parameter for determining plant respiration, but currently there are no mature techniques for mapping biomass distribution for large areas (Liu et al., 2002). To estimate biomass, two methods are often used to reduce this data constraint. One is to assign representative biomass values by cover type (Liu et al., 1999). The other method is to relate the total biomass to remotely sensed LAI using vegetation indices (Liu et al., 2002). As an alternative to VI's, SMA and forest canopy modelling can provide more accurate LAI estimation (Peddle et al., 1999a; Peddle and Johnson, 2000; Peddle et al., 2004), or in the case of canopy reflectance models, can be used to derive biomass (Pilger et al., 2003).

2.4.5 Available Soil Water-holding Capacity (AWC)

Available soil water-holding capacity (AWC) is defined as the portion of water in the soil that can readily be extracted by plant roots, or the water held in the root zone between field capacity and wilting point (Liu et al., 1997). Available soil water-holding capacity is an important factor influencing site water balance, which in turn influences photosynthesis rate, carbon allocation, and nutrient cycling (Running et al., 1989). Therefore, AWC needs to be determined for local and regional ecosystem modelling. The most common method to estimate AWC is from soil texture

based on current soil databases . For example, the Soil Landscapes of Canada (SLC) database was used for obtaining AWC for modelling Canadian-wide carbon cycling and water balance (Liu et al., 1997; Liu et al., 2002).

For ecosystem modelling, studies have indicated that a topographic index is an important variable (Band et al., 1993). Compared to the method of estimating AWC from soil series data, the use of topographic data to estimate AWC may provide more information and may be reasonable to assume that topographic data could reflect or represent relative changes over an entire landscape more accurately than soil series data (Zheng et al., 1996).

2.4.6 Climate Inputs to BEPS

Climate factors have been used in numerous modelling efforts. Much of this effort has been directed at global climate change and its effects on plants. When BEPS was applied to the Canadian landmass, meteorological data were obtained from the Median Range Forecast (MRF) Global Flux Archive from the National Center for Environmental Prediction (NCEP), distributed by the National Center for Atmospheric Research (NCAR, Colorado, USA). The data (radiation, temperature, humidity, precipitation and snow pack) were bilaterally interpolated to each pixel at 1 km and daily interval (Liu et al., 1997). For some studies, like this research, study areas are not large and limited climate stations available for the study site; we can extrapolate the climate data to whole study areas using topographic data and other information.

2.5 Chapter Summary

Global warming is a serious challenge to all mankind, and there is an important relationship between vegetation and climate. Remote sensing can link biophysical and structural parameters (e.g. LAI) and function (e.g. photosynthesis) through modelling approaches. Accordingly, remote sensing is the commonly used technique to facilitate an understanding of the role of terrestrial ecosystems in the global carbon cycle. Techniques for retrieving biophysical parameters from remotely sensed images include traditional vegetation indices methods, SMA, and radiative transfer modelling. These parameters have been integrated with other information such as meteorological data, and can be input to different process-based ecosystem simulation model which may be used to monitor forests productivity and the rates of exchanges of energy and matter with the atmosphere and hydrosphere. The modelling results can be applied to guide the practice of sustainable forest development. BEPS, used in this study, is one of the most important of those models which can output NPP and evapotranspiration from local to regional scales. It is, therefore, important to better understand the sensitivity of this model to different inputs to improve our ability to use remotely sensed inputs to BEPS in mountainous terrain. This improved understanding could also result in suggested improvement to future versions of BEPS and possibly an explicit topographic component being integrated to BEPS to make it more broadly applicable to a greater range of terrestrial ecosystems.

CHAPTER 3

3.0 Methods

3.1 Introduction

Beginning with a description of the study site and forest dynamics, field methods and equipment, this chapter describes the methods and experimental design used in the sensitivity test of the BEPS model. For this study, intensive field measurements using four optical LAI estimation instruments (Ceptometer, TRAC, LAI-2000, and hemispherical photograph system) and two kinds of direct ground-based LAI estimation methods (litterfall and allometric technique) on 81 field plots of different species composition were taken during the summers from 2000 to 2004. Basic forest measurement techniques were used to characterize the trees within each plot including: species, diameter at breast height, height, crown diameter, and cores. The crown closure of stands was also measured using a spherical densitometer. These data were used to help estimate stand level LAI and biomass. The preparation for BEPS inputs is then discussed in this chapter, including satellite image pre-processing, classification, spectral mixture analysis, and climate data analysis.

The BEPS carbon model sensitivity analysis is presented in three parts: 1) the general sensitivity of modeled NPP to each of BEPS inputs; 2) the sensitivity of each BEPS input to topographic influence of those mountainous areas; and 3) with corrected inputs, estimating the NPP distribution of the study areas.

3.2 Study Area

The study area is located in the Kananaskis region of Alberta in the Canadian Rocky Mountains and is centered at $115^{0}4'20''$ W, $51^{0}1'13''$N. This ecological zone is characterized by varying soils and forests due to its climatic and topographic diversities. The dominant conifer trees in the area include lodgepole pine (*Pinus contorta* var. *latifolia* Dougl ex. Loud), white spruce (*Picea glauca* (Moench) Voss), and Douglas fir (*Pseudotsuga menziesii* (Mib.) Franco). The dominant deciduous tree species include trembling aspen (*Populus tremloides* Michx.) and balsam poplar (*Populus balsamifera* L.). Typical stands were chosen from the study areas. They are pure stands of lodgepole pine, trembling aspen, white spruce and mixed-wood. The mixed-wood stands refer to any secondary tree species that make up greater than 20% of the overstory canopy (Archibald et al., 1996).

3.3 Data Sets

3.3.1 Field Data Collection

3.3.1.1 Forest Stand Properties

For this study, field data were collected with colleagues and graduate students from Dr. Peddle's lab from early July until late August in 2003 and 2004. A total of 40 20m x 20m field plots were established throughout the study area. In addition, another 41 10m x 10m field plots previously established in 2000 and 2001 were also used as ground truth information. Figure 3.1 shows the locations of ground plots. 76 plots were covered within the study area.

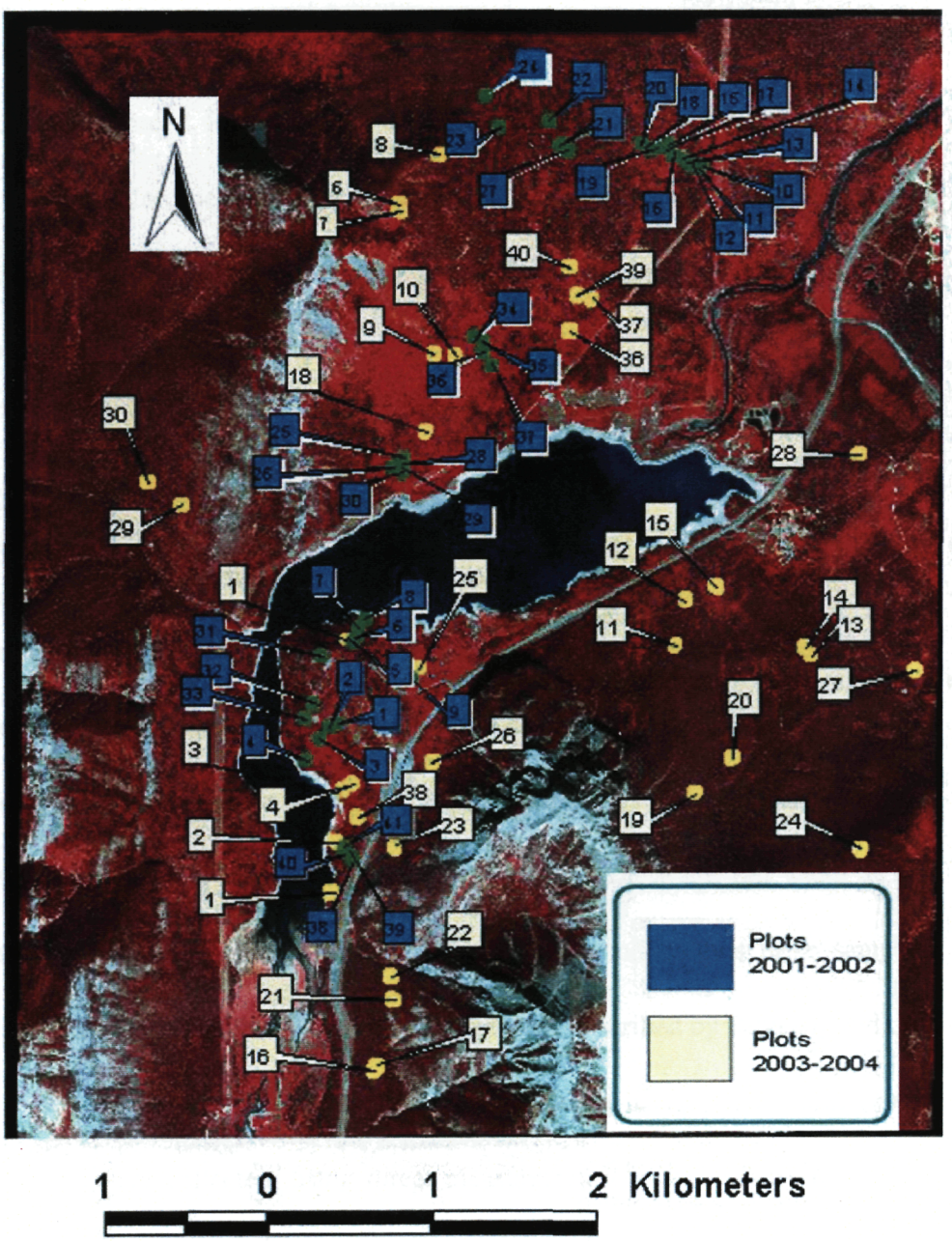

Figure 3.1 Study Area - Field plot locations

Measurements recorded for each plot included diameter at tree breast height (DBH), tree height, height to canopy and crown diameter, geographical coordinates, slope, aspect, tree cores and LAI. Five GPS points, one at plot center and one at each corner, were recorded for each plot. Two tree cores were taken for every species within each plot. In order to describe the plot terrain, a terrain survey was done using standard methods over the plot area. Tree crown closure was recorded with a densiometer.

3.3.1.2 Endmember Spectra Collection

For spectral mixture analysis high quality field spectra are an important requirement. A full range (350-2500 nm) spectroradiometer from Analytical Spectral Devices (ASD) was used to measure the spectral signatures of dominant forest species samples from the Kananaskis study area. Sampling intervals were ~3nm between 350 and 1000 nm and ~10nm between 1000 and 2500nm. These are full width at half maximum spectral resolutions. The ASD interpolates and outputs these sampling intervals to 1nm bandwidths. Using the field methods described by Peddle (1998), the spectra for each end-member component, such as sunlit background, sunlit canopy and shadow, were collected, using direct measurements optically thick stacks, and shadowed targets, respectively.

Ideal weather conditions were necessary for ground spectra capture because slight variation in incident radiation can greatly affect the spectral signature of the targets. When capturing spectra, the device requires calibration against a white

reference panel to convert to reflectance measurements. The panel is used to measure irradiance, which is corrected according to manufacturer provided calibration coefficients. All ASD radiance measurements were then corrected to reflectance using measured coincident irradiance from a calibrated spectralon® panel. As an example, Figure 3.2 shows the spectral signature of white aspen in the study areas.

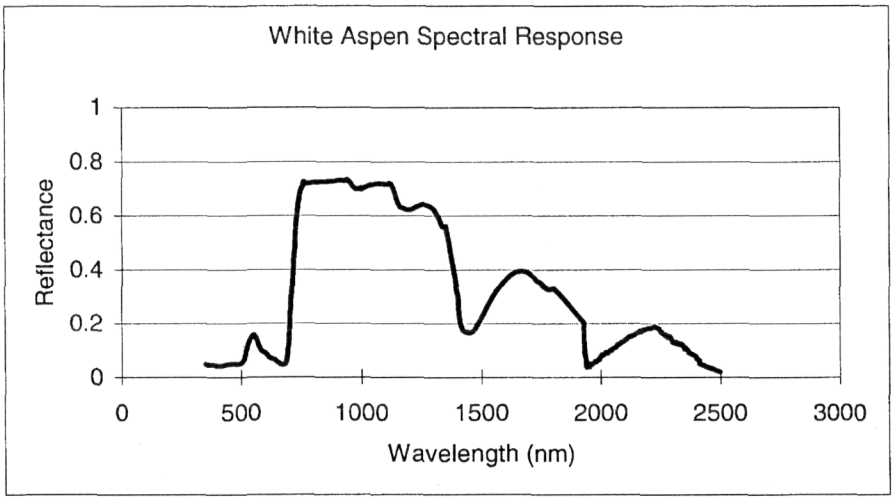

Figure 3.2 Spectral signatures of white aspen.

3.3.1.3 Ground-based LAI measurements

Systems used to measure LAI included the LAI-2000, TRAC, Ceptometer and Hemispherical photo system. In a plot, 9 points were chosen for LAI-2000, Ceptometer and Hemispherical photo system measurements of LAI. Two 30 m transects were used for the TRAC. Transects were perpendicular to the direction of shadow and maintained the same level of elevation. Each transect has 2 readings, back and forth. Because both the TRAC and the Ceptometer require direct solar radiation, the work with them was carried out between 10:30am and 2:30pm. In

contrast, the LAI-2000 and the Hemispherical photo system were used after sunset due to requirement for diffuse radiation.

3.3.2 Remote Sensing Imagery

3.3.2.1 IKONOS Data

Digital multispectral IKONOS satellite data were acquired on August 27th of 2001 at a solar azimuth of 157.21 and a solar zenith angle of 42.57 degrees. Five separate wavelength bands for IKONOS data included four multispectral (MS) bands at four meter spatial resolution and one meter panchromatic data (Table 3.1). For this study, bands MS-2, MS-3, and MS-4 were chosen. MS-1 was not used due to the influence of atmospheric scattering on the blue band.

Table 3.1 IKONOS Spectral Band Characteristics for multispectral and panchromatic bands

Band	Spectral Range (nm)	Bandwidth (nm)	Band Center (nm)	Spatial Resolution
Panchromatic	525.8 - 928.5	403	727.1	1 m
MS-1 (Blue)	444.7 - 516.0	71.3	480.3	4 m
MS-2 (Green)	506.4 - 595.0	88.6	550.7	4 m
MS-3 (Red)	631.9 - 697.7	65.8	664.8	4 m
MS-4 (VNIR)	757.3 - 852.7	95.4	805.0	4 m

3.3.2.2 Image Preprocessing

Preprocessing was required to bring the data to a format suitable for quantitative analysis and, in particular, to enhance direct inter-site comparability. There were four steps involved in the image preprocessing, including radiometric, atmospheric, geometric and topographic correction applied to the data acquired at the

research areas. From a previous study, Pilger (2004) performed radiometric, atmospheric and geometric image correction. Firstly, the calibration of the imagery was done with the post-launch calibration coefficients of IKONOS to convert digital numbers (DN) to top of the atmosphere radiance.

IKONOS Radiance (mW/cm^2-sr):

$$L_\lambda = DN / \text{Calibration coefficient} \qquad \text{(Equation 3-1)}$$

This equation was applied to all of the three IKONOS bands. Converting radiance (mW/cm^2-sr) to surface reflectance (Price, 1987) used the following equation:

$$p_\rho = (\pi * L_\lambda * d^2 / (ESUN_\lambda * \cos(\theta_s)) \qquad \text{(Equation 3-2)}$$

p_ρ= at-satellite exo-atmospheric reflectance (unitless)

L_λ= radiance W $m^{-2}sr^{-1}$ μ m^{-1} (for IKONOS)

d = earth to sun distance in astronomic units

ESUN = Mean solar exo-atmospheric irradiances or solar flux (W m^{-2}) for IKONOS

θ_s= solar zenith angle (which is 90 degrees minus the sun elevation or sun angle)

A simple dark object subtraction technique was used for atmospheric correction. The radiance measured from a dark object in dark cast shadows and dark forest pixels was assumed to have arisen from atmospheric scatter.

With measured GPS points, the image data for the test site were geometrically transformed and registered to a standard local map projection (UTM, NAD 83) to facilitate linkage with the ground data.

3.3.2.3 Topographic Correction

The variation in the surface topography of the study site was considerable.

Consequently, similar forest stand on different slopes and aspects could have dissimilar spectral responses. Topographic correction was required to reduce the effect of topographically induced variations. A variety of approaches exist to correct for topographic effects. Those include the cosine, Minnaert, statistical-empirical, and C corrections (Teillet et al, 1982). Also, Gu and Gillespie (1998) introduced a new method, which tries to normalize the sun-canopy-sensor (SCS) geometry and is more powerful to remove topographic effects than the former methods. Soenen et al. (2003, 2005) introduced a modification to the SCS model to better characterize diffuse irradiance by introducing a semi-empirical moderator (C) to account for diffuse radiation. Results showed that SCS+C provided improved corrections compared to the SCS and the photometric approaches. Accordingly, this method for topographic correction was used in this study. The formulation for this new SCS+C correction is:

$$L_n = L\frac{\cos(\alpha)\cos(\theta)+C}{\cos(i)+C} \qquad \text{(Equation 3-3)}$$

where i is the solar incidence angle, L the uncorrected reflectance, α is the terrain slope, and θ is the solar zenith angle (SZA). The C term is the moderator, which is determined based on Teillet et al. (1982) who proposed the semi-empirical moderator (C) to the cosine correction. Based on an examination of image data, a linear relationship exists between L and cos(i) in the form:

$$L = a + b\cos(i) \qquad \text{(Equation 3-4)}$$

The parameter C is a function of the regression slope (b) and intercept (a):

$$C = \frac{a}{b}$$

3.3.3 Digital Elevation Data

A digital elevation model (DEM) with 25m spatial resolution was provided from the Miistakis Institute for the Rockies. To facilitate the required image preprocessing and climate data extrapolation, the terrain slope and aspect were first derived from the 25m DEM. Next, the 25m resolution data including DEM, slope, and aspect were resampled to 4m using a nearest neighbor resampling algorithm. It is acknowledged that this approach is less than ideal, and that this resampling does not increase the topographic information content to 4m since it was derived at the 25m scale. However, it was decided to tolerate this since the field plots used for this validation (10m, 20m) were smaller than the DEM resolution and further due to DEM and plot registration, the actual field plot would not be expected to align with DEM pixels. Using nearest neighbor, no DEM interpolation was performed.

3.3.4 Climate Data

Climate data for summer 2003 were collected at the Kananaskis climate station. The original data were observed at hourly intervals, and converted into daily average data. Those included solar radiation (kj $m^{-2}day^{-1}$), minimum temperature (^{o}C), maximum temperature (^{o}C), precipitation (mm), and relative humidity (%) (Appendix 1).

3.4 BEPS Model Parameterization

The following describes the parameterization for the BEPS model. The BEPS model directly takes default biophysical and biochemical parameters the FOREST-BGC parameters for the Rocky Mountains. These were held constant in this study (e.g., for conifer, specific leaf area: 25 m^2 kg^{-1} C, maximum stomatal conductance: 1.6 mm sec^{-1}, maximum photosynthetic rate: 5 umol m^{-2} sec^{-1}, leaf maintenance respiration: 0.2 g kg^{-1} day^{-1}, stem maintenance respiration: 0.2 g kg^{-1} day^{-1}, root maintenance respiration: 0.4 g kg^{-1} day^{-1} There are four inputs prepared for running BEPS in this study including land cover, LAI, climate data, and soil water. These four parameters were varied for the BEPS model sensitivity tests.

3.4.1 Tree Species Classification

With the chosen multi-spectral bands, green, red and near infrared, the maximum likelihood (ML) supervised classification algorithm was used to classify land cover at the study site. Initially, ten classes including vegetation and other ground objects were produced with this method. The classes are shown in Figure 3.3 and 3.4, and included several mixed species classes. All of the classification work was executed for both original data and corrected data using the SCS+C topographic correction method. Figure 3.3 and 3.4 show the results of image classification for original data and topographically corrected data, respectively.

Training sets or regions of interest (ROIs) were based on the ground plots. Post-classification work, such as class combination and classification accuracy

estimation was done. The forest classes were combined to three categories, conifer, deciduous species and mixed forest. Table 3.2 shows the overall accuracy of classification for forests using the 76 ground plots as ground truth data. The overall accuracy of classification for forest is 69.4% using original data and 70.6 using SCS correction data, respectively.

Table 3.2 Overall accuracy of maximum likelihood supervised classification

	Conifers (%)	Deciduous trees (%)	Mixed forests (%)	Average (%)
Original data	82.2	59.7	42.6	69.4
SCS correction	83.5	59.5	59.0	70.6

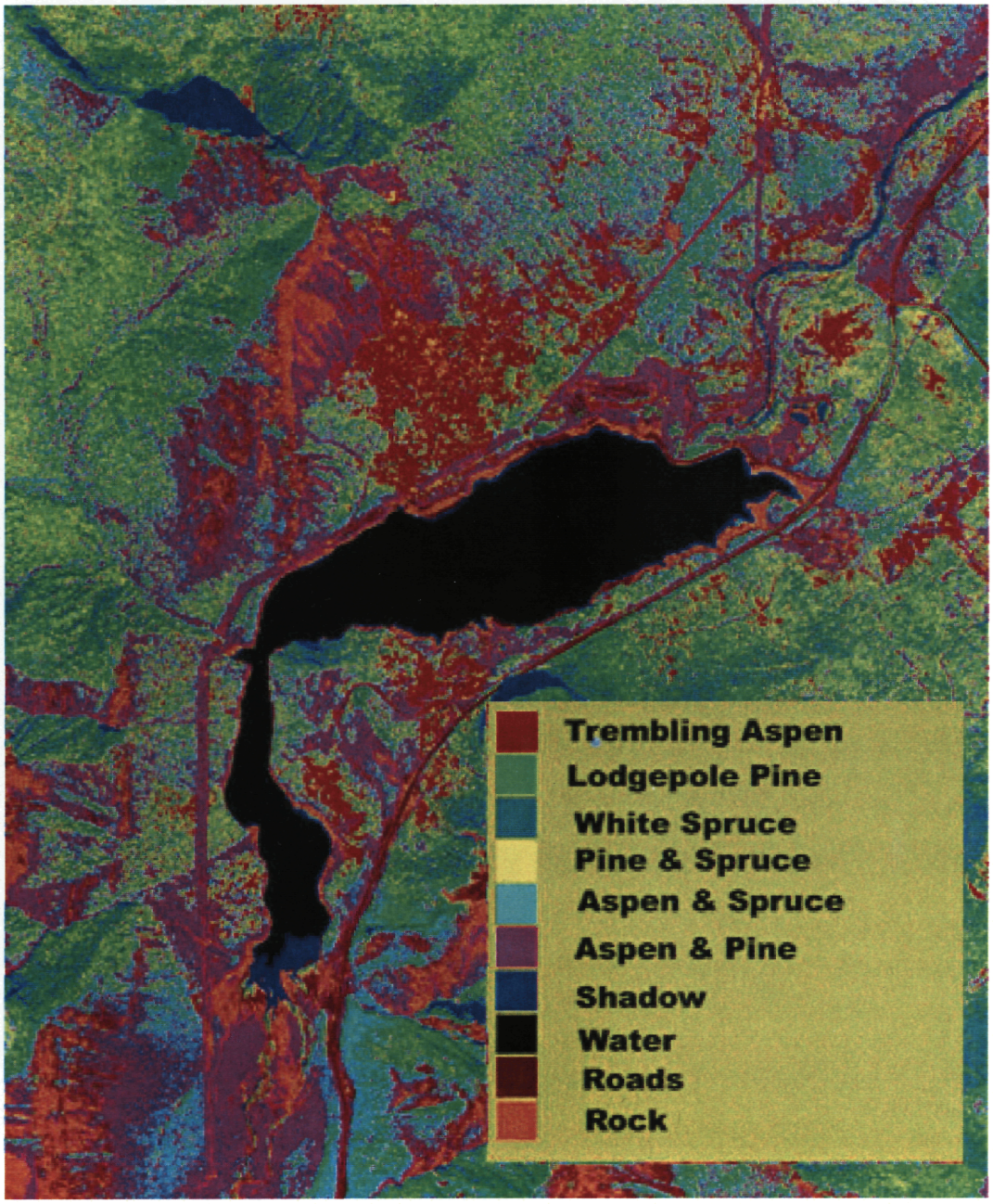

Figure 3.3 ML classification using original image data

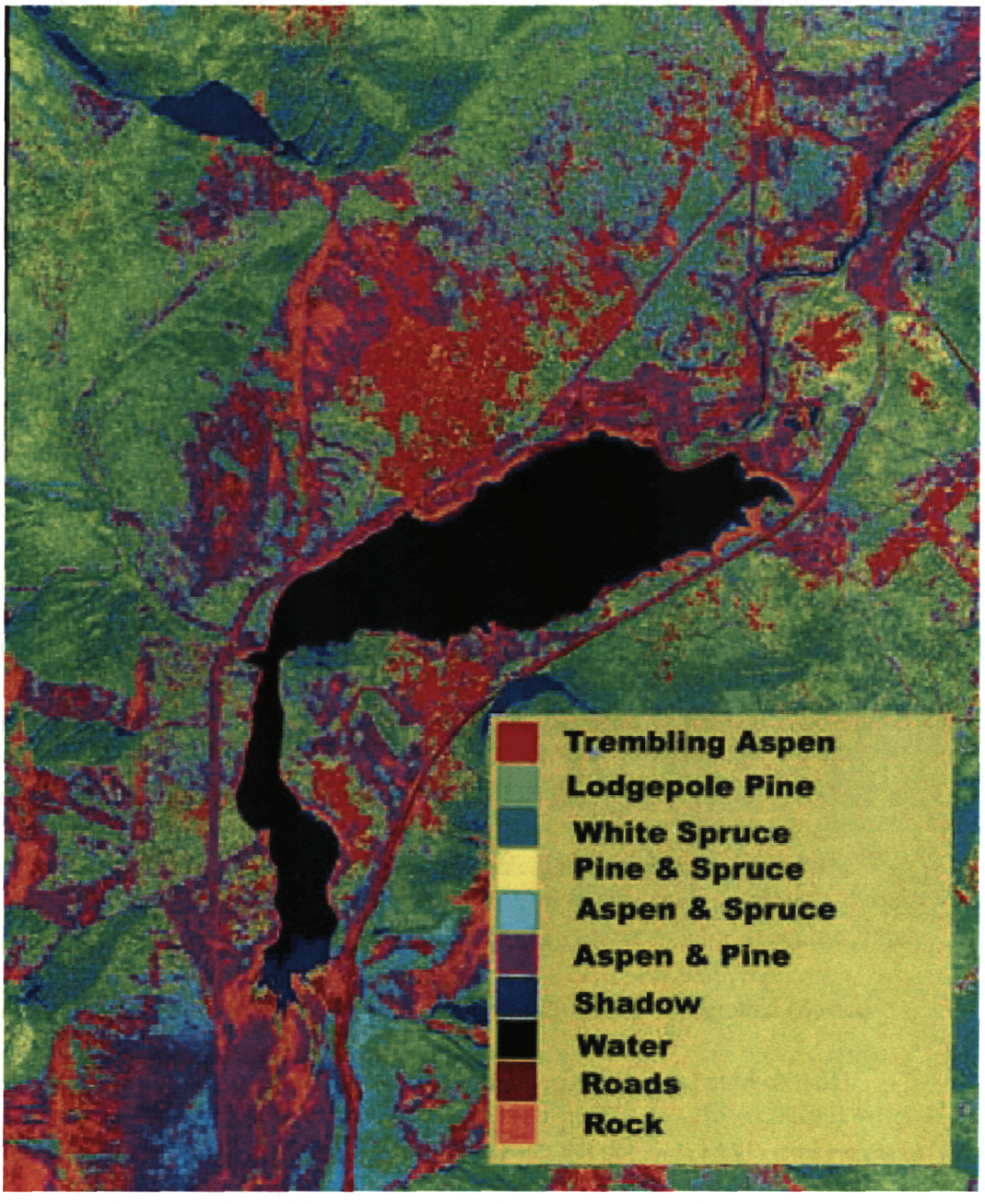

Figure 3.4 ML classification using topographically corrected image data

3.4.2 LAI and Biomass Estimation Using SMA

Leaf area index and biomass (Bio) are important variables in the BEPS model. As mentioned in Chapter 2, there are three main methods used for estimating forest

biophysical parameters: forest canopy model inversion, traditional spectral vegetation indices and Spectral Mixture Analysis (SMA). The forest canopy modelling method is robust and promising for forest parameter retrieval. For example, Peddle (2004) estimated LAI within 0.53 LAI compared with ground-based LAI validation data. Pilger (2004) also used this method to simulate the forest structure parameters. According to Hall et al (1995), SMA extracts information about the forest canopy, forest understory as well as shadow fractions while NDVI provides information solely from mean pixel-level reflectance. Comparing to vegetation indices, SMA is more accurate in estimating biophysical properties of forest biophysical attributes (Peddle et al., 1999; Hall et al 2003) and was readily accessible in this research. As a result, a sub-pixel analysis (SMA) method was chosen for retrieving LAI and biomass in this study.

The overall reflectance of an image pixel is function of the spectral components or endmembers within the pixel image scene. In a forest context, three endmembers are often identified: sunlit canopy (C), sunlit background (B) and shadow (S). Table 3.3 shows the reference endmember values based on ASD measurements of the dominant species for the IKONOS bands (ASD data averaged over each band range). The process for estimating LAI and aboveground biomass involved the following 3 steps.

Table 3.3 Reference endmember values based on ASD measurements of the dominant species.

Trembling Aspen	**IKONOS 2 (%)**	**IKONOS 3 (%)**	**IKONOS 4 (%)**
Sunlit Canopy	12.80	9.44	68.35
Sunlit Background	11.45	8.18	56.23
Shadow	0.61	0.8	5.21
Lodgepole Pine			
Sunlit Canopy	3.85	6.89	36.70
Sunlit Background	11.60	3.88	16.83
Shadow	0.52	0.76	4.47

a) Allometric equations of field-plot data

Usually dry weights (kg) are related to height (cm) or dbh (cm) to derive allometric equations from field plot data for the biomass estimation. For this study, some empirical equations (Table 3.4) were chosen since they were derived from the southwest of Alberta, Rocky Mountain forest areas (Hall, 2004). Based on the number of tree species and stems in each plot, dry biomass per unit area (ton ha^{-1}) was calculated for all plots. Thus, allometric equations were used to determine aboveground dry biomass per unit area.

Table 3.4 Empirical equations for estimating biomass by tree species

Tree Species	Equations
Trembling Aspen	$0.34961+0.01916D^2H$
Lodgepole Pine	$8.24948+0.01597\ D^2H$
White Spruce	$6.09159+0.1499\ D^2H$
Poplar	$10.8106+0.01352\ D^2H$

Note: D, tree diameter at tree breast height; H, tree height.

b) Empirical models of biomass and LAI using IKONOS data and SMA

Empirical models of stand biomass and LAI were developed using IKONOS shadow fraction image of each tree species built with ENVI SMA software. Field plot data of LAI and biomass and corresponding IKONOS shadow fraction data were used in the models. Based on tree species, trembling aspen and lodgepole pine, the statistical relations of stand level shadow fraction data to biomass and LAI were established.

c) Biomass and LAI calculations

The understanding from the models developed using field plot data and IKONOS shadow fraction data were extrapolated to landscape-level mapping using shadow fraction images. This leads to a pixel-by-pixel map depicting discrete levels of dry biomass (ton ha^{-1}), and LAI.

Lodgepole pine is not only a dominant species for conifers, but is a dominant tree species for the whole study area as well. Furthermore, for white spruce and mixed forests there are not enough sampling plots to be statistically used with confidence to estimate the LAI and biomass. As a result, both LAI and biomass estimation for conifers and mixed forests depend on the shadow fraction image for lodgepole pine.

3.4.3 Available Soil Water Capacity

Soil moisture is affected by aspect, slope and elevation. Also, soil moisture is one of the main factors that influence the nature and distribution of plant species. Soil water content has been most commonly described by a compound terrain

attribute, the wetness index (ω) (Band et al., 1993). The calculation of this index is based on the idea of local slope and upslope contributing area affecting the soil moisture status in the calculation unit (Equation 3-5):

$$\varpi = \ln\left(\frac{A_s}{\tan\beta}\right), \quad A_s = \frac{A_T}{\lambda^2} \qquad \text{(Equation 3-5)}$$

where β is slope, λ is the pixel resolution, As is the specific catchment area , and AT is the upslope contributing area. Zheng at el. (1996) used this index to estimate available soil water capacity and it was found that the index related well to mapping waterlogged soils. This technique was used to estimate soil water capacity for the study area. First the wetness index was derived using Geographic Information System (GIS) software. AWC ranges estimated using wetness index were from 0 to 15.3. Then the relationship between wetness index and ground soil series data was established based on the digitized soil map in the study area (Davidson, 2002). As a result, soil water-holding capacity map was produced (Figure 4.1 in Chapter 4). The estimated ranges for AWC is from 0.0 to 28.6 cm. Through a preliminary sensitivity test of NPP to the variation of AWC, NPP did not change when AWC was larger than 10 cm. The estimated AWC was converted from original ranges (0.0, 28.6 cm) into scaled ranges (0, 10 cm).

3.4.4 Climate Variables

Climate information is valuable in understanding the ecology of systems and

indispensable input in BEPS to simulate carbon cycling. This information is unavailable at the landscape scale. Using the measured meteorological data of 2003 at the Kananaskis climate station and topographic information, climate variables extrapolated for each day of the tree growth season from June 1 to August 31 of 2003 were solar radiation (Rad), maximum temperature (T_{max}), minimum temperature (T_{max}), precipitation (PPT), and humidity (Hum). The accuracy of those estimated climate values in the study site were not evaluated due to the lack of measured site data. The extrapolation of climate variables measured from the climate station was performed using C^{++} software (Appendix 2) as described in the following sections.

3.4.4.1 Solar Radiation

Radiation is a measure of the total amount of energy received on a surface for a given area. The amount of solar radiation received at a location influences plant growth and site productivity. In this paper, an algorithm for solar radiation given by Swift (1976) was used to calculate the daily total of potential solar radiation on mountain slopes (R_{corr}) represented by the equation:

$$R_{corr} = R_{slope} / R_{horiz} * R \qquad \text{(Equation 3-6)}$$

where R_{slope} (W m^{-2}) is the potential radiation on a slope, R_{horiz} (W m^{-2}) is the potential radiation on a flat surface, and R is the measured radiation on a flat surface (base station measurement). This method requires an estimate of solar radiation on horizontal surfaces and a ratio, f (slope/flat), to determine how much radiation falls on identically located sloping surfaces. The only inputs necessary for the calculation are

latitude, slope, aspect, Julian date, and the measured solar radiation in the base station.

3.4.4.2 Temperature

If there are a number of climate stations within a study area, temperature data for specific locations is often interpolated for locations without measured data. The interpolated temperature may be further modified by elevation, slope and leaf area index (LAI). Among all of those factors, the lapse rate (cooling with elevation) is estimated by:

$$F(elev)=\frac{T_{high}-T_{low}}{E_{high}-E_{low}} \times 1000 \qquad \text{(Equation 3-7)}$$

where E_{high} is the elevation (in meters) of the highest weather station, E_{low} is the elevation of the lowest weather station, and T_{high} and T_{low} are the corresponding temperature values recorded at those stations. In this thesis, the lapse rate of -6.0 ^{0}C km^{-1} for maximum temperature estimation and -3.0 ^{0}C km^{-1} for minimum temperature estimation were used (Bolstada et al., 1998). With the local lapse rate, the site temperature was estimated using equation:

$$T = T_b + AZ \times F(elev) \qquad \text{(Equation 3-8)}$$

where T is the predicted daily maximum or minimum temperature, T_b is the corresponding daily maximum or minimum base station temperature, AZ is the elevation difference between the base station and study site. The further adjustment for the estimated temperature was carried out based on a similar method used by Running

and Nemani (1987):

$$T_{cell}=T \times f\ (slope/flat) \times f\ (LAI) \qquad \text{(Equation 3-9)}$$

where T_{cell} (^{0}C) is final estimated maximum temperature or minimum temperature of every pixel. The f (slope/flat) is the ratio of slope radiation to flat surface radiation, and f (LAI) (^{0}C LAI^{-1}) is the LAI correction accounting for the effect of dense forests on reducing temperature.

3.4.4.3 Precipitation

On a given mountain slope, precipitation will, in general, increase with elevation (Daly et al., 1994). Reasonable estimates of precipitation could be obtained through interpolation from known points if the number of reference stations and the distribution of those stations was sufficient, e.g., using the PRISM model (Daly et al., 1994). The measured daily precipitation in the base station can be extrapolated according to a ratio of annual precipitation of study site: base station (Running and Nemani, 1987). This ratio map was produced based on the past isohyet maps. However, because those maps were not available in this study area, the surfaces of past precipitation isohyet maps were instead derived using the database from Environment Canada:

(http://www.msc.ec.gc.ca/climate/climate_normals_1990/show_stations_e.cfm?province=AB). Data from 13-climate stations were chosen based on their distance from the center of the study site (Table 3.5). Alternatively, an annual or monthly iosline map of precipitation could be determined by interpolating the climate station data around the study areas.

Further, ratio maps of monthly precipitation of study site: base station were produced. As an example, Figure 3.5 shows the ratio isoline map of June.

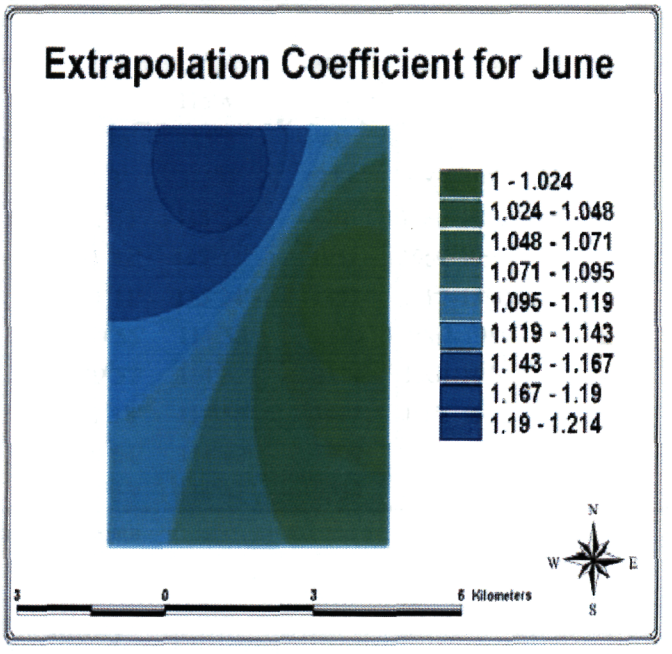

Figure 3.5 Ratio of precipitation of study site: base station for June

Then the pixel-based precipitation was estimated using Equation 3-10 (Running and Nemani, 1987):

$$P_{cell} = P_{cell0} / P_{b0} * P_b \qquad \text{(Equation 3-10)}$$

where P_{cell} is an estimate of pixel-based precipitation, P_{cell0} is the precipitation on the study site from the isohyet maps, P_{b0} is the precipitation on the base station from the isohyet maps, and P_b is the precipitation measured on the base station.

Table 3.5 Measured average precipitation (mm) for June- August by climate stations

Station	latitude	longitude	elevation	data period	June	July	August
Kananaskis	51°2'	115°2'	1391	1939-1990	82	45	67.7
K_Boundary	51°59'	115°7'	1463	1962-1986	92.6	45	N
K_Lo	51°37'	115°4'	2073	1958-1990	86.1	58.1	66.5
Mockingbird	51°26'	115°5'	1905	1962-1990	89.6	96.2	70.4
Pigeon Lo	51°3'	115°4'	1829	1960-1982	103.2	65.4	N
Shining Bank	51°51'	115°58'	829	1968-1980	99.3	103.6	74.8
Bluehill Lo	51°42'	115°13'	1951	1962-1990	100.1	107.2	71
Banff	51°11'	115°34'	1397	1887-1990	60	51.2	51.3
Moose	50°55'	114°50'	2434	1962-1990	75.6	68	65.9
Sugarloaf	49°57'	114°32'	2514	1961-1990	N	42.1	42.2
Ghost	51°18'	114°56'	1417	1958-1990	88.6	91.3	69.3
Elbow	50°54'	114°42'	1400	1958-1990	102.5	66.7	75.7
Junction	50°53'	114°41'	2239	1963-1990	96.6	67.1	77.1

Note: N means no data.

3.4.4.4 Humidity

The method for estimating humidity assumes that daily minimum air temperature is the same as dewpoint, $T_{min}= D_{ew}$ (Running and Nemani, 1987; Thornton et al., 1997). For relative humidity estimates, the Murray (1967) formulation is used. The saturated vapor pressure (Pa) at the average daytime site temperature T_a (^{0}C) is:

$$E_s(T_a)=610.78\exp\left[\frac{17.269T_a}{273.3+T_a}\right] \qquad \text{(Equation 3-11)}$$

where T_a (^{0}C) is the weighted average air temperature of maximum air temperature, T_{max} and minimum air temperature, T_{min}. T_a was estimated by Parton and Logan (1981):

$$T_a = 0.606\, T_{amx} + 0.394\, T_{min} \qquad \text{(Equation 3-12)}$$

Ambient vapor pressure (Pa) at the site minimum temperature T_{dew} is:

$$E_m(T_{dew}) = 610.78 \exp\left[\frac{17.269 T_{dew}}{273.3 + T_{dew}}\right] \qquad \text{(Equation 3-13)}$$

Consequently, the estimated relative humidity is:

$$H = \frac{E_m(T_{dew})}{E_s(T_a)} \times 100 \qquad \text{(Equation 3-14)}$$

3.5 General Sensitivity Test of BEPS in Kananaskis Forests

Because woody biomes have a similar behavior within their forest stands (White et al., 2000), and conifers dominate the forest species composition (>60%) for the whole study area, only conifer species were selected to conduct this sensitivity analysis. Table 3.6 shows all of the inputs of BEPS and their value ranges measured in the study area. The range values were computed over the period from June to August. Using those measured data, the sensitivity of modeled NPP to each input variable was tested.

Table 3.6 All of inputs for BEPS and their measured values in the study area

Variables	Mean	Maximum	Minimum
Land cover (conifer)			
LAI (conifer)	3.2	8.0	0.5
Radiation (KJ m^{-2} day^{-1})	20960	70000	0
T_{max} (0^C)	23.7	33	11
T_{min} (0^C)	5.5	15.7	-3.1
Precipitation (mm day^{-1})	1.5	24.9	0
Humidity (g kg^{-1})	6.8	11.7	2.6
Biomass (T ha^{-1})	141	250	52
AWC (m)	0.15	0.25	0.05

3.5.1 Sensitivity of NPP to the input variables in forest growth season

Typical pixels for a small area were selected to test the effect of varying each parameter by a constant step independently of other parameters. This means that only a single climate input variable or forest site parameter was altered in each sensitivity run. Input parameter changes were prescribed according to the range of variability measured for the Kananaskis lodgepole pine forest (Table 3.6). Although the BEPS model can produce outputs of GPP, NPP, autotrophic respiration, and evapotranspiration (ET), this research only considered NPP since it is the primary information of interest.

For example, the climate data, biomass and available soil water content were held constant while only varying LAI based on the LAI maps produced to query how LAI affects NPP estimation. Each parameter was varied within its measured range of variability. NPP growth from June to August (92 days) was simulated.

3.5.1.1 Tree Species

Forest species are among the most basic variables to determine the carbon pool size as well as energy dynamics within the forests. Typical stands were chosen from the study area. They were pure stands of conifers, deciduous forests and mixed-wood. In the study area, conifers have the largest LAI, and deciduous trees have the smallest LAI.

3.5.1.2 LAI

Leaf area index is a key variable in the process-based ecological model simulation. It is linked to every physiological activity of plants, such as canopy interception, evaporation, transpiration, canopy light attenuation, photosynthesis, and so forth (Running et al., 1989). Davidson (2000) tested the sensitivity of NPP to LAI variation from 1 to 8 with the carbon model FOREST-BGC, and results indicated that NPP was very sensitive to changes in LAI. For this study, to determine the influence of LAI on NPP, LAI was varied from 1 to 16 in steps of 1. Accordingly, the sensitivity of modeled NPP to LAI ranges measured in the study site was assessed. Also, the saturation of LAI for NPP estimation could be derived.

3.5.1.3 Biomass

Because biomass was not directly connected to the estimation of gross primary production (GPP), but was involved in estimating forest respiration in the BEPS model, modeled NPP should decrease as a function of respiration with the increase of forest biomass only if biomass is varied. For this study, the test was conducted using the variation of biomass from 20 to 220 (ton ha^{-1}) in steps of 20.

3.5.1.4 AWC

Water is not only the material necessary for photosynthesis, but it is the product of photosynthesis as well. It is the media to affect the whole process of photosynthesis. Since it is affected by precipitation and soil characteristics, the

influence of precipitation and available water-holding capacity (AWC) on NPP should be tested. The stand level AWC can be estimated through a soil texture map (Crossley, 1952). The sensitivity test was performed using the variation of AWC from 5 to 25 cm. The test ranges of AWC was more narrow than the estimated AWC (0.0, 28.6 cm).

3.5.1.5 Climate variables

Short wave solar radiation is another one of the key variables in BEPS. Because NPP changes more quickly at low radiation, radiation was varied from 3 to 15 (MJ $m^{-2}day^{-1}$) in steps of 3 (MJ $m^{-2}day^{-1}$), and from 15 to 70 (MJ $m^{-2}day^{-1}$) in steps of 11 (MJ $m^{-2}day^{-1}$). Net primary productivity was modeled with minimum temperature varied from –4 ^{0}C to 16 ^{0}C in steps of 2 ^{0}C, and maximum temperature varied from 11 to 33 ^{0}C in steps of 2 ^{0}C, respectively. To test the influence of precipitation (PPT) variation on NPP calculation, the model was run with precipitation varied from 0 to 23 mm day^{-1}. When PPT was less than 3 mm, the variation step was 0.5 mm; otherwise the step was 3 mm. Specific humidity was varied from 1 to 16 (g kg^{-1}) in steps of 1.5.

3.5.2 NPP Independent Variation Sensitivity Analysis

To test the effect of varying each parameter independently of other parameters, the sensitivity analysis was carried out by increasing the parameter from the mean (M) minus a standard deviation (Stdv), producing NPP (NPP.), to the mean plus a standard deviation producing NPP (NPP_+) (White et al., 2000). Among the 9 input variables for

BEPS, tree species is a non-quantitative factor, which cannot be tested by varying the variable throughout a range. Alternatively, to determine the change of NPP with the variation of tree species, the most different species types, conifer and deciduous trees were chosen. Then a change rate was defined as: $(NPP_+-NPP_-)/NPP_+*100$, indicates that how a model input varying from M-Stdv to M+Stdv affects the modeled NPP output. The larger the change rate, the more important the individual input.

3.5.3 Factorial Sensitivity Test

The purpose of the factorial sensitivity analysis was to reduce a large number of variables to a smaller number of factors for modeling purposes and to help create the potential variables modeled. For n-factors in a two level experiment, 2^n experimental runs were required. Fractional factorial analysis can also help to identify important model factors and the potential interactions between two or more factors with less time runs. For example, the half-fraction factorial design of full factorial design with n parameters, 2^{n-1} simulations were done, and simulation time is halved with similar results to the full factorial (Box et al. 1978). However, the disadvantage of this technique lies in information lost and confounding patterns introduced. Table 3.7 shows the design of the one-eighth fraction factorial analysis (Henderson-Sellers and Henderson-Sellers, 1996). There are 8 input variables for BEPS model after removing the non-quantitative variable, tree species. According to the technique introduced by Box et al. (1978), one-eighth factorial analysis (32 time runs) was designed (Table 3.7) and 32 effects could be identified.

Table 3.7 Design matrix for 8-factor, one-eighth fraction factorial experiment for conifers. Column one shows the number of simulation runs, and columns two–nine show the eight parameters set in the simulation. A plus symbol represents that the parameter was set at M+Stdv while a minus symbol indicates M-Stdv. Column ten shows the 92-day mean NPP (g C m^{-2} day^{-1}) from the simulation using high or low level values of input variables.

Runs	LAI	Rad	T_{max}	T_{min}	PPT	Hum	Bio	AWC	NPP
1	-	-	-	-	-	+	-	+	1.19
2	+	-	-	-	-	-	+	-	2
3	-	+	-	-	-	+	+	-	0.99
4	+	+	-	-	-	-	-	+	2.49
5	-	-	+	-	-	+	-	-	1.18
6	+	-	+	-	-	-	+	+	1.81
7	-	+	+	-	-	+	+	+	0.99
8	+	+	+	-	-	-	-	-	2.39
9	-	-	-	+	-	-	-	-	0.94
10	+	-	-	+	-	+	+	+	1.71
11	-	+	-	+	-	-	+	+	0.66
12	+	+	-	+	-	+	-	-	2.39
13	-	-	+	+	-	-	-	+	0.69
14	+	-	+	+	-	+	+	-	1.07
15	-	+	+	+	-	-	+	-	0.39
16	+	+	+	+	-	+	-	+	2.18
17	-	-	-	-	+	+	+	+	0.89
18	+	-	-	-	+	-	-	-	2.3
19	-	+	-	-	+	+	-	-	1.29
20	+	+	-	-	+	-	+	+	2.19
21	-	-	+	-	+	+	+	-	0.82
22	+	-	+	-	+	-	-	+	2.17
23	-	+	+	-	+	+	-	+	1.36
24	+	+	+	-	+	-	+	-	2.26
25	-	-	-	+	+	-	+	-	0.54
26	+	-	-	+	+	+	-	+	2.11
27	-	+	-	+	+	-	-	+	1.06
28	+	+	-	+	+	+	+	-	1.98
29	-	-	+	+	+	-	+	+	0.19
30	+	-	+	+	+	+	-	-	1.66
31	-	+	+	+	+	-	-	-	0.93
32	+	+	+	+	+	+	+	+	1.68

3.6 Sensitivity Analysis of BEPS to Topographic Influences

In addition to the biological and climatic factors, forests are also influenced by topographical variables. For instance, slope, aspect, and elevation can profoundly affect the composition of vegetation. BEPS does not account for this directly, at present. Therefore, the "flat-Earth" approaches adapted by original BEPS model could cause biases when it is applied to mountainous region (Liu et al., 2003). In the following section, the NPP sensitivity analysis to inputs that are not topographically corrected is compared with those that are topographically corrected. This comparison is based on landcover classification. For the whole study area (38.7 km^2), the Julian day 216 was chosen for the test because it was deemed a typical normal day (daily climate data are not extreme). It is noted that the results would not be sensitive to change in this specification. For each of the inputs, the model was run twice using the topographically corrected (SCS+C, Soenen et al., 2005) and uncorrected (original) datasets. The comparison of two-time modeled NPP was conducted with relative difference using equation 3-15:

$$\text{Relative difference}=(NPP_{scs}-NPP_o)/NPP_{scs}*100 \quad \text{(Equation 3-15)}$$

where NPP_{scs} is modeled NPP using SCS+C topographically corrected data; and NPP_o is modeled NPP using the original, uncorrected data. SCS+C was chosen since it is a recent approach shown to be superior both theoretically and empirically to a wide variety of other topographic corrections tested for this Kananaskis study area (Soenen et al., 2005).

3.6.1 Tree Species

Using the topographically corrected inputs, the BEPS model was run twice with corrected and uncorrected classification images, respectively. As mentioned above, there were two kinds of classified images, which were based on original 3 bands or those topographically corrected data. The imagery was classified to 11 classes and forest classes were combined to conifer, deciduous and mixed forests. The overall classification accuracy was 69.4 for original image data and 70.6 for topographically corrected imagery. From this experiment, we can find what is the influence of tree species on NPP estimation before and after topographic correction.

3.6.2 LAI

Based on the SMA method, a fraction of spectral mixture analysis was produced. Further LAI was then mapped with shadow fraction image by tree species. BEPS model was run twice using the topographically corrected inputs and topographically corrected LAI or uncorrected LAI. That is, the SMA used topographically corrected and uncorrected image data to derive shadow fractions that were then used to predict LAI. Accordingly, we can compare those two results from different LAI, and evaluate how topography influences on LAI estimation.

3.6.3 Biomass

The procedures used for testing the influences on biomass estimation are similar to that for the LAI test. The SMA method used topographically corrected and

uncorrected image data to derive shadow fractions. A separate regression equation of SMA shadow fraction with biomass measured in the fields was established and then the biomass in the study area was estimated. Using the topographically corrected and uncorrected biomass as inputs for BEPS model, the model was run twice. Accordingly, the two sets of results can be compared as a relative difference between them using corrected biomass and uncorrected biomass data.

3.6.4 Climate Input Variables

All five climate inputs (solar radiation, precipitation, maximum temperature, minimum temperature, and humidity) are dependent on the topographic data when extrapolated from the base climate station. Therefore, topographic sensitivity analysis to those variables is very important for this complex terrain study site. For a given test, one of those climate inputs was kept constant when the model was running. This means that the constant input is not topographically corrected. The model needs to be run twice for every variable sensitivity analysis to allow for the comparison. The first model run used all of the topographically corrected inputs, and the second model run used topographically corrected inputs except one variable that was not topographically corrected. After these two model runs, the amount of the modeled NPP for each run is compared. As a result, the influence of topography on a specific BEPS input can be given by the difference of the comparison.

3.7 Application of BEPS to the Study Area—Carbon Estimation

Following the set of comparison described above, the BEPS model was run using all of the topographically corrected inputs to produce NPP estimates for conifers, deciduous trees and mixed wood in the growing season (June to August). The distribution of carbon stocks as NPP in the study areas was then mapped from these results.

3.8 Chapter Summary

In this chapter, the methodologies used for this research included the preparation of BEPS inputs, the sensitivity of modeled NPP to each of those input variables, and the sensitivity of modeled NPP to the variation of topography. Two datasets, topographically corrected and uncorrected, were prepared to test the sensitivity of modeled NPP to each of its input variables and how each was affected by topography. After topographic correction of the IKONOS remote sensing data, much effort was made to parameterize the BEPS inputs. To reflect the variation of soil water, a wetness index was derived to estimate available soil water capacity using a GIS method. Based on endmember spectra taken from the field, linear spectral mixture analysis was conducted for the LAI and biomass estimates. All of the climate data measured at a weather station were extrapolated with a DEM and other auxiliary information.

Following the completion of parameterization for BEPS run, a sensitivity analysis was conducted. The sensitivity analysis was designed to test how the

modeled NPP was sensitive to the variation of each BEPS input. The results of factor analysis are designed to help find which are the most important inputs for the BEPS model, and the interaction effects of the input variables. For this mountainous area, the sensitivity of BEPS to topographic influence is indispensable to know before the BEPS is applied. Therefore, the effect of topography to each of BEPS inputs was tested through modeled NPP. After the sensitivity analysis, the NPP distribution of the study areas was mapped using topographically corrected inputs to derive carbon maps.

CHAPTER 4

4.0 Results and Discussion

4.1 Introduction

The results presented here are divided into three sections. The first section presents the results of the ground measurements and BEPS inputs estimated by means of the modelling approaches described in Chapter 3. The second section shows the results of general sensitivity test of BEPS NPP outputs to the variability of the BEPS model inputs. The third section shows the influence of topography on the NPP estimation by each of the model inputs, and the last section describes the estimation of forest NPP growth during the summer of 2003.

4.2 Field Results and BEPS Inputs

4.2.1 Field Measurement Results

The field forest structure data collected during summer 2003-2004 at Kananaskis is summarized in Table 4.1. All of the stand plots from 2001 to 2004 were randomly chosen. The apparent difference of estimated biomass using the data collected during 2001-2002 (Pilger, 2004) and the data collected during 2003-2004 was found, so only the field forest stand data taken during the summer of 2003-2004 was used for this study since these data were collected during this research and were well known and documented. In total, there were 35 plots within the study area used

for LAI and biomass estimation. Four forest types: trembling aspen, lodgepole pine, mixed wood, and white spruce were categorized. The mixed wood category includes a mixture of coniferous and deciduous trees. However, there were just two mixed wood plots. The following comparison, including average DBH (cm), tree height (m), stem density (stems ha-1) and biomass (T ha-1), was carried out among trembling aspen, lodgepole pine, and white spruce. According to the statistical results in Table 4.1, white spruce had the highest biomass and trembling aspen had the lowest stem densities compared to other species present. Lodgepole pine had the largest tree height and stem densities, but it had the smallest DBH value. Trembling aspen had the largest standard deviation for both tree height and DBH among the three kinds of forest stands due, in part, to the tree composition of different age classes.

Table 4.1 Statistics of plots by species from plot data collected in 2003-2004

	Trembling aspen	Lodgepole pine	Mixedwood	White spruce
No. of plots	14	13	2	6
Mean DBH (cm)	20	16.2	24.2	21.8
Min. DBH (cm)	14.7	12.8	19.8	13.4
Max. DBH (cm)	24	22.6	31.8	31.8
StdDev. DBH (cm)	3.5	1.8	6.6	2.9
Mean tree height (m)	14.2	15.2	16	14.9
Min. (m)	9.8	10.0	14.5	8.5
Max. (m)	18.0	18.4	17.9	20.3
StdDev.(m)	2.7	1.7	1.7	0.9
Mean density (stems ha^{-1})	1218	1794	1525	1150
Min.(stems ha^{-1})	725	1200	750	750
Max.(stems ha^{-1})	1825	3025	1650	1675
StdDev.(stems ha^{-1})	315.9	710.6	368.3	512.7
Mean biomass (T ha^{-1})	136.7	140.4	185	178.6
Min. (T ha^{-1})	51.9	58.0	N	109.2
Max. (T ha^{-1})	230.5	196.8	N	198.4
StdDev. (T ha^{-1})	45.5	34.4	N	34.2

Note: N means that no statistics were done due to the lack of enough ground plots.

4.2.2 BEPS Inputs

Daily-based landscape climate data were produced by extrapolating the weather station data measured in 2003. Available soil water capacity (AWC) (cm) was estimated with respect to the derived wetness index (Figure 4.1).

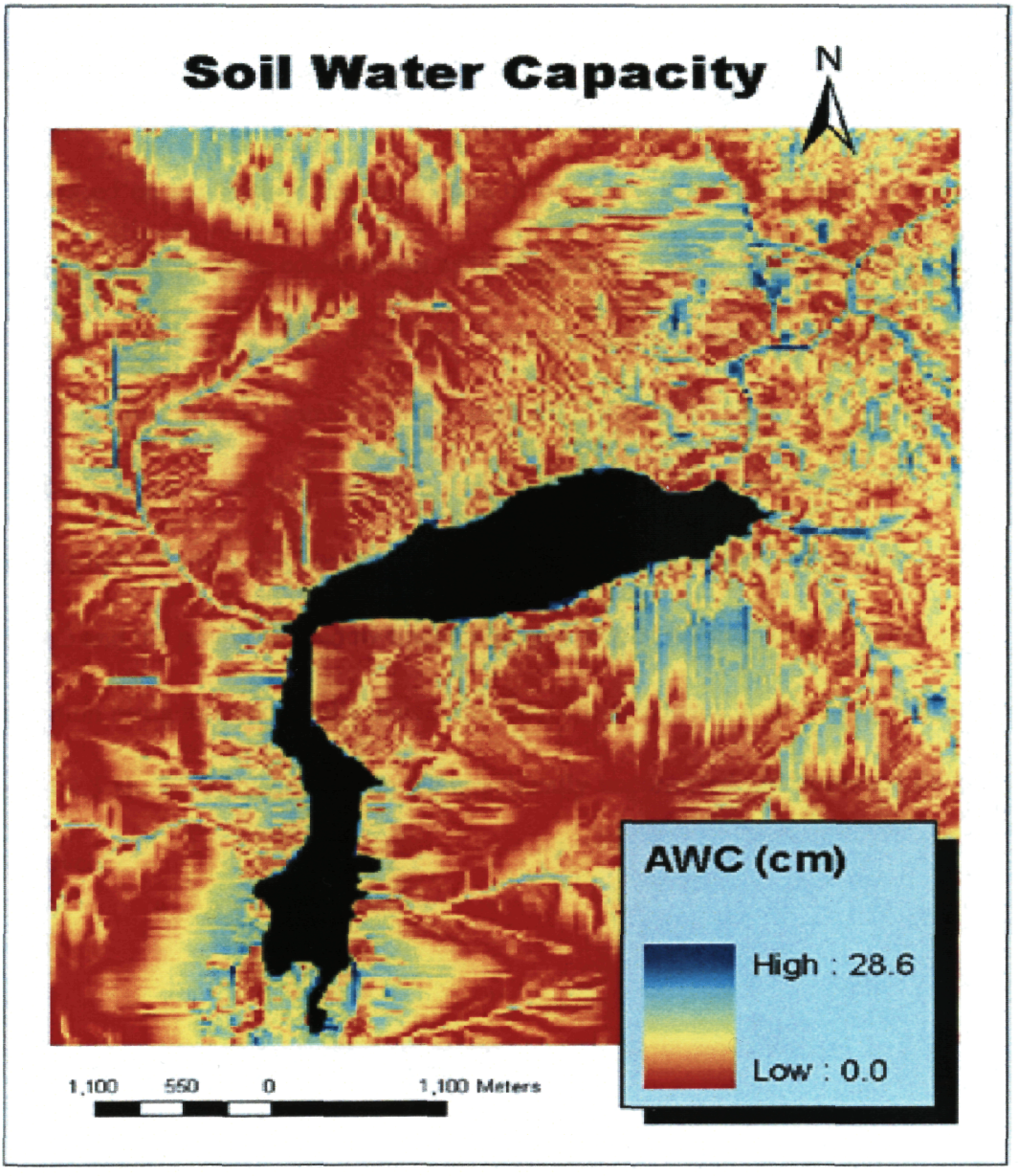

Figure 4.1 AWC (cm) distribution in the study area

Table 4.2 Equations derived from SMA to estimate LAI and biomass for aspen and pine

Species / Data	Trembling aspen	R^2/P	Lodgepole pine	R^2/P
Original	$LAI = 3.8991F^{0.8693}$	0.4943/ 0.005	$LAI = -204.5\ F^2 + 138.38\ F - 20.596$	0.6678/ 0.007
	$Biomass = 1717.5\ F^2 - 616.03\ F + 155.28$	0.5692/ 0.01	$Biomass = 3260.1\ F^2 - 3073.5\ F + 828.95$	0.6233/ 0.008
SCS+C	$LAI = 4.4032F^{1.0499}$	0.4727/ 0.007	$LAI = -262.08\ F^2 + 216.32\ F - 41.801$	0.7137/ 0.004
	$Biomass = 2040.2\ F^2 - 879.1\ F + 194.79$	0.5664/ 0.01	$Biomass = 4028.3\ F^2 - 4277.5\ F + 1241.1$	0.5951/ 0.011

Note: F, shadow fraction; R, regression coefficient; P, level of statistical significance.

Based on the shadow fraction images of trembling aspen and lodgepole pine using SMA, the regression equations for estimating stand level LAI and biomass were established (Table 4.2). Two data sets, original satellite image (original), and topographically corrected satellite image data (SCS+C) were used. There was no distinct improvement for the estimation accuracy of LAI and biomass when SCS+C data were used. Further, LAI and biomass were mapped with the derived equations in Table 4.2 and the produced shadow fraction images. Figure 4.2 and 4.3 show biomass distribution using topographically uncorrected and corrected data, respectively. Figure 4.4 and 4.5 show LAI derived from topographically uncorrected and corrected data, respectively.

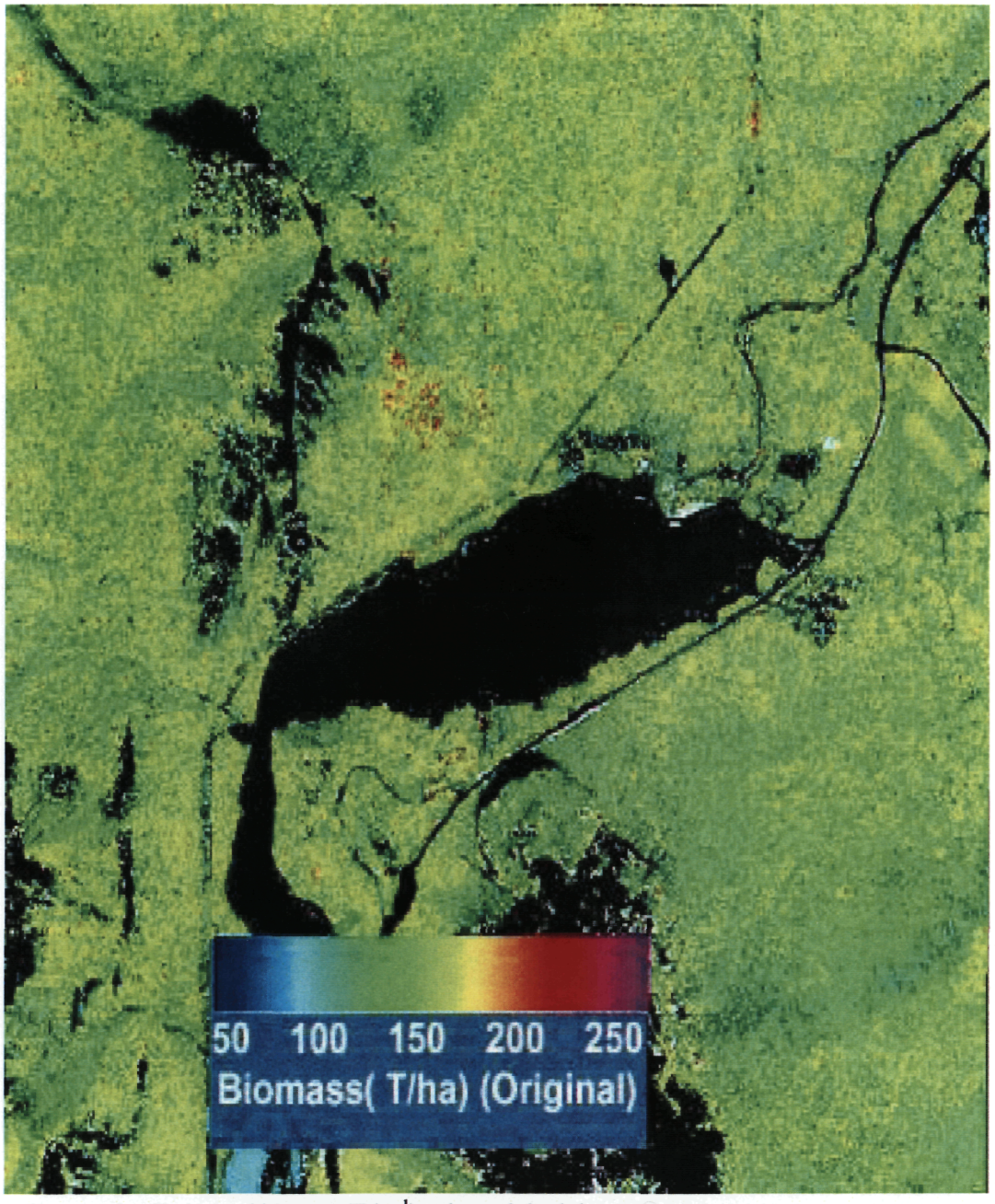

Figure 4.2 Estimated biomass(T ha^{-1}) using original data

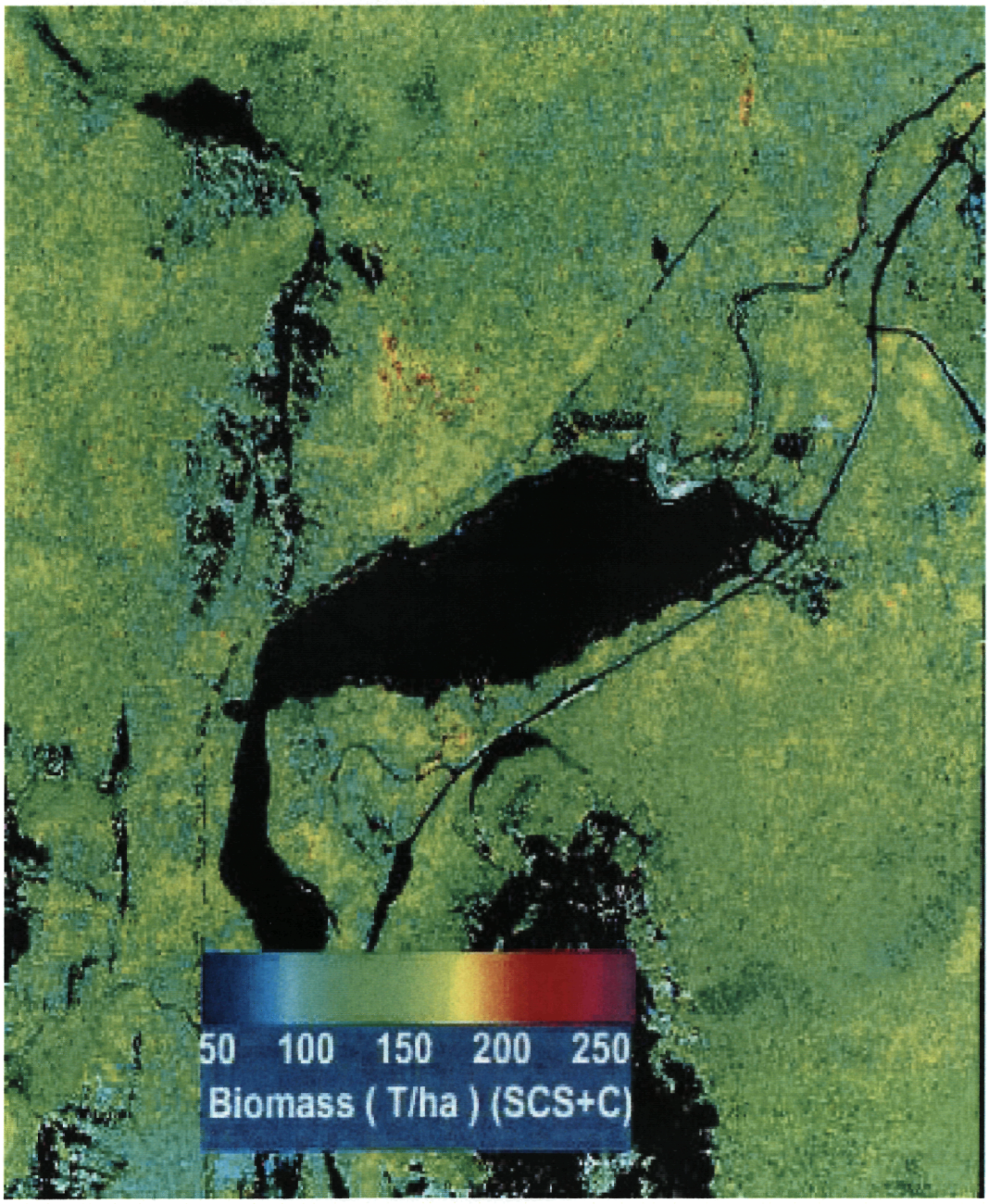

Figure 4.3 Estimated biomass(T ha^{-1}) using SCS+C data

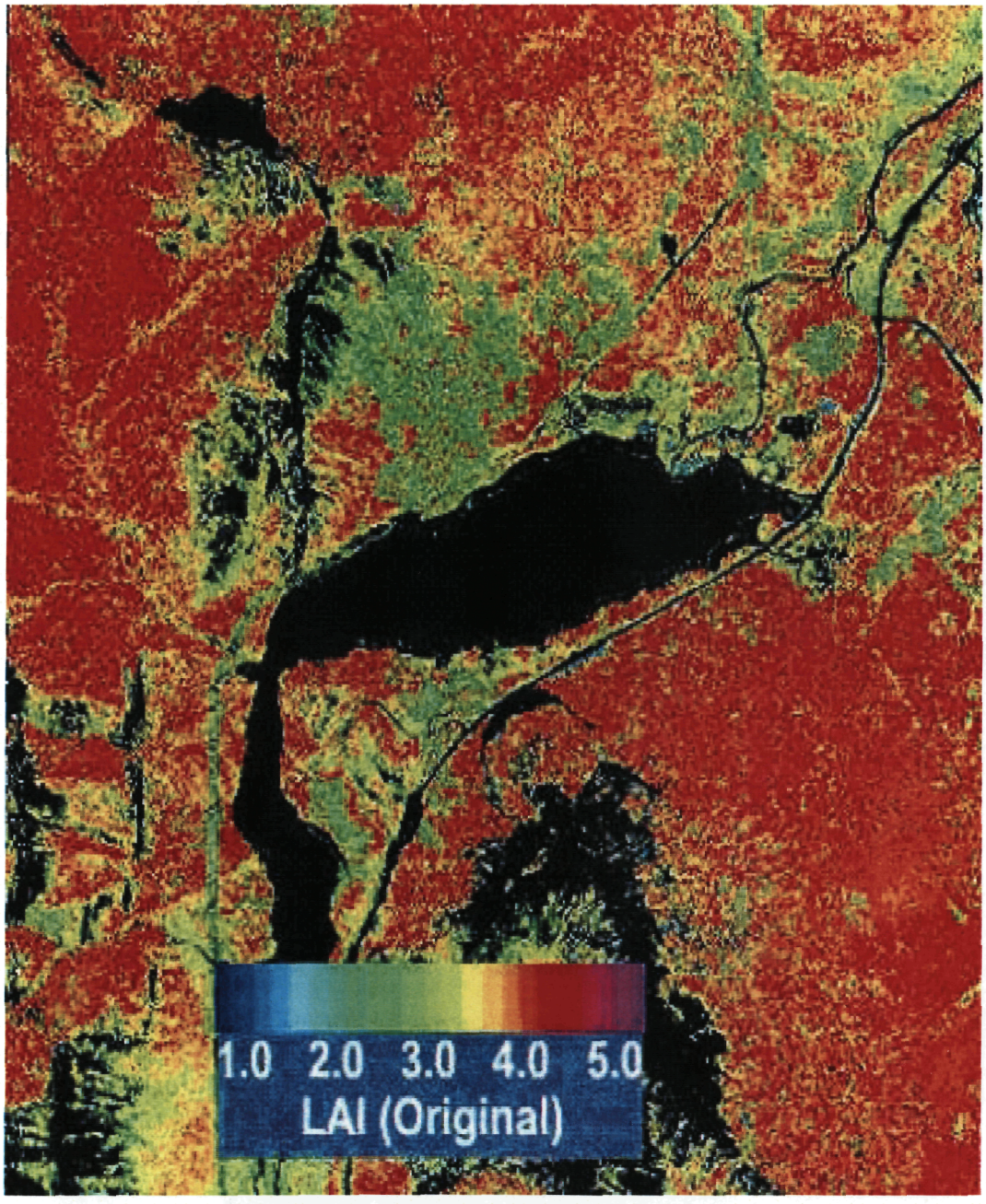

Figure 4.4 Estimated LAI using original data

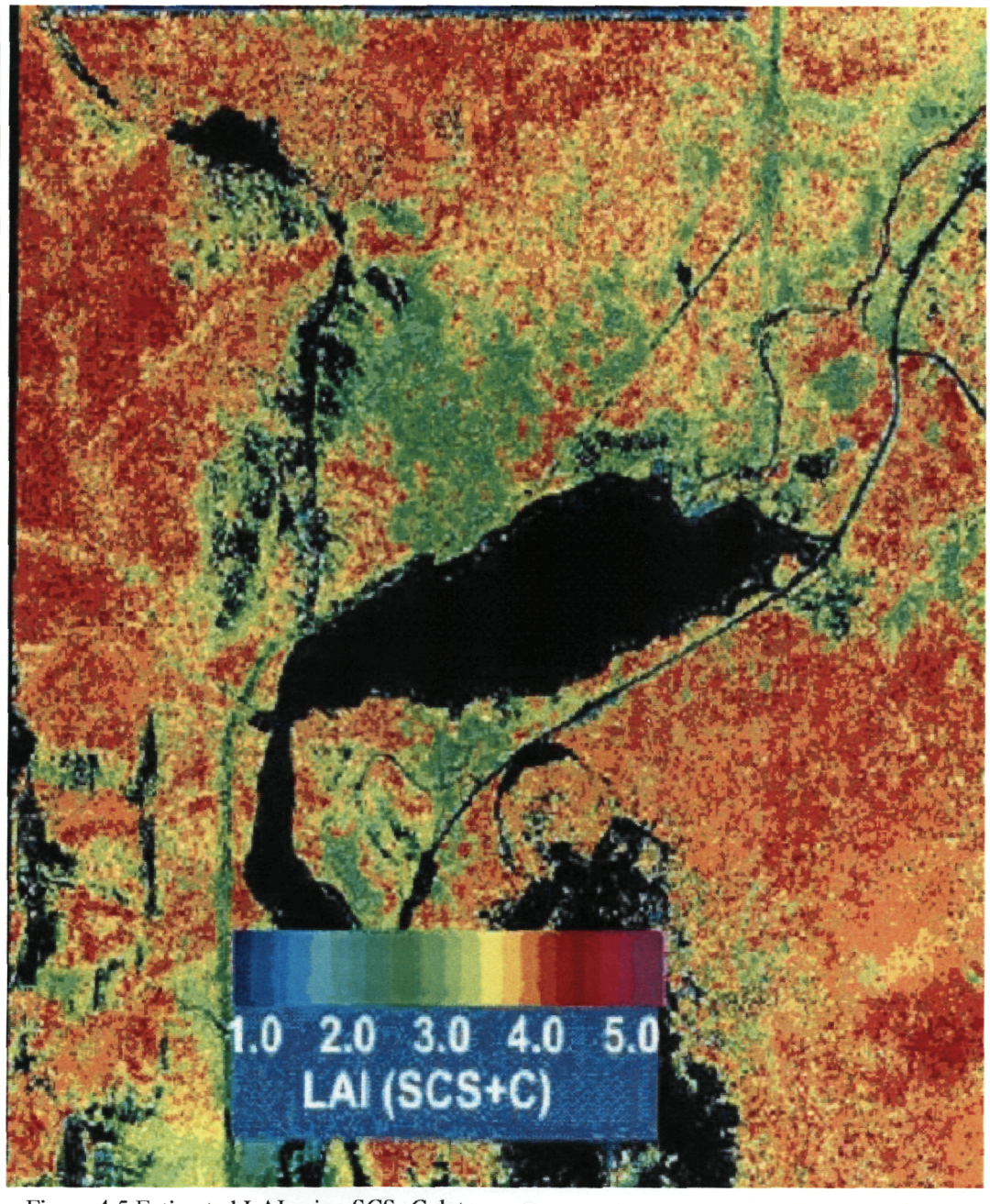

Figure 4.5 Estimated LAI using SCS+C data

4.3 Results of General Sensitivity For BEPS

4.3.1 Modeled NPP for Each of the Model Inputs

4.3.1.1 Tree Species

Figure 4.6 describes the changes of NPP values of different forest stands from June to August, and Figure 4.7 shows the average NPP values of different tree species. For coniferous, deciduous and mixed forests, average NPP from June to August were 1.4, 3.2, and 2.8 g C m^{-2} day^{-1}, respectively. Deciduous forests had the largest amount of modeled NPP value compared with coniferous and mixed forests.

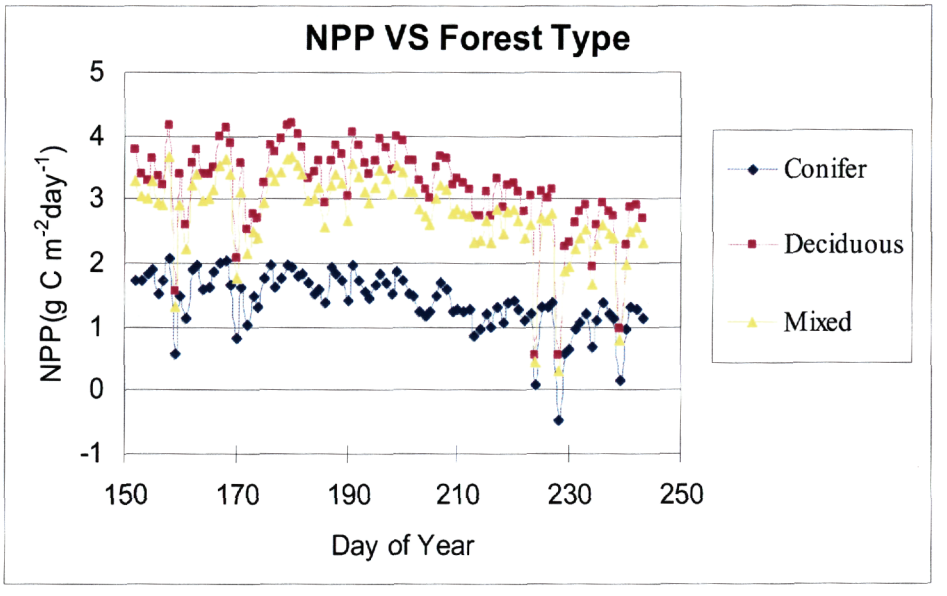

Figure 4.6 NPP changes with forest types

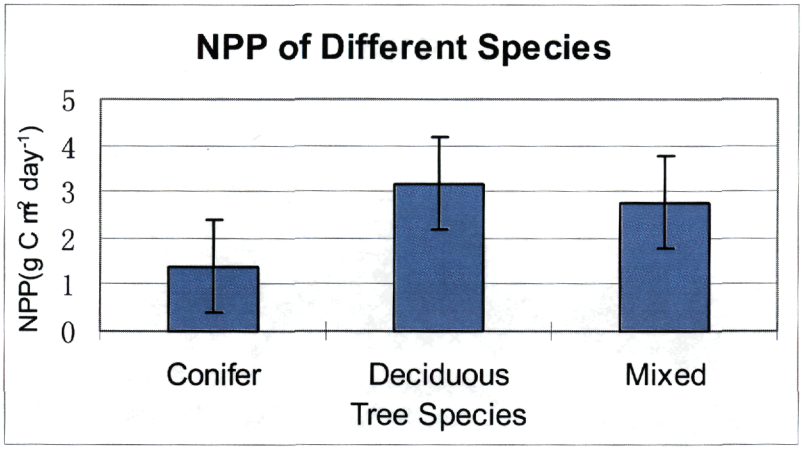

Figure 4.7 Average NPP values of different forest types

4.3.1.2 LAI

According to the modeled results shown in Figures 4.8 and 4.9, NPP was very sensitive to LAI. At the beginning, the rate of change of NPP varied with LAI increase. For example, within an LAI range of 1 to 8, NPP had an almost positive linear relationship with LAI (Figure 4.9). However, as the LAI increased further, NPP began to be saturated. For LAI>12, the change rate of NPP became very slow, and modeled NPP saturation was reached.

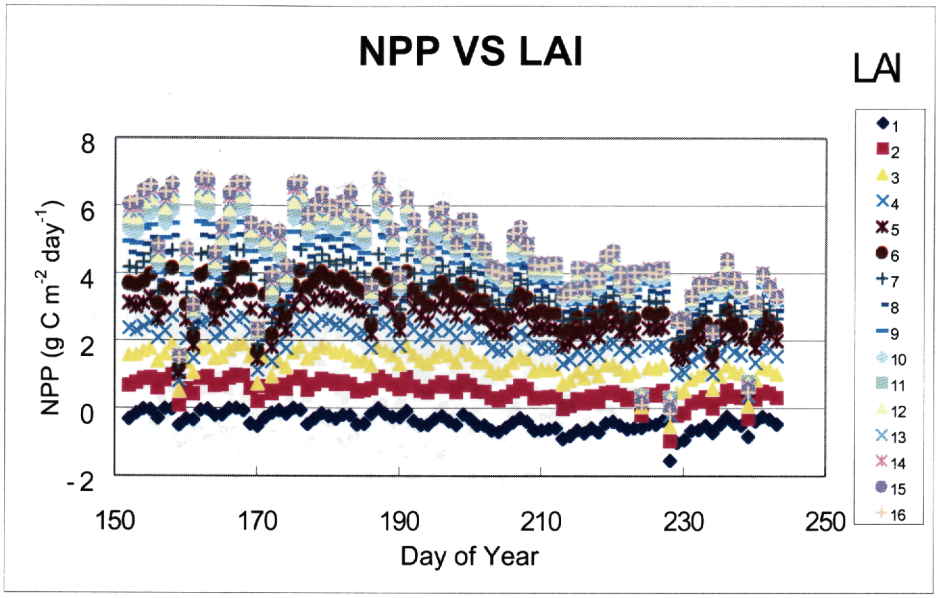

Figure 4.8 NPP changes with LAI and time

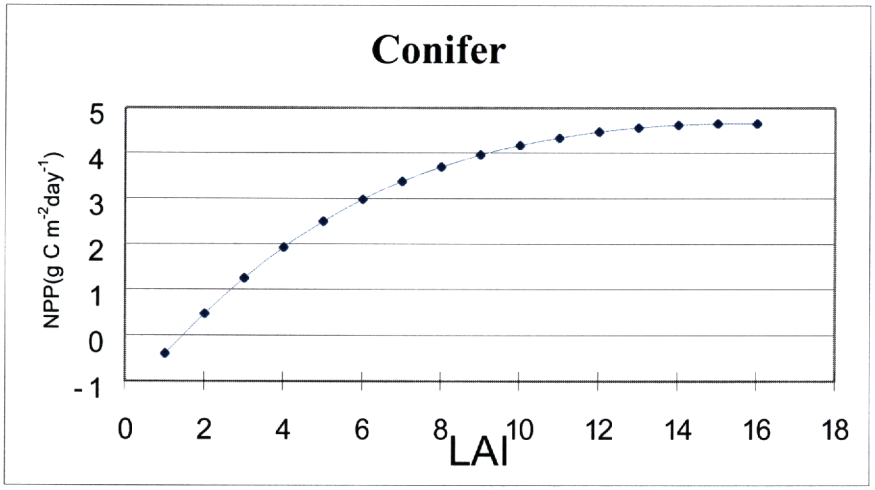

Figure 4.9 Changes of average NPP values with LAI

4.3.1.3 Solar Radiation

Figure 4.10 and Figure 4.11 show that NPP was very sensitive to the variation of solar radiation, especially when the radiation was less than 26 MJ $m^{-2}day^{-1}$. However, radiation was saturating when greater than 26 MJ $m^{-2}day^{-1}$, which largely

happened in June and July. This means that the NPP estimation could have unpredictable errors in these two months.

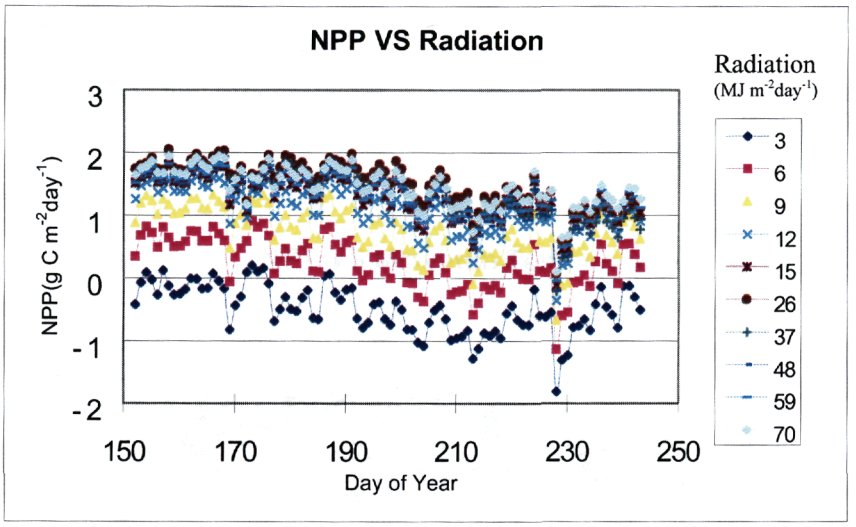

Figure 4.10 Changes of NPP with solar radiation and time

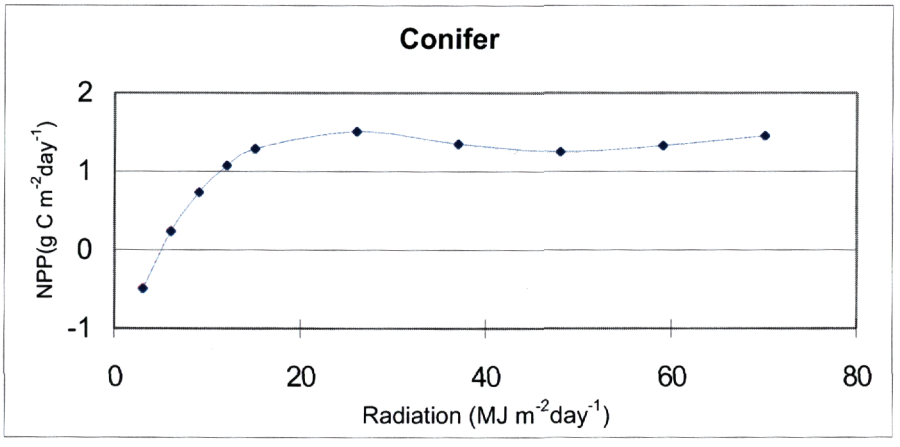

Figure 4.11 Average NPP changes with daily solar radiation

4.3.1.4 Minimum Temperature

When minimum temperature reached 0 ^{0}C, forests in the growth season produced the largest amount of NPP (Figure 4.12, and 4.13). With increased daily

minimum temperature, NPP values decreased. Generally, NPP will increase with the increase of daily average temperature. After it reaches its largest value, NPP will decrease with temperature increase because autotrophic respiration of forest also increases and higher temperatures can cause leaf stomatal closure.

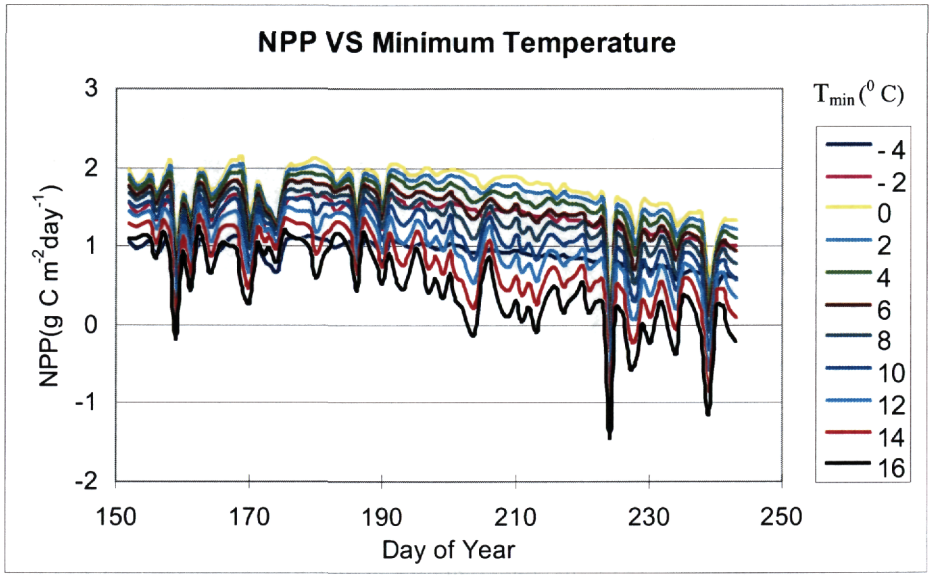

Figure 4.12 Changes of NPP with minimum temperature (T_{min}) and time

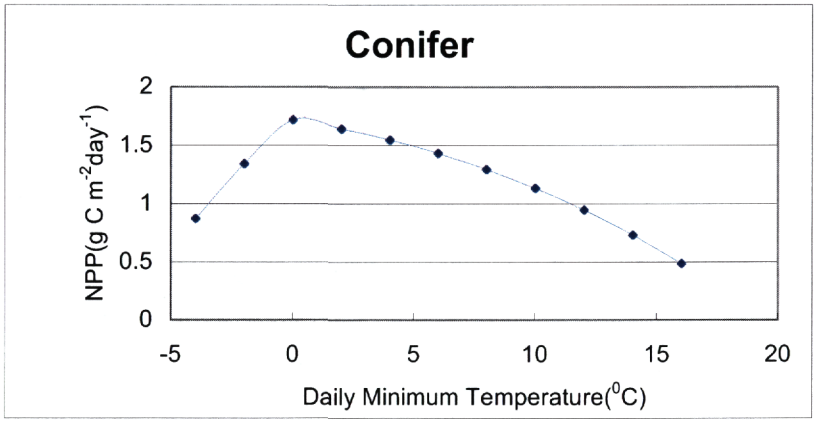

Figure 4.13 Average NPP changes with daily minimum temperature

4.3.1.5 Maximum Temperature

According to Figures 4.14 and 4.15, when daily maximum temperature reached 21 ^{0}C, NPP reached its largest value, and NPP dropped when daily maximum temperature was greater than 21 ^{0}C.

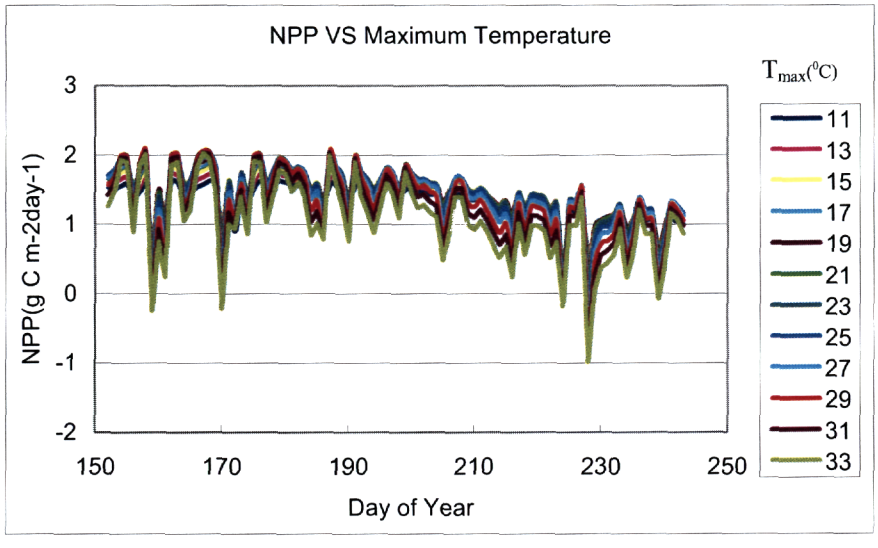

Figure 4.14 Changes of NPP with maximum temperature (T_{max}) and time

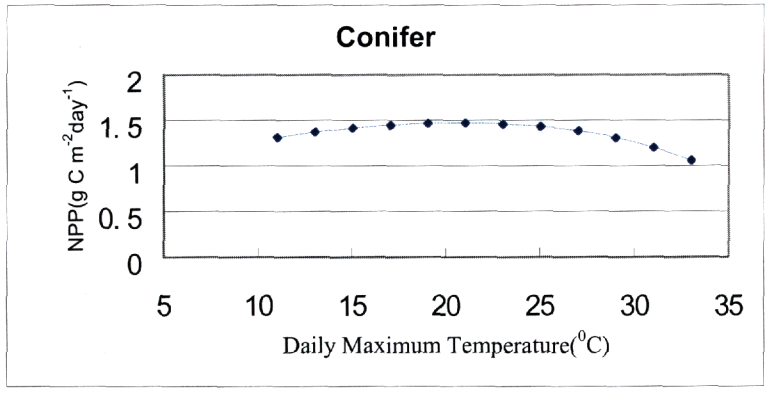

Figure 4.15 Average NPP changes with daily maximum temperature

4.3.1.6 Humidity

Although the influence of humidity on NPP modelling was relatively small, Figures 4.16 and 4.17 still showed that the modeled values of NPP increased with increased humidity. Because of low humidity in August, the modeled amount of NPP appeared less than that of June and July (Figure 4.16).

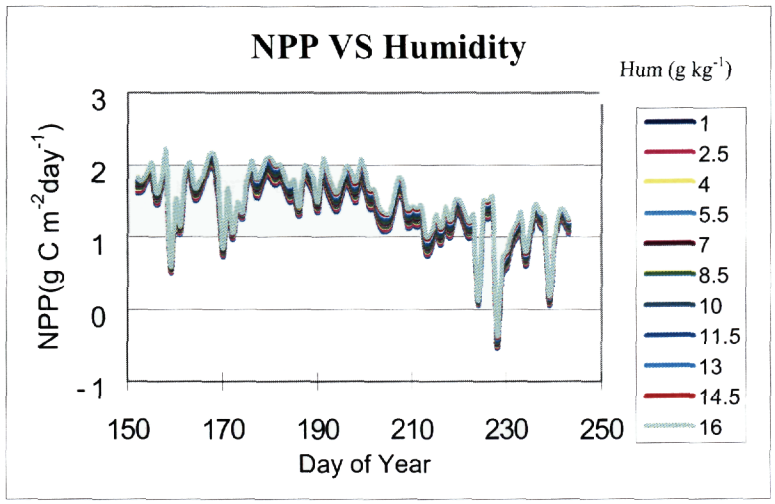

Figure 4.16 Changes of NPP with humidity (Hum) and time

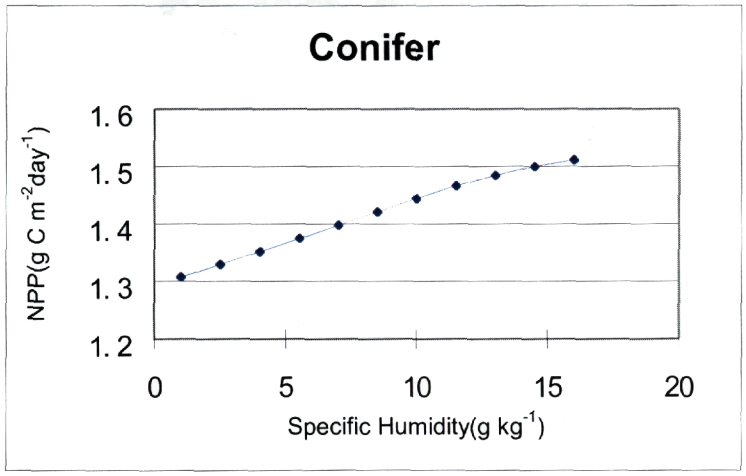

Figure 4.17 Average NPP changes with daily humidity

4.3.1.7 Biomass

Theoretically, NPP will increase with increased forest biomass. Usually forest dry biomass can be directly converted to carbon using a carbon conversion coefficient for different species (Lavigne et al. 1997). Modeled NPP varied with forest biomass as displayed in Figures 4.18 and 4.19. NPP decreased with increased biomass. This occurred because biomass used in BEPS was a variable involved in the calculation of forest respiration (R), but not gross primary production (GPP). Therefore, the modeled NPP linearly decreased with the increase of forest biomass since the NPP was the balance of GPP and R.

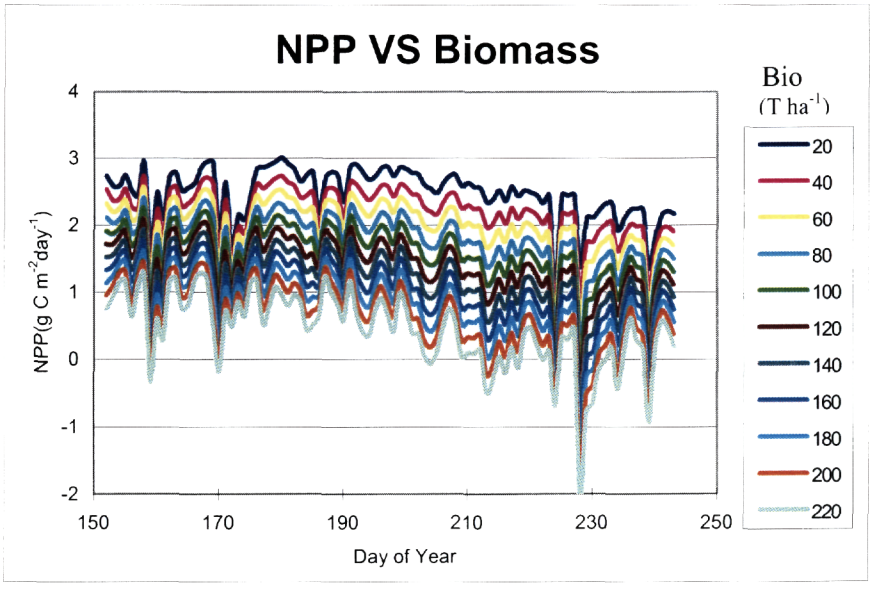

Figure 4.18 Changes in NPP with biomass (Bio) and time

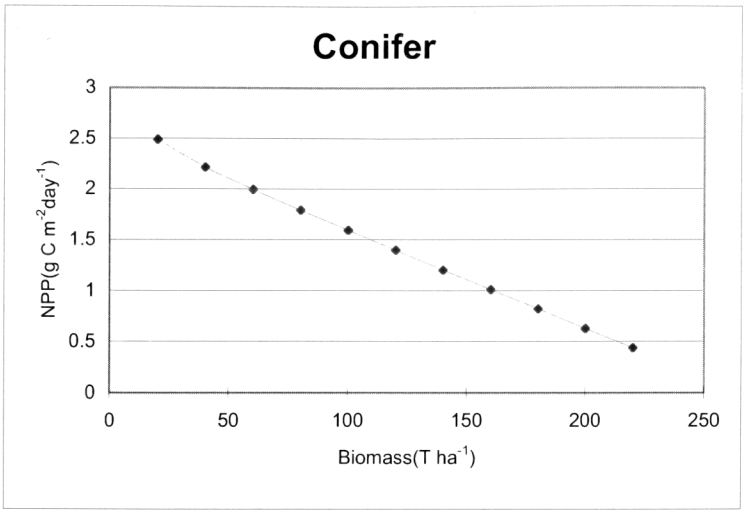

Figure 4.19 Average NPP changes with biomass

4.3.1.8 Precipitation and AWC

From the individual modeled results (Figures 4.20 and 4.21), both precipitation and AWC had no influence on the estimation of NPP using average precipitation and AWC data measured in the study areas. Therefore, another modelling test was performed in which precipitation and AWC were varied simultaneously. Figure 4.22 shows that when daily precipitation was greater than 1.0 mm or AWC greater than 0.1 m, NPP was not controlled by precipitation.

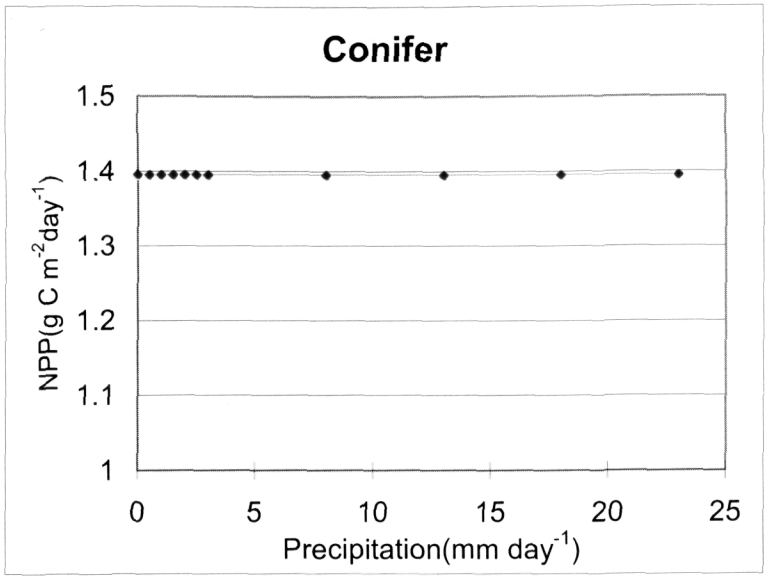

Figure 4.20 Average NPP changes with precipitation

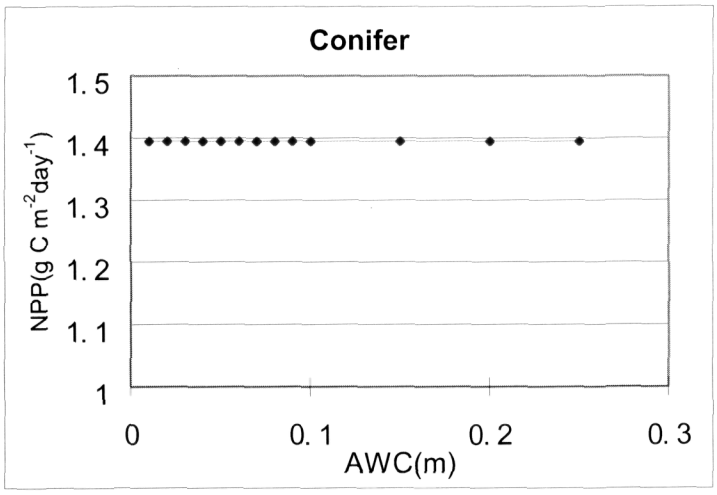

Figure 4.21 Average NPP changes with AWC

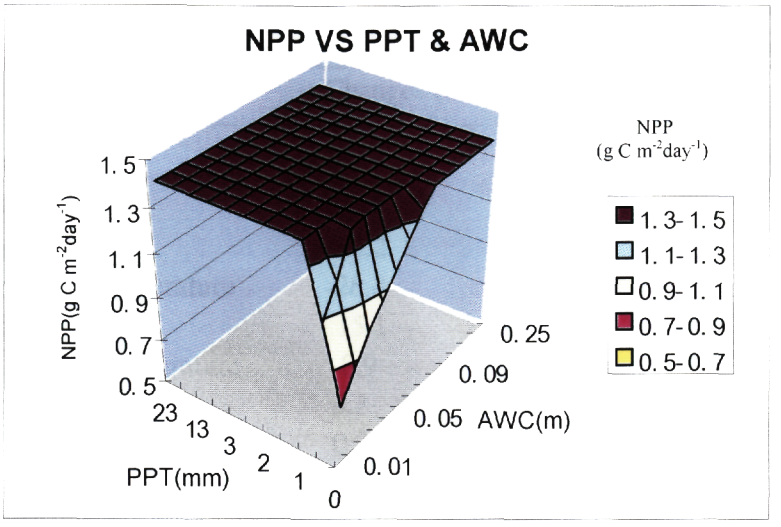

Figure 4.22 Average NPP changes with precipitation (PPT) and AWC

4.3.2 NPP Independent Variation Sensitivity Analysis

Results from the sensitivity analysis in which parameters were independently varied from –1 to +1 standard deviations (Stdv) above the mean are shown in Table 4.3. The change rates of NPP were interpreted as indicators to determine how important each input was in controlling simulated NPP. According to the sensitivity analysis results, the most important input variables for BEPS were LAI, followed by tree species, biomass, minimum temperature, radiation, maximum temperature, and humidity. For precipitation and AWC, either minus a standard deviation or plus a standard deviation to the mean, NPP did not change because precipitation was still greater than 1 mm, and AWC was greater than 0.1 m (see also Figure 4.22).

Table 4.3 Change in simulated mean NPP (g C m^{-2} day^{-1}) caused by varying the parameter from the mean minus 1 Stdv to the mean plus 1 Stdv.

Factors	Changes (%)	Order of Important
LAI	57.3	1
Tree species	54.2	2
Biomass	-30.2	3
Minimum temperature	-28.8	4
Radiation	15.1	5
Maximum temperature	-8.9	6
Humidity	3.3	7
Precipitation	0.00	8
AWC	0.00	9

4.3.3 Factorial sensitivity test

The results derived from the fraction factorial analysis are shown in Tables 4.4 and 4.5. The main effects of input variables (Table 4.4) were similar to the independent parameter variation analysis (Table 4.3). Because the non-quantitative factor, tree species was not included in the fraction factorial analysis, it was not listed in the Table 4.4. The order of importance of input variables for BEPS were LAI, followed by biomass, minimum temperature, radiation, maximum temperature, and humidity, precipitation and AWC. Again, NPP was not sensitive to water variables within the ranges from the mean minus a standard deviation to the mean plus a standard deviation. Interaction effects are shown in Table 4.5. The most significant influence of factor interaction effects on NPP was the interaction between daily maximum and minimum temperature, -0.141. However, compared to the main effects, interaction effects were generally smaller. Results from the factorial analysis given in Tables 4.4–4.5 showed that the main effects were dominant over the interaction effects.

Table 4.4 Main effects of parameter variation in conifers. Effect columns indicated that the NPP (g C m^{-2} day^{-1}) variation due to varying a parameter from the mean minus 1 Stdv to the mean plus 1 Stdv.

Factor	Effect	Factor	Effect
LAI	1.143	Biomass	-0.385
Minimum temperature	-0.383	Radiation	0.247
Maximum temperature	-0.184	Humidity	0.031
Precipitation	0.023	AWC	0.012

Table 4.5 Two- and three-factor interaction effects of parameter variation in conifers. The interaction columns show the expected interaction effect on NPP (g C m^{-2} day^{-1}) caused by varying the shown parameters from minus 1 Stdv to mean plus 1 Stdv.

Factor	Interaction effect	Factor	Interaction effect	Factor	Interaction effect
T_{max}*T_{min}	-0.141	LAI*Rad	0.093	T_{min} *Bio	-0.082
Rad*T_{max}	0.075	LAI* T_{max}	-0.058	Rad* T_{min}	0.047
T_{max}*Bio	-0.033	T_{max} *AWC	0.032	Rad*Hum	0.031
PPT*AWC	-0.029	T_{max} *PPT	0.023	LAI*AWC	0.021
LAI*Hum	0.017	Hum*Bio	-0.017	Hum*Bio* T_{max}	–0.017
Rad*Tmax*Bio	0.017	Rad*AWC	-0.016	LAI*Bio	0.011
PPT*Hum	-0.011	PPT*Hum* T_{max}	-0.011	Rad* T_{max} *PPT	0.011
T_{max}*T_{min} *PPT	-0.005	T_{min} *PPT	-0.005		

4.4 Results of Topographic Influence on NPP Estimation

For testing topographic influences to each of BEPS model inputs, the BEPS model was run two times. The first run was conducted using all of the topographically corrected data. The average NPP estimate for all forest types (conifer, deciduous and mixed wood) was produced and will be referenced as the corrected (or "right") value to be compared with the estimated NPP using topographically uncorrected data. The second run was done using all of the topographically corrected inputs but except one variable, which is topographically uncorrected and is the input of interest. The total average NPP for the three types of forest species is weighted by the correspondent

pixel numbers of each forest type. The NPP derived from these two model runs was compared only taking account for whole forest, not for individual forest species.

4.4.1 Tree Species

Table 4.6 shows the influence of topography on NPP calculation through forest species. Compared to original imagery (number of forest pixels=1827302), the numbers of pixels for forest areas derived from topographically corrected SCS image data is 1834034, increasing 0.64%. This is probably contributed to the conversion of non-vegetation classes into forest class after topographic correction. However, the total average amount of NPP still decreased 0.26%.The overall average (Avg) NPP for all forest types (conifer, deciduous and mixed) is 1.822 g C m^{-2} day^{-1} before topographic correction and 1.806 g C m^{-2} day^{-1} after topographic correction, respectively. The relative difference (-0.26%) was calculated using average NPP, which was weighted by the number of forest pixels. This suggested that NPP difference before and after topographic correction was not significant.

Table 4.6 Results of topographic influence on NPP (g C m^{-2} day^{-1}) estimation by tree species

Species	Conifer	Deciduous	Mixed	Total	Relative difference (%)
Original					
# of Pixels	1061526	118437	647339	1827302	
Avg NPP	1.542	1.749	2.295	1.822	
SCS+C					**-0.26**
# of pixels	1105333	117976	615725	1839034	
Avg NPP	1.533	1.701	2.316	1.806	

4.4.2 LAI

Table 4.7 shows the topographic influence on NPP estimation by LAI. Using topographically corrected LAI data, the modeled NPP decreased 0.8% ((1.806-1.82)/1.806) compared to the original. It is suggested that topography has little influence on NPP through LAI.

Table 4.7 Topographic influence on NPP (g C m-2 day-1) estimation by LAI

	Conifer	Deciduous	Mixed	Total	Relative difference (%)
Original					
LAI	1.541	1.702	2.299	1.82	**-0.80**
SCS+C					
LAI	1.533	1.701	2.316	1.806	

4.4.3 Solar Radiation

Table 4.8 showed the topographic influence of solar radiation variation on NPP estimation. The modeled NPP increased 3.49% ((1.806-1.743)/1.806)) using topographically corrected radiation compared to the modeled NPP using the original data. This means that topography has the largest influence on solar radiation compared to all of the model inputs.

Table 4.8 Topographic influence on NPP (g C m^{-2} day^{-1}) estimation by solar radiation

	Conifer	Deciduous	Mixed	Total	Relative difference (%)
Original					
Radiation	1.466	1.679	2.253	1.743	**3.49**
SCS+C					
Radiation	1.533	1.701	2.316	1.806	

4.4.4 Minimum Temperature

Table 4.9 shows the topographic influence on NPP estimation by minimum temperature. The modeled NPP decreased 1.89% ((1.806-1.84)/1.806)) using topographically corrected minimum temperature compared to the modeled NPP using the original data. Because the elevation of most study sites was higher than the base climate station, the average minimum temperature of topographically corrected data would be expected to be lower than the original weather station data. As a result, lower minimum temperature likely caused a lower modeled NPP value.

Table 4.9 Topographic influence on NPP (g C m^{-2} day^{-1}) estimation by minimum temperature

	Conifer	Deciduous	Mixed	Total	Relative difference (%)
Original					
T_{min}	1.563	1.747	2.311	1.84	**-1.89**
SCS+C					
T_{min}	1.533	1.701	2.316	1.806	

4.4.5 Maximum Temperature

Table 4.10 shows the topographic influence on NPP estimation by maximum temperature. The modeled NPP decreased 2.02% ((1.806-1.842)/1.806)) using topographically corrected maximum temperature compared to that modeled using the original data. The explanation is similar to that for minimum temperature because lower maximum temperature likely caused a lower modeled NPP value.

Table 4.10 Topographic influence on NPP (g C m^{-2} day^{-1}) estimation by maximum temperature

	Conifer	Deciduous	Mixed	Total	Relative difference (%)
Original					
T_{max}	1.553	1.879	2.309	1.842	**-2.02**
SCS+C					
T_{max}	1.533	1.701	2.316	1.806	

4.4.6 Precipitation

Table 4.10 shows the topographic influence on NPP estimation by precipitation. There was no difference between overall average NPP estimated before and after topographic correction. From the former discussion (Figures 4.20 and 4.21), since precipitation and AWC had no influence on the estimation of NPP using average precipitation and AWC data measured in the study areas, the results in Table 4.11 are reasonable.

Table 4.11 Topographic influence on NPP (g C m^{-2} day^{-1}) estimation by precipitation

	Conifer	Deciduous	Mixed	Total	Relative difference (%)
Original					
Precipitation	1.533	1.701	2.316	1.806	**0.0**
SCS+C					
Precipitation	1.533	1.701	2.316	1.806	

4.4.7 Biomass

Table 4.12 shows the topographic influence on NPP estimation by biomass. The modeled NPP increased 1.45% ((1.806-1.78)/1.806)) using topographically corrected biomass compared to that modeled using the original data. This increase might be from the increase of forest areas after the topographic correction.

Table 4.12 Topographic influence on NPP (g C m^{-2} day^{-1}) estimation by biomass

	Conifer	Deciduous	Mixed	Total	Relative difference (%)
Original					
Biomass	1.536	1.699	2.233	1.78	**1.45**
SCS+C					
Biomass	1.533	1.701	2.316	1.806	

4.4.8 Humidity

Table 4.11 shows the topographic influence on NPP estimation by humidity. The modeled NPP increased 2.41% ((1.806-1.762)/1.806)) using topographically corrected humidity compared to that modeled using the original data. In a forest, humidity cycle goes like: during the day the humidity decreases from morning until the warm part of the day and then increases again as night falls. Warm air can hold more moisture so that higher temperatures during mid-day cause the humidity to decrease. Because most stand plots situate at higher position than that of base climate station, the average temperature of topographically corrected data would be expected to be lower than the original weather station data for most pixels. Therefore, the humidity derived from the topographically corrected data would be higher than that measured in the climate station.

Table 4.13 Topographic influence on NPP (g C m^{-2} day^{-1}) estimation by humidity

	Conifer	Deciduous	Mixed	Total	Relative difference (%)
Original					
Humidity	1.512	1.685	2.226	1.762	
SCS+C					**2.41**
Humidity	1.533	1.701	2.316	1.806	

4.4.9 All Inputs

Table 4.14 shows the topographic influence on NPP estimation by all the inputs of the BEPS model. The modeled NPP increased 3.49% ((3320.7-3204.9)/ 3320.7)) using topographically corrected inputs compared to that modeled using the original data. The negative error (3.49%) caused by topography is significant if the BEPS model is applied to a regional or global scale. For example, the annual NPP for Canada in 1994 was 1.49 Gt C $year^{-1}$ for all land covers and 1.1 Mt C $year^{-1}$ for matured forest, respectively (Xu et al., 2004) and the error induced by topography for forest in that year was about 38.4 ton C. This simulated result indicated that we should take the topographic effects into account when we apply BEPS to montane environment.

Table 4.14 Topographic influence on NPP (g C m-2 day^{-1}) estimation by all input variables

Species	Conifer	Deciduous	Mixed	Total	Total NPP (kg day^{-1})	Relative difference (%)
Original					**3204.9**	
# of Pixels	1061526	118437	647339	1827302		
Avg NPP	1.542	1.749	2.295	1.822		
SCS+C					**3320.7**	**3.49**
# of pixels	1105333	117976	615725	1839034		
Avg NPP	1.533	1.701	2.316	1.806		

Also, topographic influences on the estimation of NPP in the Kananaskis Rocky Mountains can be seen in Figure 4.23. It is indispensable to take the impact of topography on NPP estimation into account.

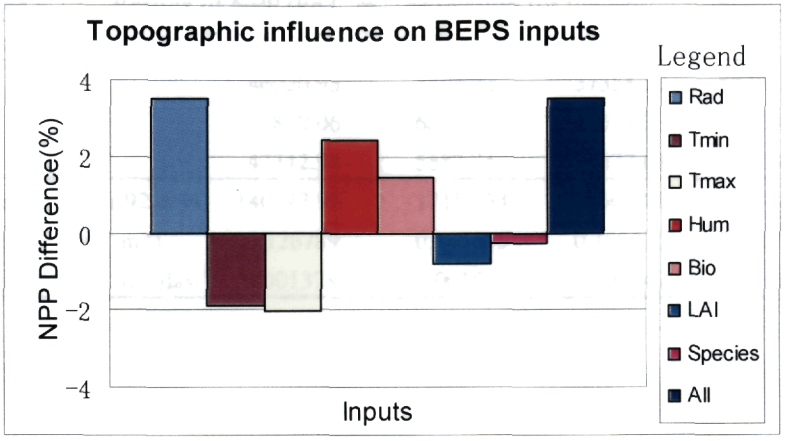

Figure 4.23 Topographic influences on all of BEPS inputs

4.5 Results of Forest Carbon Growth from June to August

Table 4.15 and Figure 4.23 show the modeled results of NPP for a total of 92 days (from June 1 to August 31). The average carbon stock of the study areas was about 0.15 kg C m^{-2} from June to August. In addition, carbon growth in July is largest among the three months. NPP is the net amount of carbon assimilated by plants per unit area and time, and NPP is allocated to aboveground and underground tree components such as leaves, stems, coarse root and fine roots to support their growth. As a result, forest carbon stock refers to dry weight of biomass for all of the tree components plus the detritus and soil carbon. In practice, the aboveground biomass is estimated using allometric equations and converted to above ground NPP by a conversion coefficient (e.g. 0.5). For example, 56% of NPP for boreal forest occurs as detritus (Gower et al. 1997). Furthermore, the northeast part of the study area has the largest carbon stock.

Table 4.15 Results of NPP (kg C m^{-2}) estimation for the period from June to August

Month	Conifer	Deciduous	Mixed	Total
6	46020.95	5403.22	37358.10	88782.28
7	50810.06	6064.57	41034.38	97909.01
8	43312.94	5687.74	37677.63	86678.31
Total (kg C for 92 days)	140143.96	17155.54	116070.11	273369.60
Average (kg C m^{-2})	0.126789	0.145415	0.188510	0.148648
Average (kg C m^{-2} day^{-1})	0.001378	0.001581	0.002049	0.001616

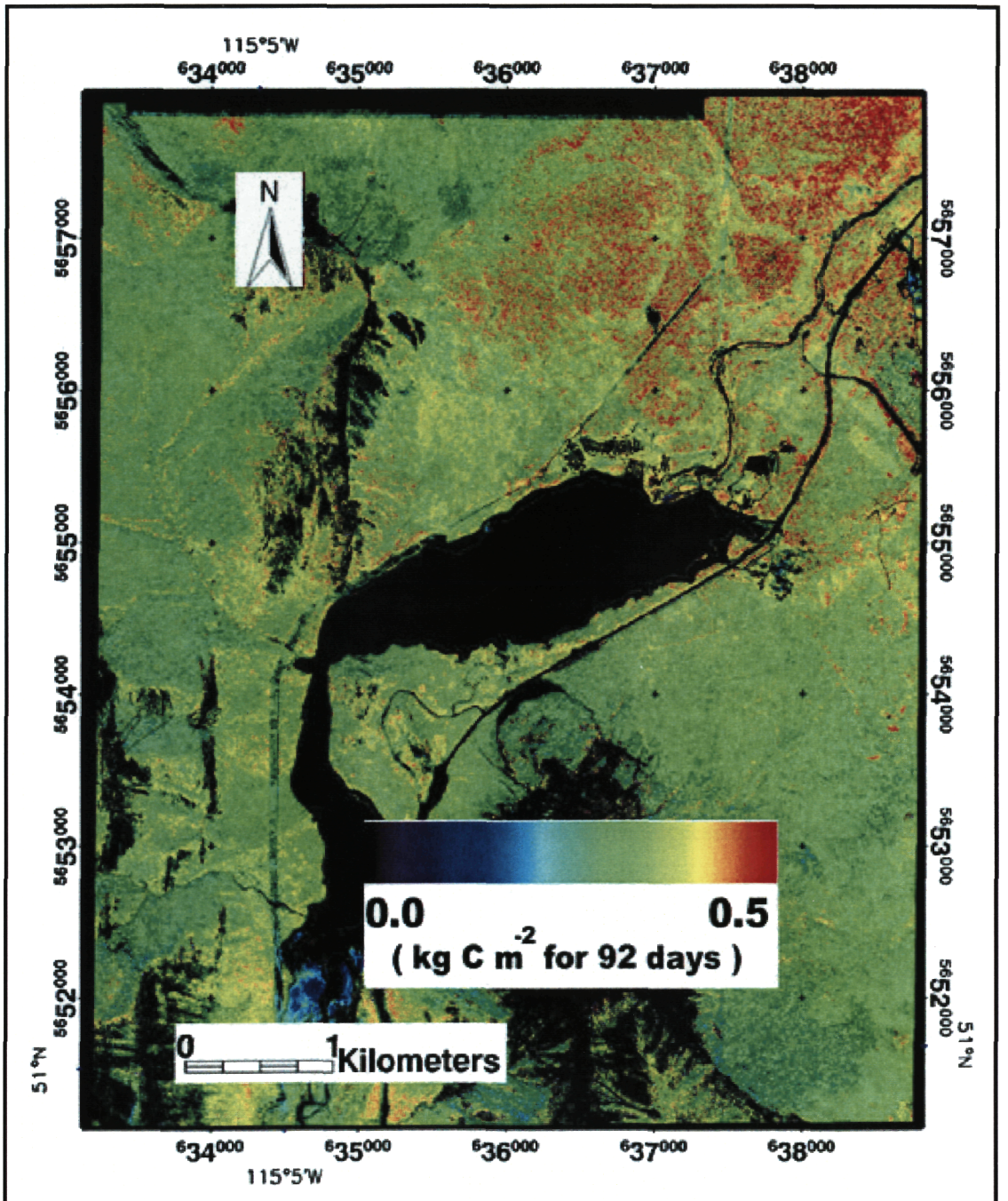

Figure 4.24 NPP (kg C m^{-2}) distribution for June-August 2003.

4.6 Discussion and Future Perspectives

4.6.1 Estimation of the Model Inputs

The accuracy of modeled NPP is highly dependent on the correct estimation of each of the model inputs. As mentioned in chapter 3, this research mainly emphasizes the areas of sensitivity of modeled NPP to the variability of model inputs and topographic effects. For mapping the tree species the maximum likelihood classification algorithm was used. The classification of tree species was a very important factor in NPP modelling because many default parameters were given depending on the forest types. The overall accuracy of classification for forest was 69.4% using original data and 70.6 using SCS correction data. To improve the accuracy of land cover classification in the future, some more sophisticated techniques can be considered. For example, artificial neutral network, which can capture non-linear information (Foody et al., 1997), and processed –based forest canopy model inversion (Peddle et al., 2004) could be used.

Regarding the estimation of climate variables, some successful software, such as MTCLIM (mountain microclimate simulator) (Hungerford et al., 1989), and PRISM (Parameter-elevation Regressions on Independent Slopes Model) (Daly et al., 1994) could be used for meteorological interpolation. But they are not very suitable for this study area because there is just one meteorological station dataset providing landscape scale climate data estimation. As a result, the previous methods for extrapolating weather station data to the study site was used, and the computer programs, which were coupled into BEPS (Appendix 2), were written for climate data

estimates. However, bias for the climate variable estimation may have existed. Furthermore, the estimated results of the weather data could not be validated due to the lack of ground-measured data.

For LAI and biomass estimates, only Trembling Aspen and Lodgepole Pine were taken into account. Other forest types, like mixed woods and White Spruce, did not have enough ground plots to establish a statistical relationship between LAI or biomass and remotely sensed information. The outcomes of estimated LAI and biomass, especially for mixed woods, were uncertain.

4.6.2 General Sensitivity Analysis

Based on the results of the general sensitivity analysis, NPP was sensitive to the variability of field-measured model input data. Leaf area index was the most important variable to drive BEPS for NPP modelling according to the results of NPP independent variation sensitivity analysis and factorial sensitivity tests. This suggests that accurate LAI estimation is indispensable for NPP modelling. Moreover, the interaction effects of the model inputs can be ignored compared to the main effects of the input variables. However, we cannot draw the conclusion that precipitation and AWC are not important depending on the test results. As discussed above, NPP was not sensitive to both precipitation and AWC when those variables were beyond a certain combined threshold, so together they do have some meaning in this regard.

Generally, varying patterns of NPP should remain consistent with those of live biomass. Luo et al. (2002) presented a close linear relationship between the potential

NPP and the area-weighted live biomass density. For this sensitivity test, a relationship between modeled NPP and biomass was found (Figure 4.25). Using the produced maps of NPP and biomass, 11 plots for Lodgepole Pine were investigated. A positive relationship between biomass and NPP existed (Figure 4.25) with R^2=0.452.

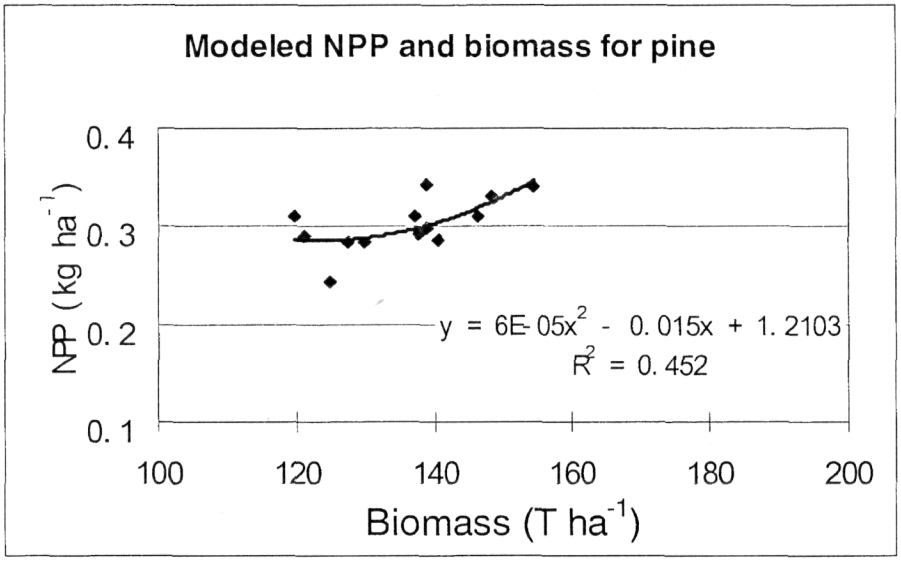

Figure 4.25 Modeled NPP and biomass for lodgepole pine using topographically corrected data

4.6.3 Topographic Influence on NPP Modelling

After the topographic correction, NPP was shown to be increased 3.49% g C m^{-2} day^{-1}. Therefore, if we want to simulate yearly or multiple-year carbon growth in this mountainous region, topographic effects should be taken into account (see 4.4.9). Topography had a relatively small influence on the other model biological input variables, such as tree species, LAI, and biomass, which reflect forest biological characteristics. In comparison, climate input variables were strongly related to

topography. Solar radiation is influenced and redistributed by topography, thus the largest NPP difference, 3.49% g C m^{-2} day^{-1} was found using the topographically corrected versus uncorrected radiation. Solar radiation received by a watershed is the energy source for controlling the growth and activity of plants and accordingly is one of the prime variables of BEPS. Therefore, the correction for radiation on a complex mountain terrain is necessary.

4.6.4 NPP estimation

Average growth rate of NPP in the forest growth season in 2003 was estimated using the topographically corrected data (Table 4.15). If 250 days were assumed for tree growth in 2003, yearly NPP production by the forests in Kananaskis was about 4.01 T ha^{-1}. This average value was based on 3.45 T ha^{-1} yr^{-1} for conifers, 3.95 T ha^{-1} yr^{-1} for deciduous trees, and 5.12 T ha^{-1} yr^{-1} for mixed woods (not enough confidence due to only two plots). This amount of modeled NPP is lower than previous findings for conifers. For example, Prescott et al. (1989) investigated NPP growth in Kananaskis region for lodgepole pine, white spruce and Douglas fir, and estimated NPP was 4.57 T $ha^{-1}yr^{-1}$, 4.32 T $ha^{-1}yr^{-1}$, and 3.83 T $ha^{-1}yr^{-1}$ for conifer, deciduous, and mixed woods, respectively. Davidson (2002) presented an estimated NPP value for coniferous forest of 4.56 T $ha^{-1}yr^{-1}$. For deciduous trees, the results derived from this study were compared with that in a boreal forest. Gower et al. (1997) gave the estimated results of NPP, 3.42 T $ha^{-1}yr^{-1}$ for conifers and 3.49 T $ha^{-1}yr^{-1}$ for deciduous

forest. As a result, the simulated NPP of deciduous forests was higher than that of boreal forests. In Davison's modeling (2002), the yearly average temperature and precipitation in 1998 were 4.3 ^{0}C and 2.2 mm day^{-1}, respectively. In comparison, the average temperature and precipitation data in 2003 were 3.9 ^{0}C and 1.4 mm day^{-1}, respectively. This can partially explain why the estimated NPP value in 2003 was lower than that in 1998.

4.7 Chapter Summary

In this chapter, the results of general sensitivity of BEPS, topographic influence on NPP modelling, and the estimates of NPP in the study area were presented, as well as any uncertainties in the results. Based on the NPP general sensitivity analysis, LAI and tree species were the two most important variables, which determined the modeled amount of NPP. Also, it was found that the effects of model input interaction could be neglected. The topographic sensitivity test indicated that it was necessary to have topographic correction for the estimation of carbon model inputs in complex terrain. The climate data were especially topographic-dependent, so it is imperative for climate data to be topographically corrected prior to model input.

Using the topographically corrected data, the carbon dynamics were simulated, with average annual NPP production by forests in Kananaskis estimated to be 4.01 T ha^{-1}. However, the accuracy for NPP modelling is highly dependent on the correct estimates of the model inputs. For this study, the emphasis was placed on NPP

sensitivity. Some results of model input estimates could not be validated because of lack of ground truth data. As a result, there may be some error or biases for NPP simulation in those cases.

CHAPTER 5

5.0 Conclusion

5.1 Summary of Results

The study implemented a comprehensive methodological framework for sensitivity analysis of NPP using satellite imagery. Ground data were collected in Kananaskis, Alberta, Canada as inputs for the ecosystem model, BEPS to be parameterized. To assess topographical influence on NPP modelling, two datasets, one that was not topographically corrected, and one that was topographically corrected, were tested and compared. General sensitivity was performed for evaluating the effect of each individual BEPS input on NPP estimates. In addition, a topographic sensitivity analysis of BEPS was done to test the topographic influence on NPP modelling through each of the model inputs. Using the corrected model inputs, the NPP modelling in the study area was done, and an estimate of carbon growth was given. Uncertainties involved in parameterization of the model inputs, and the results of sensitivity analysis indicated the need for accurate estimates of the model inputs.

5.2 Conclusion

This study has systematically evaluated the applicability of an ecosystem model, BEPS in a complex area of mountainous terrain in Kananaskis, Alberta, Canada. A number of major conclusions regarding this sensitivity experiment in the region have been drawn.

- According to the results of the randomized model runs, modeled NPP was sensitive to most of its inputs. The strongest predictors of NPP for the BEPS model were LAI and forest species, suggesting that accurate LAI estimates and tree species classification were very important under the range of conditions simulated. Also, the interaction effects of the input variables were very small, compared to main effects from each of the inputs.
- The results from the topographic sensitivity showed that topography influenced the NPP estimation in this montane ecosystem. Topography caused negative biases of about 3.5% of the modeled NPP, which is equivalent to 140 kg C ha^{-1} yr^{-1}. Moreover, the climate variables had greater influence than biological variables, such as LAI, tree species, and biomass. Out of all of the input variables, solar radiation was the variable most greatly influenced by topography.
- With corrected datasets, the estimates of NPP in 2003 was estimated at 4.01 T $ha^{-1}yr^{-1}$, which was close to field-measured, 4.24 T $ha^{-1}yr^{-1}$.
- Some uncertainties in this study existed because of the lack of ground-sampled plots. As a result, biophysical parameter extraction from satellite imagery was limited for some species, such as white spruce, and mixed forests.

5.3 Contributions to Research

This research, for the first time, presented the performance of BEPS applied to a complex mountainous terrain. Opposing the original "Earth flat" assumption of BEPS, the results of this research showed that the influence of topography on NPP estimates must not be neglected. Additionally, the general sensitivity experiments showed that the most important input variables for BEPS were forest type and leaf area index. Therefore, much attention should be paid to the derivation of those key inputs.

Furthermore, because this research has exposed the weakness of BEPS used for a montane region, the modification of BEPS is recommended for its general use globally and in those large mountainous regions in particular.

5.4 Future Research Work

To resolve the "flat Earth" problem for BEPS, some modifications should be made for its general use (Liu et al., 2003). Although the climate data were extrapolated with topographic data in this research, more sophisticated treatment should be given to BEPS for its future use for large areas. In addition, because carbon cycling is closely related to water dynamics for forest ecosystems, lateral water redistribution in mountainous regions must be taken into account (Band et al., 1993). Furthermore, to improve the classification accuracy, some advanced techniques, such as canopy reflectance model methods (Peddle, et al, 2004) can be used. Meanwhile, the spectral signals of various cover types in a pixel do not always mix linearly.

Therefore, linear mixture analysis techniques have limitations in some circumstances. Some non-linear mixture modelling methods, such as artificial neutral network (ANN) (Foody et al., 1997) could be used for retrieving the forest biophysical parameters.

This modelling experiment was conducted from June to August. The influence of snowfall, a dominant part of the yearly amount of precipitation, was not considered in this research. In future work, annual simulation should also be done so as to more comprehensively study the forest growth. More attention could be also given to precipitation, which is a very important factor to control forest growth.

Finally, uncertainties existed because of the limited number of ground plots, especially for mixed species and white spruce. Accordingly, it is necessary to take more ground samples for those forest stands in future research.

REFERENCES

Amthor J. S.,J. M. Chen ,J. S. Clein, S. E. Frolking, M. L. Goulden, R. F. Grant, J. S. Kimball, A. W. King, A. D. McGuire, N. T. Nikolov, C. S. Potter, S. Wang, and S. C. Wofsy, 2001. Boreal forest CO2 exchange and evapotranspiration predicted by nine ecosystem process models: Intermodel comparisons and relationships to field measurements. *Journal of Geophysical Research*, 106 (D24): 33623-33648.

Archibald, J.H., G.D. Klappstein, and I.G.W. Corns, 1996. Field Guide to Ecosites of Southwestern Alberta. Special Report 8 – Canadian Forest Service, Northwest Region, Northern Forestry Centre, Canada. UBC Press, Vancouver, British Columbia, Canada.

Asner, G.P., C.A. Wessman, and J. L. Privette, 1997. Unmixing the directional reflectances of AVHRR sub-pixel landcovers. *IEEE Transactions on Geoscience and Remote Sensing*, 35(4): 868-878.

Band, L. E., Patterson, P., Nemani, R., and Running, S. W, 1993. Forest ecosystem processes at the watershed scale: incorporating hillslope hydrology. *Agricultural and Forest Meteorology*, 63: 93-126.

Bartona, C.V.M. and Northb, P.R.J, 2001. Remote sensing of canopy light use efficiency using the photochemical reflectance index Model and sensitivity analysis. *Remote Sensing of Environment*, 78, 264– 273.

Bolstada, P.V., L. Swiftb, F. Collins, J. Rigniired, 1998. Measured and predicted air temperatures at basin to regional scales in the southern Appalachian mountains. *Agricultural and Forest Meteorology*, 9 1:161- 176.

Box, G. E. P., W. G. Hunter, and J. S. Hunter, 1978. Statistics for Experimenters. John Wiley, New York, 653 pp.

Cao, M., and FI Woodward, 1998. Dynamic responses of terrestrial ecosystem carbon cycling to global climate change. *Nature*, 393: 249–252.

Chen, J. M. and S. Leblanc, 1997. A 4-scale bidirectional reflection model based on canopy architecture. *IEEE Transactions on Geoscience and Remote Sensing*, 35:1316-1337.

Chen, J.M., 1996. Optically-based methods for measuring seasonal variation in leaf

area index of boreal conifer forests. *Agriculture and Forest Meteorology*, 80:135-163.

Chen, J. M. and J. Cihlar, 1996. Retrieving leaf area index for boreal conifer forests using Landsat TM images. *Remote Sensing of Environment*, 55:153-162.

Chen J.M. , J. Liu , J. Cihlar , M.L. Goulden,1999. Daily canopy photosynthesis model through temporal and spatial scaling for remote sensing applications. *Ecological Modelling*, 124:99–119.

Chen, J. M., W. Chen, J. Liu, J. Cihlar, 2000. Annual carbon balance of Canada's forests during 1895-1996. *Global Biogeochemical Cycles*, 14(3): 839-850.

Chen J. M., G. Pavlic, L. brown, J. Cihlar, S. Leblanc, H.P. White, R.J. Hall, D.R. Peddle, D.J. King, J.A. Trofymow, E. Swift, J.Van der Sanden & P.K.E Pellikka, 2002. Derivation and validation of Canada-wide course-resolution leaf area index maps using high-resolution satellite imagery and ground measurements. *Remote Sensing of Environment*. 80:165-184.

Crossley, D.I., 1952. The soil of Kananaskis Forest Experiment Station in the sub-alpine forest region in Alberta. Silviculture Research Notes No.100. Forest Branch. Canada Department of Resources and Development, Ottawa, 32pp.

Davidson, D., 2002. Sensitivity of NPP Models to Remotely Sensed LAI. Masters Thesis; Department of Geography, University of Lethbridge.

Daly, C., Neilson, R.P., and Phillips, D.L., 1994. A statistical-topographic model for mapping climatological precipitation over mountainous terrain. *Journal of Applied Meteorology*, 33:140-158.

Falkowski P., R. J. Scholes, E. Boyle, J. Canadell, D. Canfield, J. Elser, N. Gruber, K. Hibbard, P. Ho¨gberg, S. Linder, F. T. Mackenzie, B. Moore III, T. Pedersen, Y. Rosenthal, S. Seitzinger, V. Smetacek, W. Steffen, 2000.The Global Carbon Cycle: A test of our knowledge of Earth as a system. *Science*, 290 (13): 291-296

Friend A. D., Stevens A.K., Knox R.G, and Cannell M.G.R, 1997. A process-based terrestrial biosphere model of ecosystem dynamics (Hybrid v3.0). *Ecological Modelling*, 95:249-287.

Farquhar, G. D., S. von Caemmerer, and J. A. Berry, 1980. A biochemical model of photosynthetic CO2 assimilation in leaves of C3 species. *Planta*, 149: 78–90.

Gemmell, Fraser, 1998. An investigation of terrain effects on the inversion of a forest

reflectance model. *Remote Sensing of Environment*, 65:155–169.

Gemmell, Fraser, Jari Varjo, Mikael Strandstrom, and Andres Kuusk, 2002. Comparison of measured boreal forest characteristics with estimates from TM data and limited ancillary information using reflectance model inversion. *Remote Sensing of Environment*, 81:365– 377.

Goel, N.S. and D.E. Strebel, 1983. Inversion of vegetation canopy reflectance models for estimating agronomic variables.1. Problem definition and initial results using the suits model. *Remote Sensing of Environment*, 13:487-507.

Goel, N. S., 1988. Models of vegetation canopy reflectance and their use in estimation of biophysical parameters from reflectance data. *Remote Sensing Reviews*, 4:1–213.

Goetz, S. J. and Prince S. D., 1996. Remote sensing of net primary production in boreal forest stands. *Agricultural and Forest Meteorology*, 78:149-179.

Gong, P., R. Pu, and J.R. Miller, 1992. Correlating leaf area index of ponderosa pine with hyperspectral CASI data. *Canadian Journal of Remote Sensing*, 18(4):275-282.

Gu, D. and A. Gillespie, 1998. Topographic normalization of LANDSAT TM images of forest based on subpixel sun-canopy-sensor geometry. *Remote Sensing of Environment*. 64:166 - 175.

Gower, S.T., Vogel, J.G, Norman, J.M., Kucharik, C.J., Steele, S.J., and Stow, T.K. 1997. Carbon distribution and aboveground net primary production in aspen, jack pine, and black spruce stands in Saskatchewan and Manitoba, Canada. *Journal of Geophysical Research*, 102:29029–29041.

Hall, F.G., Y.E. Shimabukuro, and K.F. Huemmrich, 1995. Remote Sensing of Forest Biophysical Structure using Mixture Decomposition and Geometric Reflectance Models. *Ecological Applications*, 5(4): 993-1013.

Hall, R.J., D.P. Davidson, and D.R. Peddle, 2003. Ground and remote estimation of leaf area index in Rocky Mountain forest stands, Kananaskis, Alberta. *Canadian Journal of Remote Sensing*, 29(3):411-427.

Hall, R.J., 2004. Modelling of tree and forest biomass. Natural Resources Canada. Unpublished data, September, 2004.

Hamilton, Jason G, Evan H. DeLucia, Kate George, Shawna L. Naidu, Adrien C. Finzi,

William H. Schlesinger, 2002. Forest carbon balance under elevated CO2. *Oecologia*, 131:250–260.

Henderson-Sellers, B., and A. Henderson-Sellers, 1996: Sensitivity evaluation of environmental models using fractional factorial analysis. *Ecological Modelling*, 86:291–295.

Houghton, R.A. and J.L. Hackler. 1995. Continental Scale Estimates of the Biotic Carbon Flux from Land Cover Change: 1850 to 1980. ORNL/CDIAC-79, NDP-050, Oak Ridge.

Houghton, R A, 2002. Terrestrial carbon sinks– uncertain explanations. *Biologist*, 49 (4): 155-160.

Hungerford, R.D., Nemani R.R., Running S.W., Coughlan J.C., 1989. MTCLIM: A mountain microclimate simulation model. Research Paper INT-414. Intermountain Research Station. Forest Service. US Department of Agriculture. US. 52 pp.

Johnson, R.L., 2000. Airborne Remote Sensing of Forest Leaf Area Index in Mountainous Terrain. Masters Thesis; Department of Geography, University of Lethbridge.

Jensen, J. R., 1996. Introductory Digital Image Processing: A Remote Sensing Perspective, Second Edition, NJ, Prentice Hall.

Kasting, James. 1998. The Carbon Cycle, Climate, and the Long-Term Effects of Fossil Fuel Burning. Consequences: *The Nature and Implication of Environmental Change*, 4(1).

Kimball, J.S., Thornton, P.E., White, M. A., and Running, S.W. 1997. Simulating forest productivity and surface--atmosphere carbon exchange in the BOREAS study region. *Tree Physiology*, 17, 589—599.

Kurz, W.A., and Apps, M.J., 1999. A 70-year retrospective analysis of carbon fluxes in the Canadian forest sector. *Ecological Application*, 9:526–547.

Lavigne, M.B., and G. Ryan, 1997. Growth and maintenance respiration rates of aspen, black spruce and jack pine stems at northern and southern BOREAS sites. *Tree Physiology* , 7:543-551.

Li, X., and A. H. Strahler, 1985. Geometric-optical modelling of a conifer forest canopy. *IEEE Transactions on Geoscience and Remote Sensing*, GE-23:705–721,

1985.

Li, X., and A. H. Strahler, 1986. Geometric-optical bidirectional reflectance modelling of a coniferous forest canopy. *IEEE Transactions on Geosciences and Remote Sensing*, GE-24:906–919.

Li, X., and A. H. Strahler, 1992. Geometric-optical bidirectional reflectance modelling of the discrete crown vegetation canopy: Effect of crown shape and mutual shadowing. *IEEE Transactions on Geoscience and Remote Sensing*, 30:276–291.

Lillesand, T. M. and R. W. Kiefe , 1994. Remote sensing and image interpretation, Third Edition, John Wiley & Sons Inc.

Liu, J., J. M. Chen, J. Cihlar, and W. Park, 1997. A process-based Boreal Ecosystems Productivity Simulator using remote sensing inputs. *Remote Sensing of Environment*, 62:158-175.

Liu, J., J. M. Chen, J. Cihlar, W. Chen, 1999. Net primary productivity distribution in the BOREAS region from a process model using satellite and surface data. *Journal of Geophysical Research,* 104(D22): 27735-27754.

Liu, J., J. M. Chen, and J. Cihlar, 2003. Mapping evapotranspiration based on remote sensing: An application to Canada's landmass. *Water Resources Research*, 39(7):4-1-15.

Liu, J., J. M. Chen, J. Cihlar, W. Chen, 2002. Net primary productivity mapped for Canadian at 1-km resolution. *Global Ecology and Biogeography*, 11:115-129.

Luo, T., W. Li, And H. Zhu, 2002. Estimated biomass and productivity of natural vegetation on the Tibetan Plateau. *Ecological Applications*, 12 (4), 980–997.

Mackay, D.S., and L.E. Band, 1997. Forest ecosystem processes at the watershed scale: dynamic coupling of distributed hydrology and canopy growth. *Hydrological Processes*, 11: 197-1217.

Murry, F.W., 1967. On the computation of saturation vapor pressure. *Journal of Applied Meteorology*, 6:203-204.

North, Peter R.J., 2002. Estimation of fAPAR, LAI, and vegetation fractional cover from ASTER-2 imagery. *Remote Sensing of Environment*, 80:114-121.

Parton, W.J., Logan, J.E., 1981. A model for diurnal variation in soil and air temperature. *Agricultural Meteorology*, 23:205-216.

Parton, W.J., Scurlock J.M.O., Ojima D.S., 1993. Observations and modelling of biomass and soil organic matter dynamics for the grassland biome worldwide. *Global Biogeochemical Cycles*, 7: 785-809.

Peddle, D.R. and S.E. Franklin, 1991. Image texture processing and data integration for surface pattern recognition. Photogrammetric *Engineering and Remote Sensing*, 57(4): 413-420.

Peddle, D.R. 1995, Knowledge Formulation for Supervised Evidential Classification. *Photogrammetric Engineering and Remote Sensing*, 61(4): 409-417.

Peddle, D.R., 1998. Field spectroradiometer data acquisition and processing for spectral mixture analysis in forestry and agriculture. First international conference on geospatial information in agriculture and forestry. Lake Burena Vista, Florita, USA. June 1-3/98. ERIM International. Vol 2, P. 645-652.

Peddle, D.R., 1999b. Integration of a geometric optical reflectance model with evidential reasoning image classification for improved forest information extraction. *Canadian J. of Remote Sensing*, 25(2):189-196.

Peddle, D.R., F.G. Hall, and E.F. LeDrew, 1999a. Spectral mixture analysis and geometric-optical reflectance modeling of boreal forest biophysical structure. *Remote Sensing of Environment*, 67: 288-297.

Peddle, D.R., R.L. Johnson, 2000. Spectral mixture analysis of airborne remote sensing imagery for improved prediction of Leaf Area Index Mountainous Terrain. *Canadian Journal of Remote Sensing*, 26 (3): 177-188.

Peddle, D.R., S.P. Brunke, F.G. Hall, 2001. A comparison of spectral mixture analysis and ten vegetation indices estimating Boreal forest biophysical information from airborne data. *Canadian J. of Remote Sensing*, 27(6): 627-635.

Peddle D.R., R.L. Johnson, J. Chihlar, and R. Latifovic, 2004. Large area forest classification and biophysical parameters estimation using the 5-scale canopy reflectance model in multiple-forward-mode. Remore Sensing of Environment, BOREAS Special Issue, 89(2):252-263.

Peterson, D. L., and R. H. Waring, 1994. Overview of the Oregon Transect Ecosystem Research Project. *Ecological Application*, 4:221-225.

Pilger, N., 2004. Canopy Reflectance Modelling Of Forest Stand Volume. Masters

Thesis; Department of Geography, University of Lethbridge.

Qi, J., Chehbouni, A., Huete, A.R., Kerr, Y.H., and Sorooshian, S., 1994. Modified soil adjusted vegetation index. *Remote Sensing of Environment*, 48:119–126.

Prescott, .E., J.P. Cobin, D. Parkinson, 1989. Biomass, productivity, and nutrient-use efficiency of aboveground vegetation if four Rocky Mountain coniferious forests. *Canadian Journal of Forest Research*, 19:309-317.

Roberts, L. 1989. How fast can trees migrate? *Science*, 243: 735-737.

Running, S.W and Nemani R.R., Hungerford R.D., 1987. Extrapolation of synoptic meteorological data in mountainous terrain and its use for simulating forest evapotranspiration and photosynthesis. *Canadian Journal of Forest Research*, 1(17):472-483.

Running, S.W., and Coughlan J.C., 1988. A general model of forest ecosystem process for regional applications. 1. Hydrologic balance, canopy gas exchange and primary production processes. *Ecological modelling*, 42:125-154.

Running S.W., R.R. Nemani, D.L. Peterson, L.E. Band, D.F. Plotts, L.L. Pierce, M.A. Spanner, 1989. Mapping regional forest evapotranspiration and photosynthesis by coupling satellite data with ecosystem simulation. *Ecology*, 70:1090-1101.

Running, S.W., 1994. Testing FOREST-BGC ecosystem process simulations across a climatic gradient in Oregon. *Ecological Application.*, 4:238-247.

Sandmeier, S. and Deering, D.W., 1999. Structure analysis and classification of boreal forests using airborne hyperspectral BRDF data from ASAS. *Remote Sensing of Environment*, 69(3): 281-295.

Soenen, S.A., D.R. Peddle and C. Coburn, 2003. Topographic correction of remote sensing imagery using a canopy reflectance model. In, Proceedings, 25th Canadian Symposium on Remote Sensing, Montreal, PQ., Canada. Oct. 14-17, 2003. Canadian Aeronautics and Space Institute, Ottawa (CD-ROM).

Soenen, S.A., D.R. Peddle and C. Coburn, 2005. SCS+C: A modified sun-canopy-sensor topographic correction in forested terrain. *IEEE Transactions on Geoscience and Remote Sensing*, 43(9):2148–2159.

Stylinski, C.D., Gamon, J.A., and Oechel, W.C., 2002. Seasonal patterns of reflectance indices, carotenoid pigments and photosynthesis of evergreen

chaparral species. *Oecologia*, 131:366-374.

Swift, L.W., 1976. Algorithm for solar radiation on mountain slopes. *Water resources research*, 12(1):108-112.

Teillet, P.M., B. Guindon, and D.G. Goodenough, 1982. On the Slope-Aspect Correction of Multispectral Scanner Data. *Canadian Journal of Remote Sensing*. 8(2):84-106.

Thornton, P. E., S. W. Running, and M. A. White, 1997: Generating surfaces of daily meteorological variables over large regions of complex terrain. *Journal of Hydrology*, 190:214–251.

Urban, D.L., 2000. Using model analysis to design monitoring programs for landscape management and impact assessment. *Ecological Applications*, 10(6): 1820–1832.

Weiss, M. and Baret, F., 1999. Evaluation of canopy biophysical variable retrieval performances from the accumulation of large swath satellite data. *Remote Sensing of Environment*, 70:293–306.

Wessman, C.A. and G.P. Asner, 1998. Successes, limitations, and frontiers in ecosystem science. Springer-Verlag, New York, Inc.

White, M.A., P. E. Thornton, S.W. Running, and Ramakrishna R. Nemani, 2000. Parameterization and sensitivity analysis of the BIOME–BGC ecosystem model: Net primary production controls. *Earth Interactions*, 4(3): 1-85.

Woodcok, C.E., John B.C., V.D. Jakabhazy, X. Li, S.A. Macomber, and Y. Wu, 1997. Inversion of the Li-Strahler canopy reflectance model for mapping forest structure. *IEEE Transaction. Geoscience Remote Sensing*, 35: 405–414.

Wulder, M.A., Franklin, S.E., Lavigne, M.B, 1996. High spatial resolution optical image texture for improved estimation of forest stand leaf area index. *Canadian Journal of Remote Sensing*, 22(6):441-449.

Xu, S., J. Chen, R. Fernandes, and J. Chilar, 2004. Effectts of subpixel water area fraction on mapping leaf area index and modelling net primary productivity in Canada. *Canadian Journal of Remote Sensing*, 30(5):1-8.

Zheng, D.L., E.R. Hunt, Jr. and S.W. Running, 1996. Comparison of available soil water capacity estimated from topography and soil series information. *Landscape Ecology*, 11(1):3-14.

Appendix 1 Climate data—Kananaskis summer 2003

Julian day (day)	Solar Radiation (kj $m^{-2}day^{-1}$)	Minimum temperature (0^c)	Maximum temperature (0^c)	Precipitation (mm)	Relative Humidity (%)
152	22898.56	7.2	20.7	0	67
153	18754.63	3.9	17.1	11.1	69.7
154	29913.71	0.7	17.3	0	43.4
155	28151.37	1.3	20.5	0	45
156	14764.03	6.5	17.9	0	56.8
157	28302.11	-0.8	17.2	0	59.7
158	26281.03	0.4	25.4	0	54.4
159	6386.098	7.1	17.1	9.1	80.6
160	14142.62	7.5	16	1	86
161	9232.409	7.1	14.5	5.9	92.9
162	27158.55	2.5	17.9	0.2	70.8
163	23004.01	1.2	20.7	0.1	62.5
164	13569.4	4.2	19.7	0	56.3
165	16253.38	4.7	18.2	0	40.8
166	18962.13	0.4	19	0	53
167	28510.6	-0.2	23.7	0	49.5
168	26706.33	1.6	24.5	0	54.6
169	26278.08	6.8	29.9	0	50.4
170	8648.917	10.1	15.7	5.1	80.8
171	16497.26	7.1	17.9	5.9	76.2
172	13306.99	-3.1	14.8	25	82.6
173	13788.34	0.9	11.6	0.3	86.3
174	11056.68	3.5	11	3.8	87.1
175	22268.69	-0.4	16.1	1.1	74.2
176	28421.68	2.1	21.2	0	57.3
177	28620.54	9.6	22.2	0	40.8
178	29352.41	7	22.9	0	50.7
179	28965.18	3.5	24.6	0	57.4
180	28909.22	3.9	28.4	0	49
181	29740.53	6	25.3	0	41.9
182	29878.32	4.4	22.9	0	30.2

Appendix 1 (a) July 2003 climate date observed at Kananaskis Meteorological Station.

Julian day (day)	Solar Radiation (kj $m^{-2}day^{-1}$)	Minimum temperature (0^c)	Maximum temperature (0^c)	Precipitation (mm)	Relative Humidity (%)
183	25368.43	5.9	16.7	1.2	33.6
184	27922.65	10.5	19.2	0	29.2
185	22729.24	8.8	22.8	0	32.4
186	9933.167	2.7	15.8	14.2	77.1
187	26403.73	0.5	19.1	0	69.1
188	21370.45	3.9	21.9	0	62.1
189	17392.42	5.1	22.8	1.4	66.6
190	11806.46	5	18.3	0	56.3
191	29944.77	1.5	24.3	0	62
192	24567.4	5.9	27.9	0	49.2
193	22422.21	7.4	28.1	1.2	43
194	18361.71	8.5	24.5	0	50.3
195	22092.96	6.7	21.2	0.1	46.9
196	25689.3	3.9	25.5	0	45.1
197	26660.2	5.4	28.8	0	44.3
198	29895.91	7.7	26.3	0	18.2
199	29077.21	1.7	29	0	34.3
200	26839.42	5.1	26.2	0	54.2
201	24312.82	6.9	29.4	0	52.3
202	28670.74	6.5	30.1	0	47.8
203	27869.04	7.2	32.2	0	38.1
204	25969.05	7.6	32.4	0	36.2
205	15280.58	9.7	22.2	1	69.6
206	18703.97	8.2	20.7	2	75.9
207	20367.1	4.1	26.1	0	56.3
208	27229.45	4.7	29.8	0	42.9
209	23701.76	8	30.2	0	46.4
210	26846.78	8.7	28.5	0	54.5
211	22187.75	7.3	30.5	0	52.5
212	19739.61	7.7	28	0	43.5
213	24145.1	9.9	31.4	0	38.9

Appendix 1 (b) August 2003 climate date observed at Kananaskis Meteorological Station.

Julian day (day)	Solar Radiation (kj $m^{-2}day^{-1}$)	Minimum temperature (0^c)	Maximum temperature (0^c)	Precipitation (mm)	Relative Humidity (%)
214	18844. 16	10. 4	28. 2	0	49. 8
215	19046. 8	9. 3	26	0	64
216	15917. 32	11. 1	23. 4	0. 6	64. 3
217	26377. 2	7. 2	29. 1	0. 1	61. 2
218	18998. 88	9. 7	26. 5	0	49. 8
219	18029. 94	6. 1	25. 2	0	61. 8
220	17510. 7	5. 9	22. 8	0	69
221	16804. 93	6. 3	27. 1	0	69. 2
222	15379. 91	8. 6	24. 4	0	64. 9
223	18053. 81	7. 9	25. 8	0	71. 2
224	3985. 56	0	26. 5	24. 9	60. 7
225	24521. 04	5. 6	26. 3	0	35. 5
226	23652. 36	5. 5	26. 9	0	30. 7
227	21220. 92	1. 2	33	0	36. 6
228	10960. 92	15. 7	28. 2	0	46. 4
229	17910. 72	12. 1	27. 6	0	55. 7
230	23289. 12	9. 9	30. 1	0	35. 4
231	15565. 91	8. 6	24. 9	5	65. 6
232	19968. 3	8. 5	24. 5	0	60. 6
233	21190. 18	5	28. 6	0	51. 9
234	12015. 03	7. 8	27	0	51. 4
235	15421. 37	6. 7	19. 3	0	36. 8
236	20383. 04	1. 3	22. 1	0	55. 7
237	18466. 77	4. 6	24. 5	0	44. 9
238	18515. 44	4. 6	27. 5	0	50. 7
239	7376. 713	5. 8	29. 9	14. 6	77. 4
240	10284. 97	4. 7	14. 6	0. 5	90
241	20994. 84	0. 8	22. 2	0	67. 6
242	20980. 22	1. 5	26	0	59. 6
243	19474. 19	3. 6	27. 3	0	53. 8

Appendix 1 (c) September 2003 climate date observed at Kananaskis Meteorological Station.

Appendix 2 C code for climate data extrapolation

```
/*****************************************************************************
   Subroutine readclimate.ccp run in the BEPS model

   Description:
   ----------
   Extrapolate climate date observed in a climate station to landscape scale
   using topographic information and empirical equations
 *****************************************************************************

   Written by:     Shiyong XU
                   February 2005
*****************************************************************************/

#include <stdio.h>
#include <stdlib.h>
#define tmax_lr -7 /* lapse rate for maximum temperature */
#define tmin_lr -3 /* lapse rate for minimum temperature */
#define base_el 1393 /* base elevation for climate station */
#define deg 0.01745329 /* converting coefficient for radian */
#define PI acos(-1.0) /* value for PI */
double rad(double, double,double, float,float); /*subroutine for calculating radiation */
double dayl(double, double) /*subroutine for calculating day length */
void readclim(lin,jday,climate,rcode) /*subroutine used by BEPS for climate data extrapolation */

int lin;          /* Line number */
int jday;         /* Julian Day */
double **climate;   /* Climate data for a line in the study area */
int short *rcode;
{
int i,j,k,day[365],ptr;
FILE *f1,*f2,*f3,*f4,*fjun,*fjul,*faug;
float radi,tmin,tmax,precip,humi;
float t_max[365],t_min[365],pre[365],rad[365],hum[365];
double denom,tat,output;
float t_avg,vpd,es,em;
float dif_lr,f;
float l0,l1,l2,d,e,t,t0,t1,t2,t3,t4,t5,t6,t7,r0,r1,r2,r3,r4,r5,r6;
float sun_c=1.95;
short *dem;
float *aspect,*slope,*f6,*f7,*f8;
l0=lat;
aspect=(float *) malloc(npixels*sizeof(float));
```

```
dem=(short *) malloc(npixels*sizeof(short));
slope=(float *) malloc(npixels*sizeof(float));
f6=(float *) malloc(npixels*sizeof(float));
f7=(float *) malloc(npixels*sizeof(float));
f8=(float *) malloc(npixels*sizeof(float));

if((f1=fopen("c:/bepsinputkan/dem","rb"))==NULL)
  {
       printf("\n Unable to open file <%s>,    exitting program ...\n\n","dem.bil");
            return 0;
           }
if((f2=fopen("c:/bepsinputkan/slope","rb"))==NULL)
{
       printf("\n Unable to open file <%s>,    exitting program ...\n\n","slope.bil");
          return 0;
           }
if((f3=fopen("c:/bepsinputkan/aspect","rb"))==NULL)
{
       printf("\n Unable to open file <%s>,    exitting program ...\n\n","aspect.bil");
         return 0;
           }
if((f4=fopen("c:/bepsinputkan/climate_daily.txt","r"))==NULL)
{
       printf("\n Unable to open file <%s>,    exitting program ...\n\n","daily.txt");
         return 0;
           }
if((fjun=fopen("c:/bepsinputkan/jun","rb"))==NULL)
{
       printf("\n Unable to open file <%s>,    exitting program ...\n\n","jun");
         return 0;
           }
if((fjul=fopen("c:/bepsinputkan/jul","rb"))==NULL)
{
       printf("\n Unable to open file <%s>,    exitting program ...\n\n","jul");
         return 0;
           }
if((faug=fopen("c:/bepsinputkan/aug","rb"))==NULL)
{
       printf("\n Unable to open file <%s>,    exitting program ...\n\n","aug");
         return 0;
           }
for (k=0;k<365;k++)
{
day[k]=0;
```

```
t_max[k]=0.0;
t_min[k]=0.0;
pre[k]=rad[k]=hum[k]=0.0;
}
for (j=jday_start;j<=jday_end;j++)
{
fscanf(f4,"%d%f%f%f%f%f\n",&(day[j]),&(rad[j]),&(t_min[j]),&(t_max[j]),&(pre[j]),&(hum[j]))
;
}
ptr=lin*NPIX_CAN + pix_offset;
fseek(f1,ptr*2,0);
fread(&dem[0],sizeof(unsigned short),npixels,f1);
fseek(f2,ptr*4,0);
fread(&slope[0],sizeof(float),npixels,f2);
fseek(f3,ptr*4,0);
fread(&aspect[0],sizeof(float),npixels,f3);
fseek(fjun,ptr*4,0);
fread(&f6[0],sizeof(float),npixels,fjun);
fseek(fjul,ptr*4,0);
fread(&f7[0],sizeof(float),npixels,fjul);
fseek(faug,ptr*4,0);
fread(&f8[0],sizeof(float),npixels,faug);
for (k=0;k<npixels;k++)
{
 /* calculate radiation */
      /* latitute of equivalent slope */
 l1=asin(cos(slope[k]*deg)*sin(lat*deg)+sin(slope[k]*deg)*cos(lat*deg)*cos(aspect[k]*deg));
 denom=(cos(slope[k]*deg)*cos(lat*deg))-(sin(slope[k]*deg)*sin(lat*deg)*cos(aspect[k]*deg));
 if (denom == 0) {
denom=.0000000001;
}
 /* time offset in hour angle between actual and equivalent slope */
l2=atan((sin(slope[k]*deg)*sin(aspect[k]*deg))/denom);
if (denom <0) {
l2=l2+PI;
}
/* declination of sun */
d=asin(.39785*sin(4.8690+(.0172*day[jday])+(.03345*sin(6.2241+.0172*day[jday]))));
/* radius vector of sun */
e=1.0-0.0167*cos((day[jday]-3)*0.0167);
r1=60*sun_c/(e*e); /* solar constant for 60 minutes */
t=dayl(l1,d); /* temporary variable,hour angle of sunset */
t7=t-l2; /* hour angle of sunset on equivalent slope */
t6=-t-l2; /* hour angle of sunrise on equivalent slope */
```

```
t1=dayl(l0*deg,d); /* hour angle of sunrset on horizontal surface */
t0=-t1; /* hour angle of sunrise on horizontal surface */
t2=t0; /* hour angle of sunset on equivalent slope */
if (t6 >t0) {
t2=t6;
}
t3=t1;
if (t7 < t1) {
t3=t7;
}
if (t3<t2) {
t3=t2;
}
t6=t6+2.0*PI;
if (t6 >= t1) {
t7=t7-2.0*PI;
if (t7<=t0) {
r4=r1*rad(l1,l2, d, t2, t3);
r3=r1*rad(l0*deg,0.0, d, t0, t1);
if (r3 != 0) {
f=r4/r3;

}
}
}
r5=fabs(f)*rad[jday];
radi=r5/cos(slope[k]*deg);

/*    calculate temperature */
 dif_lr=(dem[k]-base_el)/1000.0;
 tmax=t_max[jday]+dif_lr*tmax_lr;
 tmin=t_min[jday]+dif_lr*tmin_lr;
 if (tmin>=tmax)
       tmin=tmax-0.5;

/* calculate humidity */
t_avg=0.606*tmax+0.394*tmin;
es=610.78*exp(17.269*t_avg/(237.3+t_avg));
em=610.78*exp(17.269*tmin/(237.3+tmin));
humi=em/es*100;
/* convert realative humidity(%) to specific humidity(g/kg) */
if(t_avg<=10) {
     humi=0.0941*humi+0.0006;}
if(t_avg>10 && t_avg<=15) {
```

```
        humi=0.1286*humi;}
if(t_avg>15 && t_avg<=20) {
        humi=0.1733*humi-0.0003;}
if(t_avg>20 && t_avg<=25) {
        humi=0.2316*humi-0.0086;}
if(t_avg>25) {
        humi=0.3043*humi+0.0006;}

/*    calculate precipitation */

if(jday>=152 && jday<=181) {
        precip=pre[jday]*f6[k];}
if(jday>=182 && jday<=212) {
        precip=pre[jday]*f7[k];}
if(jday>=212 && jday<=243) {
        precip=pre[jday]*f8[k];}

  climate[k][0]=radi;
  climate[k][1]=tmin;
  climate[k][2]=tmax;
  climate[k][3]=precip;
  climate[k][4]=humi;

} // end of pixel
  free(dem);
  free(slope);
  free(aspect);
  fclose(f1);
fclose(f2);
fclose(f3);
fclose(f4);
fclose(fjun);
fclose(fjul);
fclose(faug);
}
/* calculate potential radiation */
double rad(double equivlat, double along,double D, float timeA,float timeB ) {
        double output=0;
output=(sin(D)*sin(equivlat)*(timeB-timeA)*3.82)+(cos(D)*cos(equivlat)*
(sin(timeB+along)-sin(timeA+along))*3.82);
return output;}

/* Requires latitude input in radians, caculate sun rise and sunset times*/
double dayl(double inlat, double declin) {
```

```
double tat;
tat=tan(inlat)*tan(declin);
if (tat <-1.0) {
return 0.0;
}
if (tat>1.0) {
tat=1.0;
}
return acos(-tat);
}
```